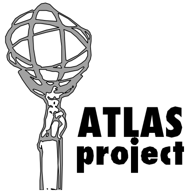

ITk Pixel – Outer Endcaps Loaded Local Supports

ATLAS ITk-Pixel Project

ATLAS ITk-Pixel Project Document No: **AT2-IP-ER-0047**	EDMS Document No: **2824412**	Created: 01/12/2022	Page: **1 of** 122
		Modified: 22/02/2023	Rev. No.: 3.6

Design Overview of the Loaded Local Supports for the ITk Pixel Outer Endcaps

Provided for the ITk Pixel Outer System Loaded Local Supports Final Design Review
28 February – 1 March 2023

This document describes the procedures and equipment for the loading of modules and on-detector services in the ITk Pixel Outer Endcaps. It also describes the validation of these procedures and equipment, plus plans for pre-production and preliminary plans for production.

Prepared by:		Checked by:	Approved by:
J. Pater (editor)		All authors (see list to left)	
P. Morettini (editor)			
D. Alvarez Feito	J. Matheson		
R. Chapple	M. Monti		
G. Chiodini	G. Miller		
S. Coelli	F. Muñoz Sánchez		
L. Cunningham	S. Passaggio		
P. Dervan	S. Ravera		
S. Eisenhardt	E. Ruscino		
G. Gariano	B. Smart		
C. Gemme	D. Vazquez Furelos		
H. Hayward	B. Vormwald		
D. Hynds	M. Wielers		
S. Koch	G. Zhang		
J. Martin			

Distribution List

Atlas ITk Collaboration , FDR Review panel

History of Changes

Rev. No.	*Date*	*Sections*	*Description of changes*
V0	01/12/2022	All	BV: First Emission (Template)
V1.0	08/12/2022	All	JRP: First version of skeleton document specific to Outer Endcaps; including suggested changes over V0 plus suggestions for authors of various sections.
V1.1	11/12/2022	All	Discussed/shared with BV as starting point to maintain parallel structure between OE, OB.
V1.2	15/12/2022	All	Included feedback from PM; shared with BV. To discuss with endcap loading community on 16-Dec-22.
V1.3	16/12/2022	All	Result of discussion with loading community
V2.0	21/02/2023	All	First complete draft – incorporated input from loading community. Included some rearranging of sections to increase clarity (JRP). Released to endcaps community for feedback on 21/02/2023.
V3.0	22/02/2023	Section 5	Some editing with HH. Section 5 sent to HH for further revision.
V3.1	22/02/2023	All but Section 5	Work in parallel with HH, PD, BS, JM working on Section 5
V3.2	23/02/2023	All	Imported new Section 5. Released as draft to EDMS for endcaps community for feedback.
V3.3	24/02/2023	Sec.2.2.3 4.1 Sec.4.5 Sec.5 Sec.7.2.1 Appendix A All	Added more on STYCAST re-workability issue Added description of module re-work method. Added description of Genova thermal cycling programme Added plots showing noise in cold MOPS operation Updated production flow diagram Added placeholder appendix for responses to actions from previous reviews Corrected typos, reformatting to remove excessive white space, fixed references.
V3.4	25/02/2023	Sec.4.5	Updated results on thermal cycling. Released to EDMS and to reviewers via the FDR indico page.
V3.5	25/02/2023	pp.1,2	Missing contributor added, correction to dates in history page. Released in place of 3.4
V3.6	26/02/2023	Fig.14 Fig.71 various	New version of Fig.14 Was missing in lower-resolution pdf Small formatting changes

Table of Contents

1 INTRODUCTION 6

2 SYSTEM OVERVIEW 7

2.1 The Outer Endcaps Loaded Local Support 7

2.2 Components and Interfaces 7
2.2.1 The local supports 7
2.2.2 Modules 8
2.2.3 Adhesives 9
2.2.4 On-detector services 10
2.2.5 Interface to the support cylinders 12
2.2.6 Interface to Type-1 cables 13
2.2.7 Interface to Type-1 cooling 13

3 DESIGN AND LOADING PROCESSES 16

3.1 General Design Considerations 16
3.1.1 Specifications and Requirements 16
3.1.2 Half-ring reference system reconstruction 16
3.1.3 Grounding and Shielding 18
3.1.4 The Half-ring Handling Frame 21

3.2 Bus tape loading 25
3.2.1 Loading Specifications 25
3.2.2 Qualification - Thermo-mechanical FEA 26
3.2.3 Preliminary Bus-Tape Gluing trials 31
3.2.4 Production Tooling and Method 34
3.2.5 Qualification - metrology 36

3.3 Power Pigtails connection 37
3.3.1 Design Concept - Tooling 37
3.3.2 Design Concept - Procedure 37
3.3.3 Preliminary trials 38
3.3.4 Trials with realistic components 42
3.3.5 Irradiation QA 43

3.4 Module Loading technique – RAL 44
3.4.1 Description of the loading process 44
3.4.2 Description of the tooling and equipment 44
3.4.3 Glue Deposition 49
3.4.4 Module placement 50

3.5 Module Loading technique – Oxford 53
3.5.1 Description of the loading process 53
3.5.2 Description of the tooling 53
3.5.3 Glue Deposition 55
3.5.4 Module placement 57

3.6 Loading technique – Genova and Lecce 58
3.6.1 Description of instrumentation and tooling 59
3.6.2 Schematic description of the loading procedure 59
3.6.3 Glue preparation and deposition 63
3.6.4 Gantry calibration for metrology 63
3.6.5 Safety Considerations 64

4 RESULTS OF LOADING DESIGN VALIDATION 65

4.1 Loading Validation at RAL 65
4.1.1 Glue thickness 65
4.1.2 Placement accuracy 66
4.1.3 Loaded modules functionality check 67
4.1.4 TFM cross-check 67

4.2 Loading Validation at Oxford 67
4.2.1 Glue thickness 67
4.2.2 Placement accuracy 68

4.3 Loading Validation at Genova 70
4.3.1 Glue thickness 71
4.3.2 Placement accuracy 74
4.3.3 Loaded modules functionality checks 77

4.4 Loading Validation at Lecce 79
4.4.1 Glue thickness 81
4.4.2 Placement accuracy 83
4.4.3 Loaded modules functionality checks 84

4.5 Thermal Cycling of a Layer-4 Half-Ring 86

5 ELECTRICAL EVALUATION AND DESIGN VALIDATION OF LLS 91

5.1 Concept of Electrical Validation 91
5.1.1 Testing Stages and Test Setups 91
5.1.2 Pre-/Post-Loading 92
5.1.3 System Test 93

5.2 Results 97
5.2.1 MOPS Readout 97
5.2.2 Module Performance Pre-Loading, Post-Loading and System Test 100

6 QUALITY CONTROL 110

6.1 Philosophy of QC Procedures 110

6.2 Outline of electrical QC setups 110
6.2.1 UK test box and environmental control 111
6.2.2 Italy test box and environmental control 111
6.2.3 Power supplies 113
6.2.4 Cables 113
6.2.5 Detector Safety and Interlock concept 113
6.2.6 Readout System 114

6.3 Site Qualification Plan 114

7 PRODUCTION PLAN 116

7.1 Number of Parts 116

7.2 Production Flow and Involved Institutes 116
7.2.1 Production Flow Diagram 116
7.2.2 Description of Production QC 117

7.3 Transport of loaded supports to Integration Sites 117

7.4 Schedule 118

8 REFERENCES 120

APPENDIX A: RESPONSES TO ACTIONS AND RECOMMENDATIONS FROM PREVIOUS REVIEWS 122

1 Introduction

The ITk Pixel Outer Endcaps (outlined in green in Figure 1) occupy the space between the Inner Support Tube (IST) and the Pixel Support Tube (PST) at either end of the detector. The space they occupy is defined by 1114 mm < |Z| < 3018 mm, 145 mm < R < 327 mm. One Endcap will be manufactured and assembled in Italy; the other in the UK.

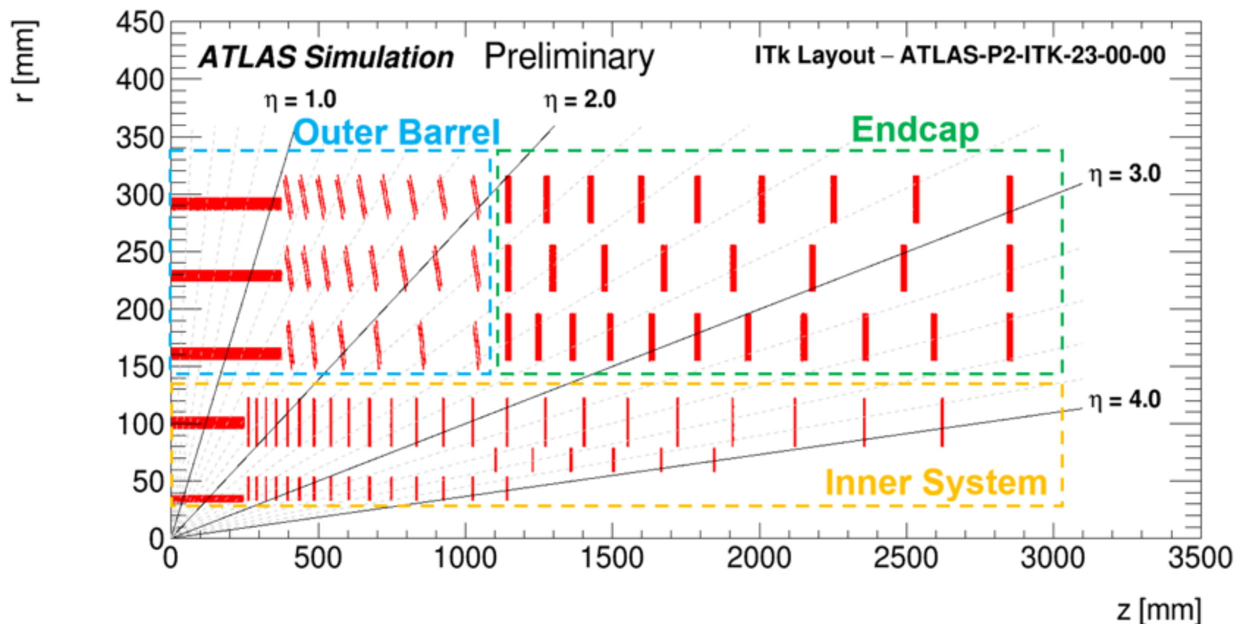

Figure 1: r-z schematic of the layout of the ATLAS ITk Pixel Detector, highlighting the regions corresponding to the Inner System (orange), Outer Barrel (blue) and Outer Endcaps (green). Only one quadrant and only active detector elements are shown.

This document describes the procedures and equipment for the loading of modules and on-detector services on the local-support structures of the Outer Endcaps. It should be noted that there are four distinct loading sites: two in the UK and two in Italy. While the basic principles of loading are common across the four sites, there are some minor differences, due for example to equipment availability; these differences will be described in this document along with the basic principles. As the requirements and specifications are identical for all loading sites, the final loaded supports will be identical independent of which site produced them.

The remainder of this document is divided into the following sections:

- An overview of the design of the Outer Endcaps, to introduce the elements involved in the local-support loading process
- A description of the general design considerations for the loading process, and the techniques used in the various loading sites
- A presentation of the results of design validations at the individual module and system levels
- Our pre-production and production plans; including quality control, site qualification, procurement, production database implementation, and schedule issues.

2 System Overview

Each ITk Pixel Outer Endcap consists of three layers (Layers 2, 3, and 4)[1] of half-ring-shaped local support structures (see Figure 2) installed into half-cylindrical global support structures together with all associated cooling and electrical services. The half-layers are assembled into full coaxial-cylindrical layers during the endcap integration process.

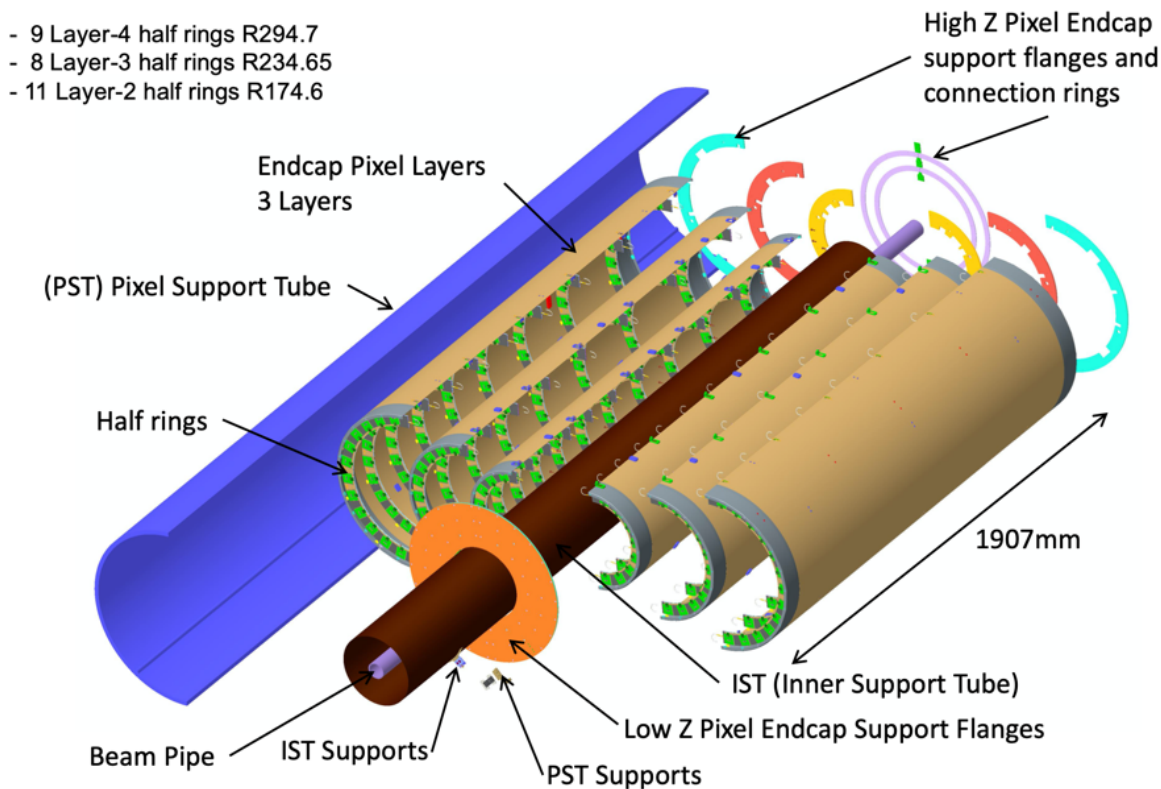

Figure 2: CAD representation (exploded view) of one ITk Pixel Outer Endcap.

2.1 The Outer Endcaps Loaded Local Support

2.2 Components and Interfaces

2.2.1 The local supports

The basic local-support structure for the Outer Endcaps is a "half-ring" (see Figure 3), which supports two serial-powering chains of modules, one chain on each face of the half-ring. Phi hermeticity is achieved by placing the modules on one face of a half-ring over the spaces between modules on the opposite face. Eta hermeticity is achieved by strategic z placement of the rings, see Figure 1.

---

[1] *Layers 0 and 1 are part of the Inner System. Layers 2, 3, and 4 are informally referred to respectively as the "Inner", "Middle", and "Outer" layers within the Outer Endcaps community and these terms sometimes appear in e.g. engineering drawings.*

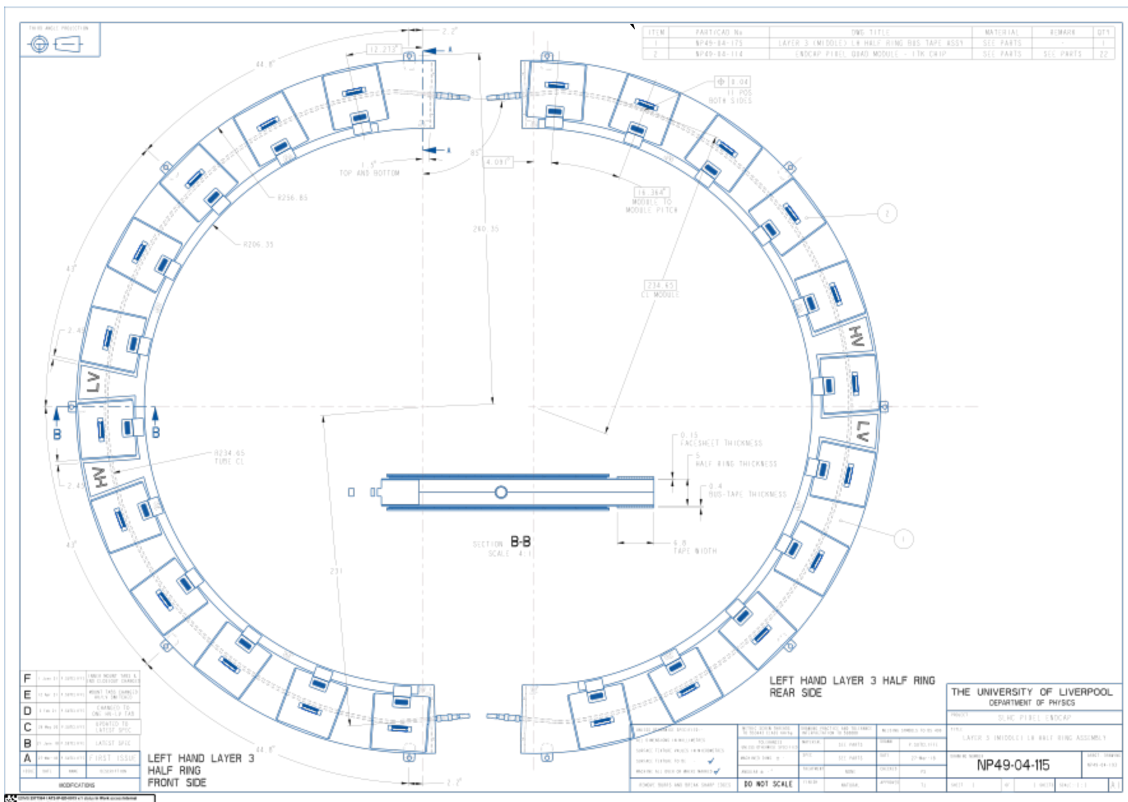

Figure 3: Engineering drawing of a fully-loaded left-handed Layer-3 Outer Endcap Half-ring (front and back views) showing the modules, bus tape, and power pigtails, the loading of which is described in this document.

Further details about the design and qualification of the Outer Endcaps' bare local support structures can be found in the documentation [1] for the ITk Pixel Outer System Bare Local Supports Final Design Review, which was held on 13-14 October 2021[2].

2.2.2 Modules

A single type of hybrid module featuring four front-end chips bump-bonded to a 150µm thick, n-in-p planar sensor is employed in the design of the Outer Endcaps; this is the same module that is employed in the Outer Barrel. The geometry of the bare "quad" module is shown in Figure 4. A flexible printed circuit glued to the back side of the sensor provides the interface between the hybrid and the outside world through two separate connectors for (i) the data and command and (*ii*) the power and DCS signals. Wire-bonds connect electrically the sensor and the front-end chips with the so-called "module flex", which is used to route the clock, input command, output data and power signals to the active elements. In addition, several NTC thermistors are placed in the flex to measure the temperature of the module.

The wire bonds between the hybrid and the flex cover completely two parallel edges of the quad module. In the Outer Endcaps the wire-bonding edges are in the roughly radial direction.

Table 1 shows the numbers of rings and modules in one Outer Endcap.

---

[2] https://indico.cern.ch/event/1075990/

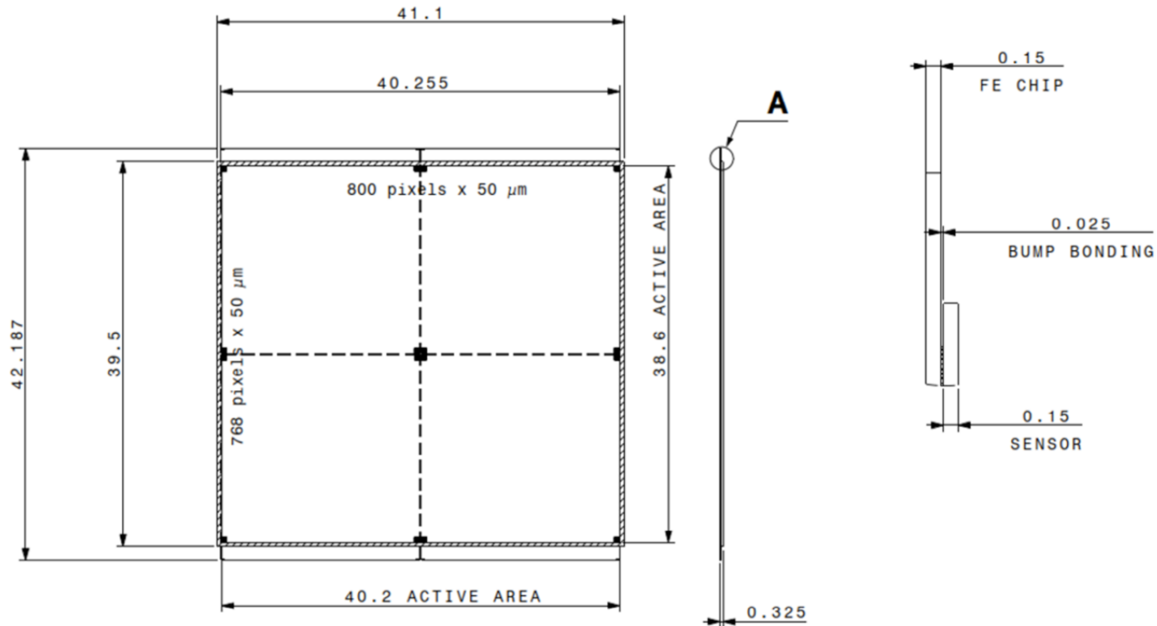

Figure 4: CAD view of the bare module used in the Pixel Outer Barrel (all the dimensions are in mm).

Ring Layer	# of Rings	SP chain length (# of Quad Modules)	# of Modules / Ring	Total # of Modules
Layer 2	11	8	32	352
Layer 3	8	11	44	352
Layer 4	9	13	52	468
				1172

Table 1: The number of rings and "quad" (incorporating four readout ASICs) pixel modules in one Outer Endcap.

2.2.3 Adhesives

Modules will be fixed directly to the carbon-fibre surfaces of the half-rings. The preference is to use a re-workable adhesive; our baseline is DOWSIL™ SE4445 CV Gel [2] (hereafter referred to in this document simply as "SE4445"), a two-part thermally-conductive silicone gel which behaves as an adhesive with room temperature cure times of a few hours (see Figure 5). Our experience so far with the re-workability of SE4445 is limited - only 30 working modules have so far been loaded across the four sites – but very positive, see Section 4.1.

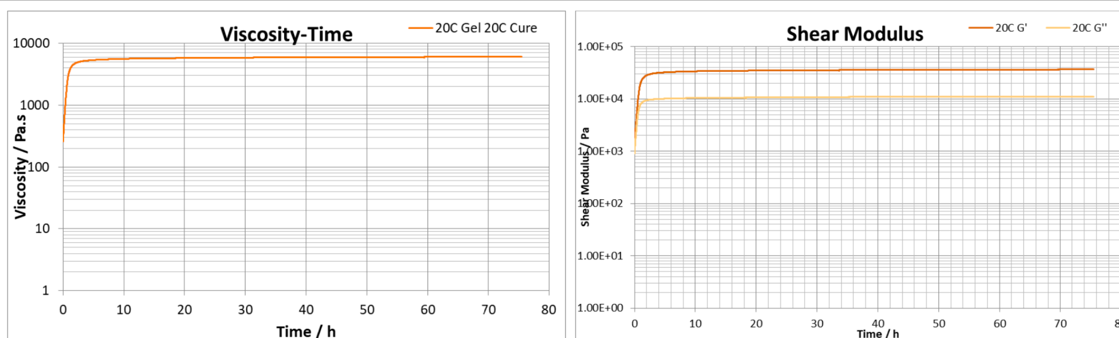

Figure 5: Room-temperature cure properties of DOWSIL™ SE 4445, from a 2019 study performed at RAL [3].

Samples of SE4445 are currently being prepared for irradiation by LBNL and subsequent mechanical testing at Purdue University. This programme is expected to be completed in the coming few months.

In case the SE4445 does not pass qualification, our fall-back option is to use STYCAST® 2850FT [4] (the same adhesive being used in the Outer Barrel). However, STYCAST is not re-workable once cured, so extreme care would need to be taken in loading and handling to avoid damage to modules. As mentioned above, the number of real modules loaded so far has been very limited – only 30. One was damaged by a malfunctioning bench power supply that was being used in the absence of 'official' power supplies but, while we cannot quantify the likelihood of such accidents with the current low statistics, we do not expect such accidents to occur with any great frequency during production loading.

Having said that, it is possible to remove a module that has been fixed down with STYCAST[3], but a programme of work would be necessary to develop a removal method that minimises the risk to the half-ring and any nearby modules and services already loaded and working. In addition, *complete* removal of residual cured STYCAST may not possible without damaging the half-ring. It should however be possible to glue another module on top of the residual glue; the thermal performance would be impaired due to the resulting thicker glue layer, but this solution would be preferable to leaving a hole in the coverage. This possibility will be investigated with urgency if SE4445 proves unsuitable in the irradiation study.

The stress on the modules due to thermal expansion and contraction when fixed to the (effectively 0-CTE) carbon-fibre local supports has been studied in the module community; results were presented in the recent ITk Pixel Modules FDR[4].

2.2.4 On-detector services

In addition to modules, the half-rings also support the Type-0 power electronics, which consist of one "bus tape" (a semi-circular copper-Kapton flex circuit which carries module power and monitoring to and from the modules – see Figure 6) per serial-powering chain, and one "power pigtail" per module, which connects the module to the bus tape. Figure 7 shows a CAD rendering of a Layer-2 half-ring with modules and Type-0 services loaded. These components, their loading, and their loading qualification, are presented later in this document.

---

[3] This destroys the module, but it wouldn't be a candidate for removal if it were usable.

[4] 31 May – 8 June 2022, https://indico.cern.ch/event/1074796/.

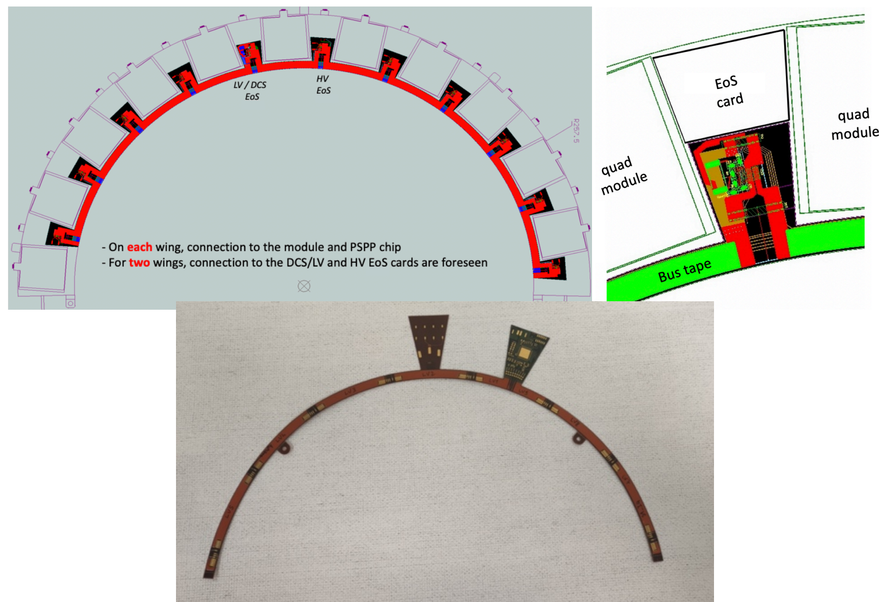

Figure 6: Top Left: The Version-5 Outer Endcap bus tape design for Layer 3 (as used on the Ring-1 electrical demonstrator) which required separate Edge-of-Structure (EoS) cards to be plugged in at the indicated locations as shown at Top Right. Bottom: A Version-6 bus tape featuring integrated EoS cards on so-called "EoS wings".

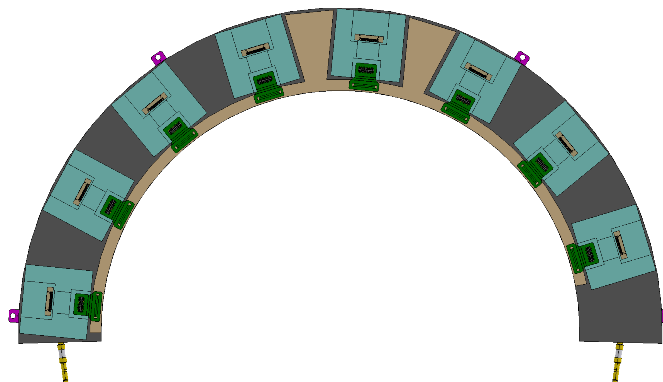

Figure 7: CAD rendering of one side of a fully-loaded Layer-2 half-ring, showing a V6 bus tape (brown), stylised quad modules (blue-green) and power pigtails (green).

It should be noted that early versions of the Type-0 electronics (before version 6 of the bus tape) required two "EoS" cards to be attached to the bus tape. The EoS cards transferred LV and DCS or HV between the Type-1 cables and the bus tape. This is the version of the Type-0 electronics that is present on the "Ring-1" electrical demonstrator discussed later in this document. Since bus tape version 6, these EoS cards have been integrated with the bus tape.

Note that data and clock and command signals follow a separate path to power and monitoring; "data PP0s", which will be added at the endcap integration phase, will connect multiple modules to bundles of twin-axial cables, which run along the inner surface of the half-cylinders (see Section 2.2.6).

All of the electrical services discussed in this document were included in the recent ITk Pixel On-detector Services FDR[5].

2.2.5 Interface to the support cylinders

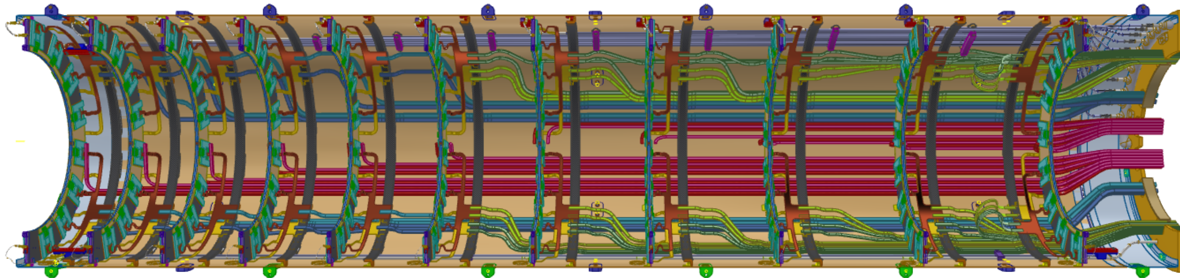

Figure 8: CAD rendering of one ITk Pixel Outer Endcap Layer-2 half-layer, showing the 11 loaded half-rings, the Type-I cooling pipes, the data PP0s, and the Type-I data and power cables.

Figure 8 shows a CAD rendering of one Outer Endcap half-layer, essentially a carbon-fibre half-cylinder into which services and loaded half-ring have been inserted. As has been shown above, the outer circumference of each half-ring has a number of fixation lugs (sometimes referred to as “mounting lugs”). As is illustrated in Figure 9, when the half-ring is installed into the half-cylinder shell during endcap integration, these lugs will be bolted into a matching array of lugs adhesively precisely bonded on to the inner surface of the half-shell. This interface was reviewed as part of the Global Mechanics and Integration (GM&I) PDR[6], see [5], and will be followed further in the GM&I FDR, currently tentatively scheduled for May 2023.

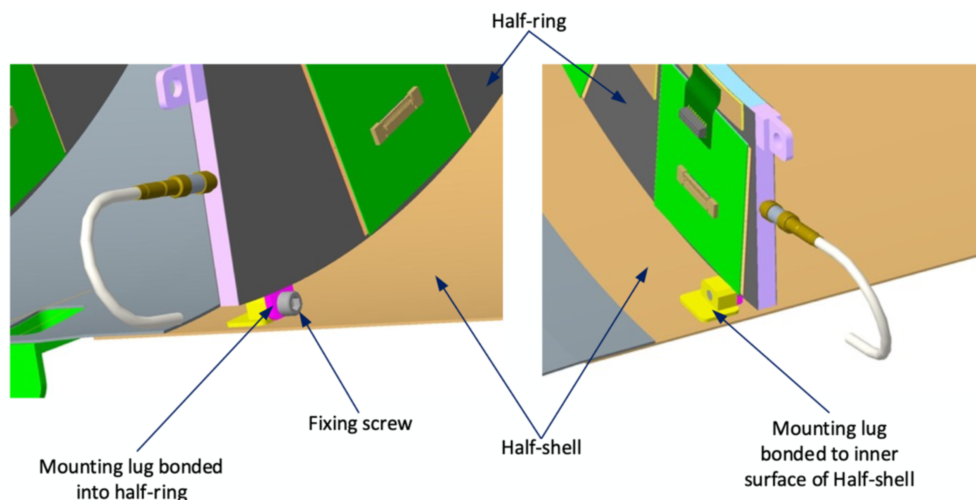

Figure 9: CAD renderings showing the concept of the half-ring mounting system. Also visible are the ceramic electrical breaks on the ends of the cooling tubes embedded in the half-ring, and the U-loop which connects the half-ring to the Type-I cooling (Type-I cooling pipes not shown).

---

[5] 30 November – 1 December 2022, https://indico.cern.ch/event/1213069/.

[6] 10-11 December 2020, https://indico.cern.ch/event/962215/.

2.2.6 Interface to Type-1 cables

As was illustrated in Figure 8 and further in Figure 9, Type-1 cables for data, low voltage, high voltage, the Detector Control System (DCS), and interlocks will run along the inner surface of the half-layer's supporting half-cylinder; this routing is illustrated more clearly in Figure 10. These cables will be put in place before half-rings are installed and will terminate in connectors which will be plugged into mating connectors located on the EoS wings of the half-ring bus tapes during endcap integration. These connections were reviewed electrically as part of the On-Detector Services FDR; the details of the installation and connection process will be reviewed in the upcoming Global Mechanics & Integration FDR.

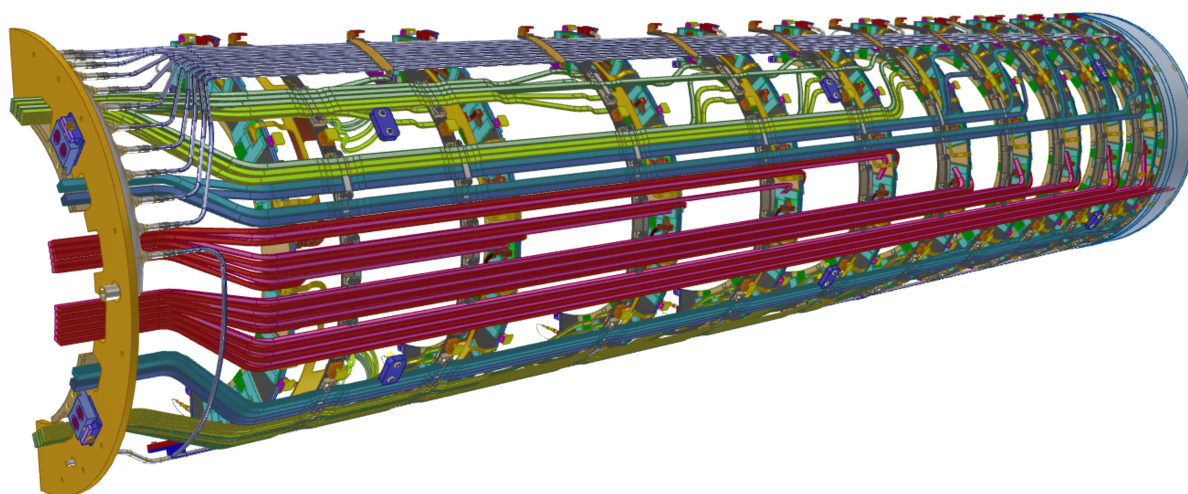

Figure 10: CAD rendering of one ITk Pixel Outer Endcap Layer-2 half-layer with the supporting half-cylinder removed from view, to show the routing of the Type-I cables and cooling pipes.

The Type-1 services will pass very close to the high-radius edges of the half-ring which form the inner radius of the gap through which the Type-1 services pass while exiting the detector. Thus, the Type-1 cables will often touch the high-radius rim of the half-rings, but the cables' insulation will prevent any electrical contact. Further, the Type-1 services will be clamped in the spaces in z between the half-rings, controlling their thermally-induced movement and preventing them from slipping back and forth and rubbing against the half-rings.

2.2.7 Interface to Type-1 cooling

2.2.7.1 Description of the Interface

The bare half-rings incorporate embedded titanium evaporators to remove the heat produced by the modules and services mounted onto their surfaces. The evaporators include ceramic electrical breaks at each end, which protrude from the half-ring; these can be clearly seen in Figure 9. Type-1 cooling pipes, similarly to the Type-1 cables described above, are installed on the supporting half-cylinders at the beginning of the half-layer integration process. When a half-ring is installed in the half-shell, a coiled capillary with a brazed weld sleeve is welded to the half-ring on the cooling inlet side. A titanium "U-loop", also shown in Figure 9, is selected for the exhaust end of the half-ring, from a variety of available sizes, to fit the individual location and is welded in place with two orbital sleeve welds, one on each end of the U-loop. This procedure was also preliminarily reviewed at the GM&I PDR and will covered at the upcoming GM&I FDR.

2.2.7.2 Welding procedure and qualification

A procedure was developed to qualify electronics as being safe to be welded next to in the ITk[7]. This procedure must be used to qualify all final electronic devices that will go into the ITk.

The procedure consists of mounting electronic devices to be qualified onto representative support structures with representative cabling. The devices have their performance tested, the cooling pipes of these support structures are then welded as they will be in the ITk, and the devices are retested. Identical devices will remain un-welded as 'control' devices for comparison. The welded and un-welded (control) devices are then put through an accelerated ageing program, consisting of operation at elevated temperatures and voltages, as well as irradiation to ITk end-of-life dosage. Throughout this, the performance of the devices will be evaluated and compared, to assess whether there is any difference in performance between the welded and un-welded devices.

Thus far, tests of the qualification procedure have been performed on prototype pixel modules (RD53a) mounted to prototype pixel support structures. The following tests have been made:

One RD53a pixel quad module was mounted to a prototype pixel end-cap half-ring ('Ring 1'), and twenty welds made on the cooling pipes of the half-ring. That module, and an identical un-welded module, were then put through the full accelerated ageing program. No effects on module performance were seen due to welding.

Two digital RD53a pixel quad modules were mounted to a prototype pixel end-cap half-ring which did not have electrical breaks. 20 welds were made on the cooling pipes of the half-ring. Module performance was tested before and after welding. No effects on module performance were seen.

One digital RD53a pixel quad module had its ground plane connected to a pixel end-cap cooling pipe, and 20 welds were made on the cooling pipe while the module was powered and running. Noise bursts were seen in the module when the welding arc formed and when the arc collapsed, but no residual effects on module performance were seen (see Figure 11).

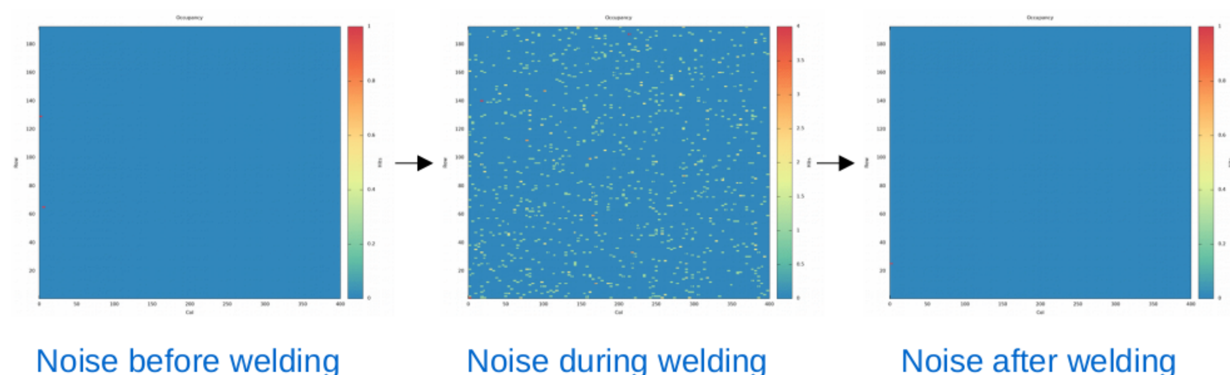

Figure 11: Noise seen in a powered digital RD53a quad module before, during, and after welding of the cooling pipe of the module's local support structure.

---

[7] A formal report from the Welding Task Force is in preparation and will be released soon.

In addition to the above tests on pixel modules, when welds were being made, an RF probe was placed near the modules. The RF spectrum was monitored and recorded. Other nearby common sources of RF were also investigated, with the RF probe in the same location next to the module; see Figure 12. Common procedures such as starting a pixel module scan, or starting a nearby workshop pillar drill, were found to produce more RF noise than welding.

Figure 12: RF scans. Yellow: RF probe voltage. Pink: RF frequency spectrum.

2.2.7.3 Modularity of Loaded Half-rings

Considerable design effort has gone into making the half-rings, bus tapes and power pigtails as modular, portable, and self-contained as possible. The three sizes of half-rings and bus tapes are identical in design except for scale, and the power pigtails are identical everywhere in the endcaps.

The front and back sides of every half-ring are identical to each other, and the half-rings could therefore be inserted into their half-layer in either orientation; the cooling inlet and outlet locations will only be determined at this moment of insertion, when capillaries will be added at the inlet. Likewise, any individual half-ring could be placed at any z position in its given half-layer.

It should be noted however that each *loaded* half-ring will be either “right-handed” or “left-handed” and must be placed in the corresponding half-layer; this is necessary to avoid an asymmetry in the z-spacing of the end modules on the mating half-rings at the top and bottom of the detector.

3 Design and Loading Processes

3.1 General Design Considerations

3.1.1 Specifications and Requirements

The specifications for local supports and loading can be found in References [6] and [7] respectively. The most important specifications can be summarised as follows:

- The thickness of the glue between the modules and the local support must be in the range 100^{+100}_{-50} µm. This value is selected considering the thermal performance requirements as well as the flatness tolerances; while thinner glue layers would be preferred from the thermal standpoint, they are disfavoured to avoid potential problems with filler particles in the adhesive.
- The modules should be placed so that there will always be at least five pixels overlap in phi with all loads applied[8].
- The default module placement accuracy for rings from Reference [7] is ±150µm, "which corresponds to standard assembly precisions". Ensuring good alignment of modules with the soldering pads on the bus tapes in the Outer Endcaps may require a tighter and more complex specification; this issue is still under study.

3.1.2 Half-ring reference system reconstruction

To be able to position the modules with the required precision, it is necessary to precisely reconstruct the reference system of the half-ring once it has been placed on the working plane. The reference system is identified by three parameters: the X and Y coordinates of the half-ring centre, and the rotation angle of the half-ring axis (for example with respect to the Y axis). The procedure to reconstruct the reference system relies on the bare half-ring elements placed with the best accuracy, in particular the two mounting lugs placed at the extreme ends of the half-ring (see Figure 3), which have to be mounted with a diametric accuracy of 50µm according to the bare local supports specifications. The main mounting hole of the lugs (see Figure 13) is not visible during the loading procedure, being covered by fixation clamps on the handling frame, and also this larger hole is too big to fit in the field of view of some of the loading sites' optical placement systems. Therefore, the position of the modules is determined by the fiducial markers ("small holes") on the lugs. The fabrication specification on the position of the fiducial markers is 20µm with respect to the mounting holes, so we can assume that the absolute position of the fiducials is known with a precision of at least 70µm.

[8] It should be noted that the Outer Endcaps layout provides generally a much-more generous overlap. The smallest (nominal) overlap anywhere in the Outer Endcaps is nine pixels, between outer-radius corners of phi-adjacent modules in Layer 2; this overlap quickly gets larger with decreasing radius due to the geometry of arranging rectangular modules around a circle.

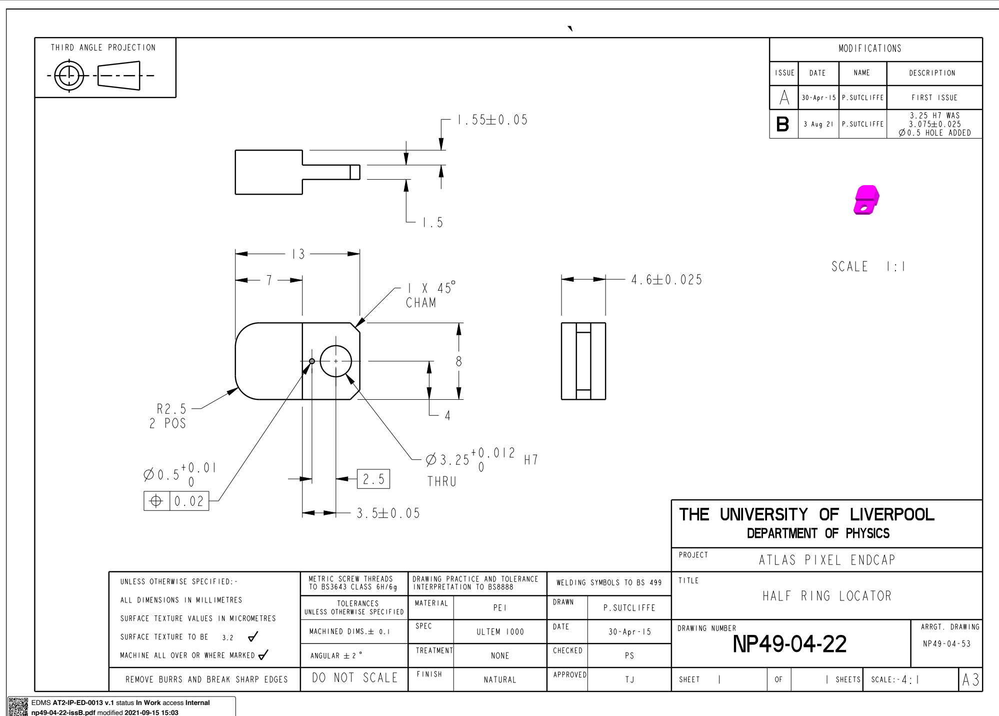

Figure 13: Engineering drawing of a half-ring mounting lug. There are several of these lugs per half-ring; the large holes fix the half-ring into its supporting cylinder; the small holes are used as fiducials for the module loading process.

The procedure to reconstruct the reference system consists of three steps, illustrated in Figure 14:

1. First, the positions of the fiducial holes of the lugs at the extreme ends of the half-ring are determined by means of a microscopic camera (see Figure 15) and the midpoint of the connecting line segment is computed.
2. Then the perpendicular to the line segment connecting the fiducial points is computed. This is the half-ring axis and provides the orientation of the half-ring with respect to the X-Y coordinates.
3. The centre of the half-ring is determined as the point along the axis having a distance from the fiducial points equal to the lugs' nominal radius.
4. To further improve the precision on the coordinates of the centre, a χ^2 fit to a circle is done on the measured coordinates of all the lugs, including the central ones which are placed with a diametric precision of 200μm. The fit-free parameters are the coordinates of the centre and the initial values are those determined in the previous steps.

The propagation of the error on the lugs fiducial points has been calculated, including a ± 25μm uncertainty on the measurement with the microscopic camera added in quadrature, and gives a total error of ±40μm on the coordinates of the half-ring centre and ± 0.01° on the angle.

Once the reference system of the half-ring has been determined, the (X, Y) of any point in the working plane can be transformed in the half-ring reference system coordinated $(r, \theta)_{HR}$ and compared with CAD. A first check can be performed comparing the measured positions of the remaining lugs with the CAD model predictions.

Another important check that must be performed is the verification of the conformity with the specifications of the positions of the pads of the power bus tape.

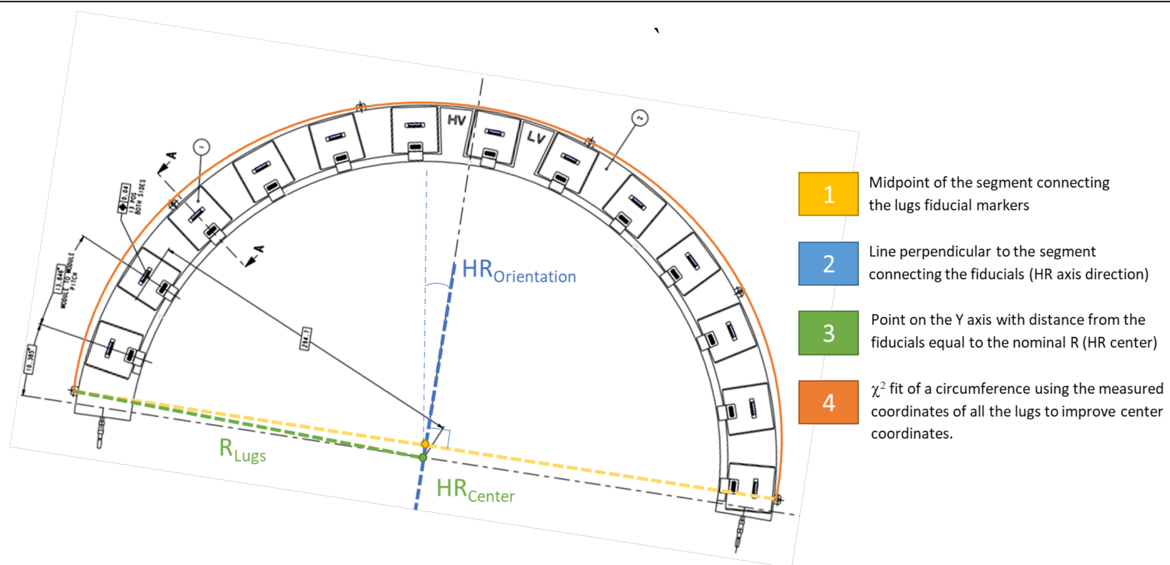

Figure 14: Reconstructing the half-ring reference system using lug fiducials.

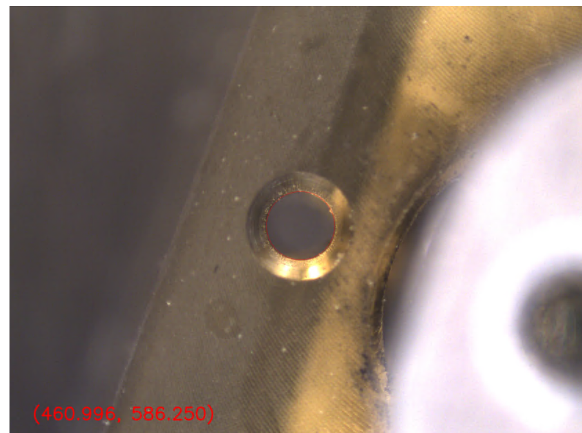

Figure 15: Example of a measurement of the position of a lug fiducial marker.

3.1.3 Grounding and Shielding

3.1.3.1 Concept

The grounding and shielding concept for the ATLAS-ITk Pixel Outer Endcaps has been addressed in previous reviews and has been documented for the Outer System Bare Local Supports FDR [1] and for the on-detector services FDR [8]. In this document, only the interface between the bus tape and the local support is discussed as it has not yet been fully covered elsewhere.

Figure 16 shows a simplified sketch of the Endcaps grounding and shielding approach.

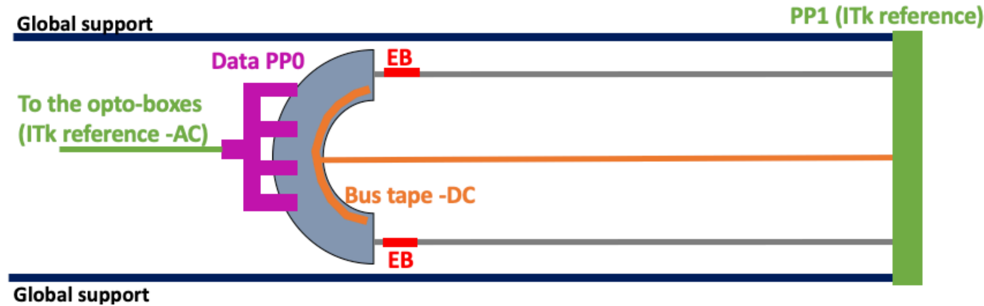

Figure 16: The ITk-Pixel Endcaps grounding approach. The local support half-ring (in grey) is connected to the ITk reference (ground) through the bus tape.

In accordance with the ITk grounding and shielding requirements [9] we need to demonstrate that the interface between the bus tape and the local support is a low impedance tie, so that the local support will be connected to the ITk reference through the power bundle.

To achieve this low-impedance tie, three "grounding pads" have been added to the back side of each bus tape prototype version 6. Silver-loaded epoxy is used between these grounding pads and the half-ring surface during bus tape loading; graphite-loaded epoxy is used on the rest of the bus tape area to achieve an adequate thermo-mechanical connection (see Section 3.2.4). Note that only one reliable grounding connection is needed, however we have six per half-ring in the current design (three per side). Clearly this is redundant, and it could be reduced by simply not using the silver loading epoxy in every pad. In Figure 17, a prototype of the bus tape is shown where the three pads are visible (right). Once one connection is done, the reference potential is driven through the local support via the Titanium pipe.

Figure 17: Left: front side of the v6 bus tape. Right: back side of the v6 bus tape where the three pads for the grounding connection are visible.

To understand if the presence of this silver might produce undesirable effects in the detector, we estimated the mass of silver epoxy to be at most of 0.045g per half-ring. We consulted the tracking simulation team and at the moment they account for 0.4 g of silver per module. Therefore, the impact of adding 0.045 g per half-ring can be considered minor.

3.1.3.2 Preliminary Qualification – Impedance measurement

A Layer-2 unpopulated (no surface-mount components added) bus tape was loaded on one side ("side A") of a prototype half-ring and the impedance was measured up to 1 MHz in several places: between the titanium pipe and a grounding pad in the LV-EoS wing, between the carbon facesheet and the same pad in the LV-EoS wing, and between the carbon face sheet at one end of the half-ring and the carbon face sheet next to the LV-EoS wing.

A second bus tape (populated) was loaded on the other side ("side B") of the same half-ring and the same measurements were carried out. Figure 18 shows photos of these measurements being performed.

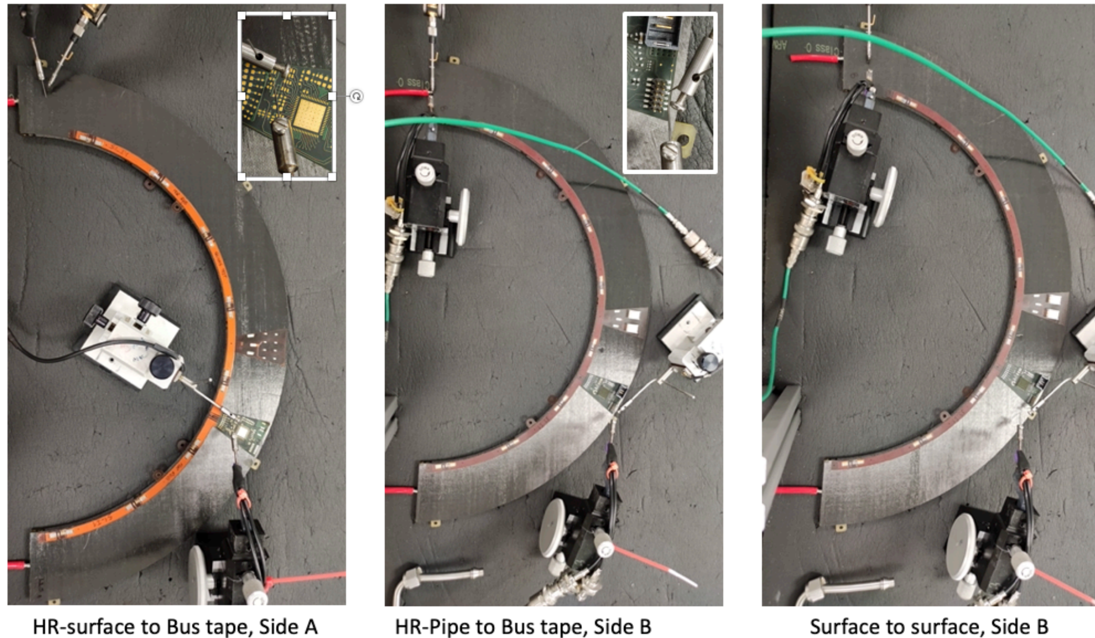

Figure 18: Photos of the measurements carried out after loading bus tapes on one half-ring prototype. Note that side A bus tape is un-populated while the one loaded to side B was populated to be as close as possible to the final one.

The impedance results up to 1 MHz are shown in In Figure 19, for side A (left) and side B (right).

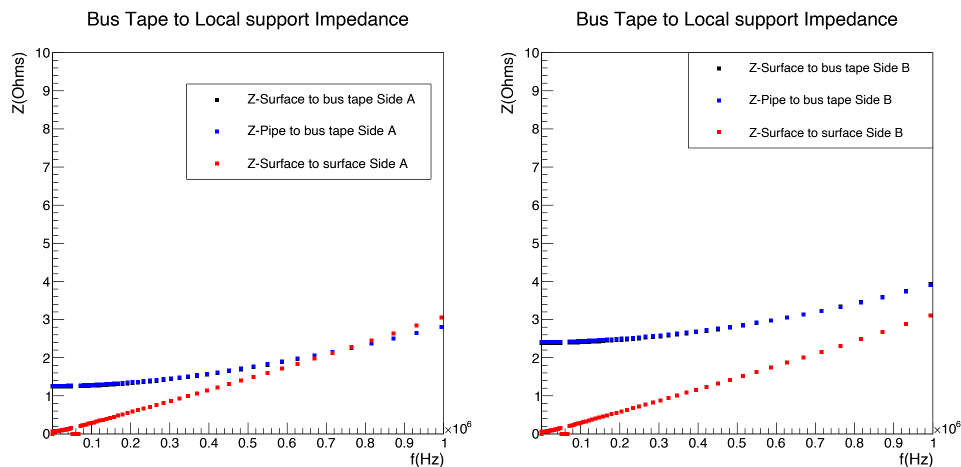

Figure 19: Impedance results for side A (left) and B (right). From the half-ring surface to the bus tape (black), from the pipe to the bus tape (blue) and from surface to the surface close to the wing (red).

The results show that the impedance measurement up to 1 MHz are well below the specification (10 Ω). Looking at these results, the use of silver loaded epoxy appears to be a reliable solution

however, samples are under preparation to qualify its electrical properties after the expected irradiation doses. Results are expected well before the loaded local supports PRR.

In addition, the overlap of the impedance curves between the pipe or carbon surface and the bus tape pad indicates that the impedance between the pipe and the surface is negligible, as expected since by design the local support is conductive.

3.1.4 The Half-ring Handling Frame

Each half-ring after construction is fixed into its own handling frame [10] for handling until integration in the half-shell (see Sec. 3.2 of Reference [1]). In this document, more emphasis is placed on the role of the handling frame during loading, tests and transport.

There are three flavours of handling frames, one for each flavour half-ring. Figure 20 shows a CAD design of a loaded Layer-2 half-ring fixed in its own handling frame. The handling frame is made of several parts, which are fabricated with high precision using a CNC machine, starting from a 1 cm thick aluminium plate for high precision tooling.

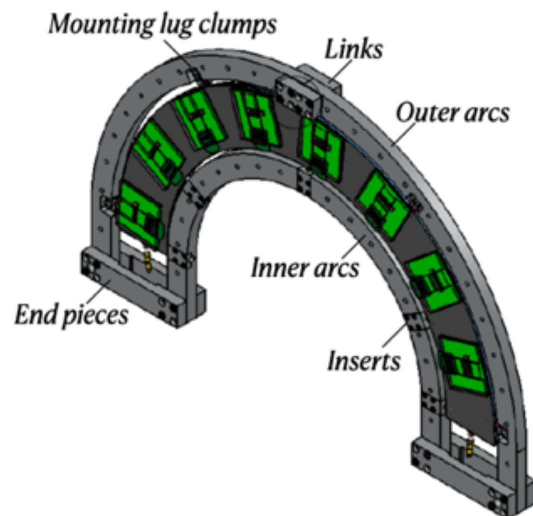

Figure 20: CAD rendering of a loaded Layer-2 half-ring fixed in its handling frame.

As can be seen in Figure 20, the handling frame is formed of *outer arcs* and *inner arcs* which are fastened together with *links* on both sides of the frame. The outer and inner arcs are fastened together with *end pieces* on both sides of the frame. All the parts are common for all handling frame flavours except the arcs.

The half-ring is rigidly fixed in the handling frame at the inner rim by screwing radial captive screws through the inner arcs into the threaded *inserts* embedded in the inner rim of the half-ring. In the outer radius other housings in the outer arcs are provided with pillars, to match the half-ring fixation lug holes. The half-ring outer rim is rigidly fixed to the handling frame by screwing *mounting lug clamps,* also provided by pillars, in the outer radius housings.

Table 2 gives the required number of parts required for each flavour of handling frame, for pre-production and production.

	HR/HS	HR pre	HR Tot	IN ARC	OUT ARC	END	LINK	INSERT	LUGS	Captive	M3x6	M2x6	M3x12
L4	9	3	39	78	117	156	234	273	234	273	234	1092	1365
L3	8	3	35	70	105	140	210	210	175	210	175	840	1400
L2	11	6	50	50	100	200	100	250	200	250	200	1000	1200
TOT			**124**	**198**	**222**	**496**	**544**	**733**	**609**	**733**	**609**	**2932**	**3965**

Table 2: Number of handling frame parts required for pre-production and production.

When the ring is rigidly fixed in the handling frame it should not be bent or twisted by the frame. This is achieved with tight geometrical tolerances for several parts: links and end pieces' hole diameters, inserts' hole diameters, the arcs' angular coverage, and the mounting surfaces for the ring lugs. The rigidity of the half-ring is necessary to avoid distortion during loading, where a load of about 250g is exerted on each module during glue curing, and to avoid large-amplitude mechanical oscillations during transportation.

During thermal cycling the mismatch between handling frame and half-ring thermal expansion coefficients would cause a half-ring deformation; this is avoided by relaxing the captive screws and the mounting-lug clamps during the cycles.

In order to optimise the final production, the Layer-2 and Layer-3 handling frames will be made in Glasgow, while the Layer-4 handling frames will be made in Lecce.

So far, as required by the project, four Layer-2 pre-production handling frames have been produced (three in Glasgow and one in Lecce), three Layer-3 pre-production handling frames have been produced in Glasgow, and four Layer-4 pre-production handling frames have been produced in Lecce.

Figure 21 shows a height map of both sides of a Layer-4 half-ring fixed in one of the handling frames produced in Lecce, which is in turn fixed on the gantry working plane, ready for module loading. The half-ring height maps are similar before and after fixation to the handling frame and gantry and a local planarity with respect to the gantry working plane better than 20μm has been measured.

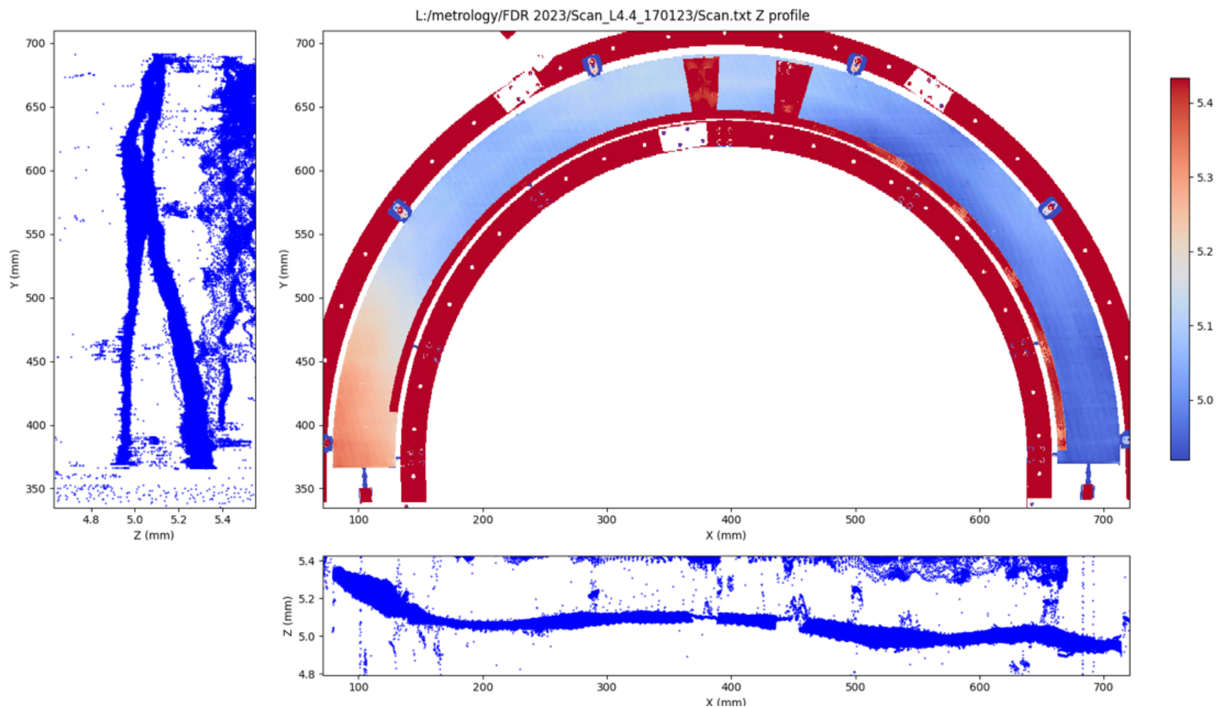

Figure 21: Centre: Height map of a Layer-4 half-ring fixed on the gantry working plate by a Layer-4 handling frame measured with a chromatic confocal optical pen. Height scatter plot along the X axis (left plot) and the Y axis (bottom plot).

The half-ring planarity with respect to the module bottom surface is given by the uniformity of the aluminium tooling plate thickness, the arc mounting points' mechanical precision, the gluing precision of the half-ring fixation lugs, the gantry working plane planarity, and the module flatness. For comparison with Figure 21, Figure 22 shows a height map of the freestanding half-ring.

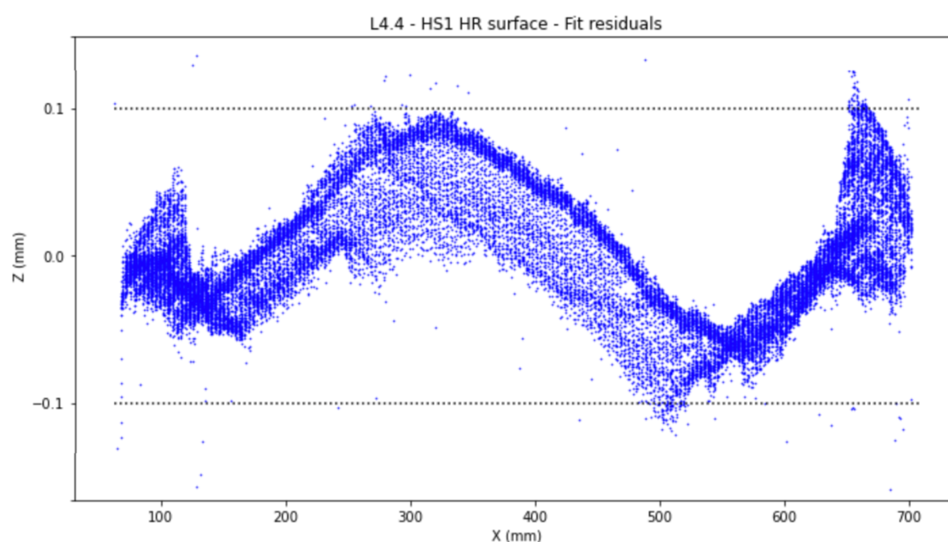

Figure 22: Height map of the (freestanding) Layer-4 half-ring of Figure 21 measured with a chromatic confocal optical pen.

The frames manufactured in Glasgow were made from high precision Al tooling plate to ensure that the parts would be able to meet the tight mechanical tolerances. Manual measurements of the parts and assembled frames showed that it was possible to match parts to within ±25µm before assembly. This was achieved by using the material as delivered. The critical variable for the successful loading of modules onto a half-ring are the planarity of the half-ring within the frame and the rigidity of attachment. On the Glasgow assembled frames the support for the half-ring mounting lug was measured to a tolerance of ±20µm, after assembly the heights of the rings were measured using a manual height gauge which gave a flatness of the frame in the region of ±50µm. A record of the measurements for a Layer-2 and a Layer-3 handling frame are shown below in Figure 23 and Figure 24 respectively.

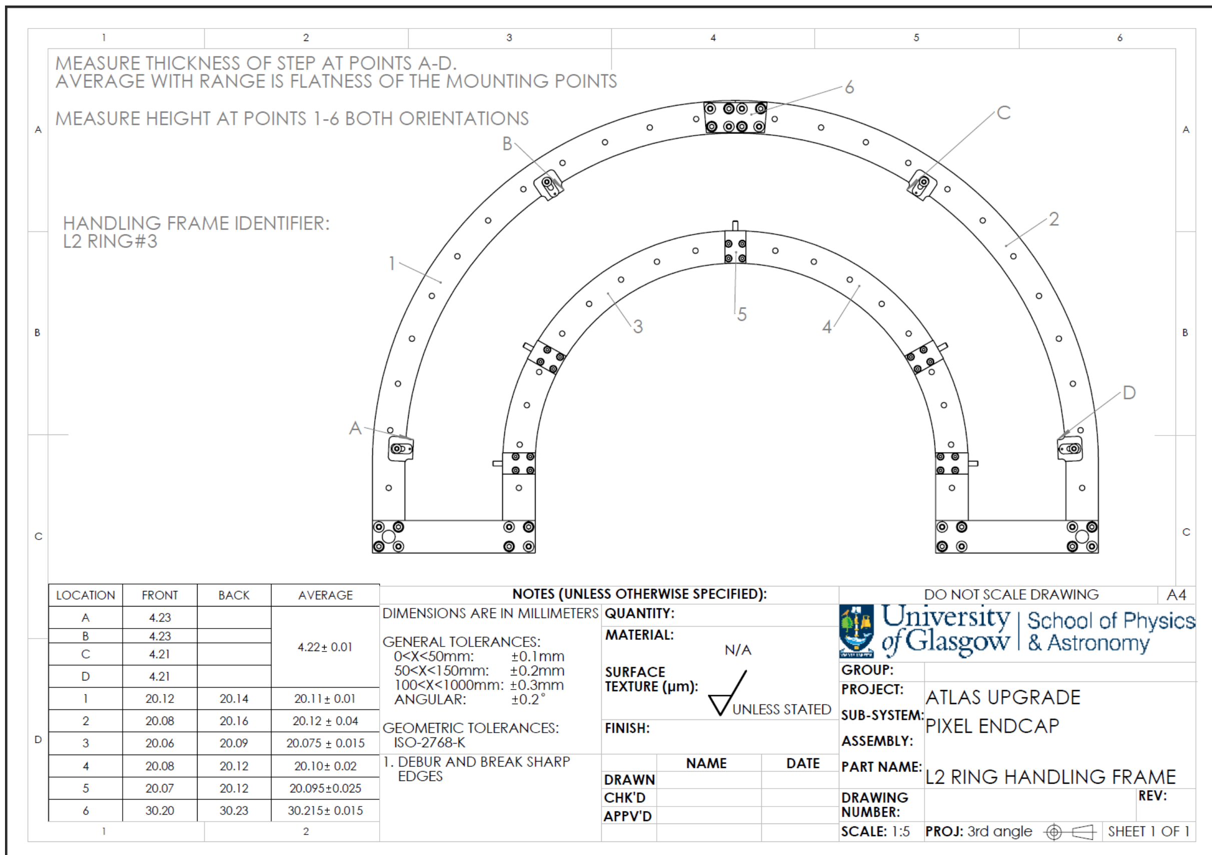

LOCATION	FRONT	BACK	AVERAGE
A	4.23		4.22± 0.01
B	4.23		
C	4.21		
D	4.21		
1	20.12	20.14	20.11± 0.01
2	20.08	20.16	20.12 ± 0.04
3	20.06	20.09	20.075 ± 0.015
4	20.08	20.12	20.10± 0.02
5	20.07	20.12	20.095±0.025
6	30.20	30.23	30.215± 0.015

Figure 23: Measurements made on a Layer-2 handling frame.

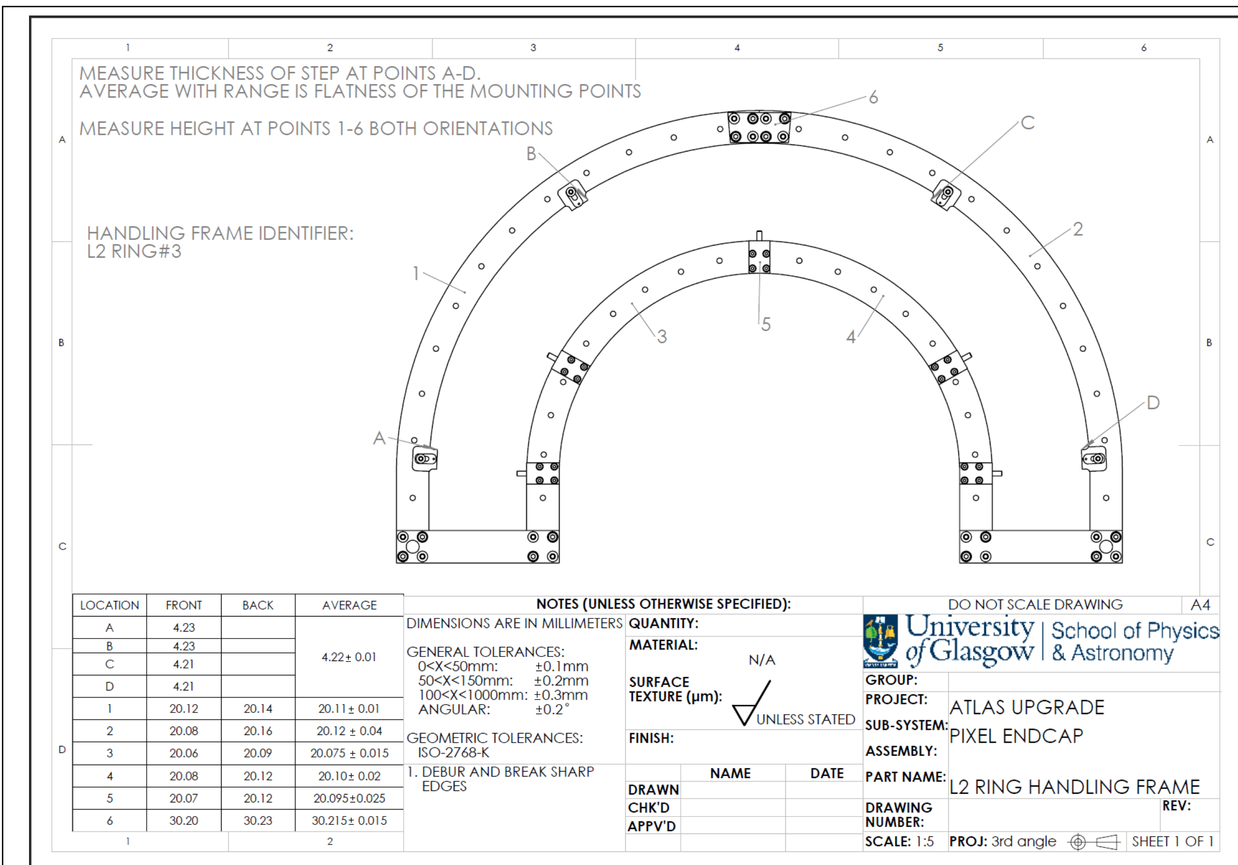

LOCATION	FRONT	BACK	AVERAGE
A	4.23		4.22± 0.01
B	4.23		
C	4.21		
D	4.21		
1	20.12	20.14	20.11± 0.01
2	20.08	20.16	20.12 ± 0.04
3	20.06	20.09	20.075 ± 0.015
4	20.08	20.12	20.10± 0.02
5	20.07	20.12	20.095±0.025
6	30.20	30.23	30.215± 0.015

Figure 24: Measurements made on a Layer-3 handling frame.

The fixation of a handling frame on the gantry working plate can be done in different ways: by screws, using the unthreaded holes in the end pieces or the threaded holes in the arcs, or by movable clamps. Whatever method is used, this operation should not distort the handling frame and calibrated metal shims can be used below the end pieces and the links if needed. Calibrated shims could also be used to improve the global half-ring planarity on the gantry.

3.2 Bus tape loading

3.2.1 Loading Specifications

- The glue layer between the bus tape and the local support must be thermally conductive to transfer heat from the bus tape to the half-ring's internal cooling pipe.
- The glue thickness must be constant across the tape area; we have assumed the same specification as for the module loading, namely 100^{+100}_{-50} µm. The thermal FEA studies presented at the Outer System Bare Local Supports FDR [1] used this glue thickness.
- The glue coverage must be sufficient to ensure that the tape won't peel or shear from the half-ring surface during handling and thermal cycling.
- The tape-loading position needs to be accurate enough to ensure that the power pigtails can be soldered to modules that have been placed within the module-loading placement specification reported above. A preliminary estimate is that the pattern of soldering pads on the bus tape must be within 100µm in r-ϕ of the mating pads on the power pigtail which plugs into the module. The radial alignment tolerance resulting from this requirement will be quite loose as the power pigtail design includes an "S bend" to accommodate the height difference between the bus tape solder pads and the top of the

module, but still needs to be quantified. There will also need to be a specification on the angular orientation of the solder pad pattern; this also still needs to be quantified.

- The bus tape is to be aligned to the inner rim of the half-ring to ±50µm. This is important to avoid:
    - clashes with the modules at the higher-radius perimeter, and
    - excessive overhang off the half-ring at the inner perimeter, which has the same nominal inner radius as the bus tape.

Preliminary bus-tape loading trials are described below, in Sections 3.2.33.2.4.

3.2.2 *Qualification - Thermo-mechanical FEA*

An FEA analysis was performed recently to assess the stresses in the glue layer between the bus tape and the half-ring.

3.2.2.1 Scope of this study

As demonstrated by previous thermo-mechanical FEA studies, performed to assess the mechanical stability of the Outer Endcap Half-rings, the Layer-4 half-ring is the worst flavour in deformation, when cooled to the working temperature: this is mainly due to the action of the CTE mismatch between the structural CFRP and the bus tape, which has copper layers in its stack-up. The ITk Pixel Local Support Design Specifications [6] define the minimum temperature that the structures could experience during a relevant failure of the cooling system to be -55°C so, under this extreme condition, the local support design must guarantee no damages. This is why the thermo-mechanical structural response of the Layer-4 half-ring, cooled down from +20°C to -55°C (ΔT = -75°) was evaluated by a specific FEA study, which was presented at the Bare Local Supports FDR [1]. Recently, the copper layers at the top and bottom of the bus tape design have been thinned from 70µm to 50µm (see Figure 25). This should lead to lower stresses in the glue layer of the bus tape than in the previous analysis, so the thermo-mechanical FEA of the Layer-4 half-ring has been repeated to evaluate the mechanical strength of the glue layer interface, which must be qualified for this review.

Changes in the FlexTape V6 (1)

- From Power Budget slide, it is possible to reduce Top and Bottom layers from 70um to 50um:

Board Stack Report

Stack Up		Layer Stack				
Layer	Board Layer Stack	Name	Material	Thickness	Constant	
1		Top Paste				
2		Top Overlay				
3		Top Solder	IMAGECURE	0,030mm	3,9	
4		Top Layer	Copper	0,070mm		50 um
5		Dielectric 1	UPISEL-N	0,050mm	3,2	
6		Dielectric 2	EPOXY GLUE	0,020mm	4,8	
7		Layer 1	Copper	0,018mm		
8		Dielectric 3	UPISEL-N	0,025mm	3,2	
9		Layer 2	Copper	0,018mm		
10		Dielectric 4	EPOXY GLUE	0,020mm	4,8	
11		Dielectric 5	UPISEL-N	0,050mm	3,2	
12		Bottom Layer	Copper	0,070mm		50 um
		Coverlay Adhesive	**EPOXY GLUE**	0,065mm	4,8	
13		**Coverlay**	**UPISEL-N**	0,030mm	3,2	
14		Bottom Overlay				
	Height =	0,466				

Figure 25: Bus tape Version-6 *updated stack-up.*

3.2.2.2 FEA model

The FEA model of the Layer-4 Half-ring, developed with Ansys software, is the same as that already used for the thermo-mechanical studies performed for the Bare LS FDR, in 2021(see the left-most part of Figure 26). The FEA model was validated by comparison with measurements of the thermo-mechanical deformation under cooling down. The stack-up of the

bus tape V.6 has been updated with the reduced thicknesses of the top/bottom copper layers (see the right-most part of Figure 26).

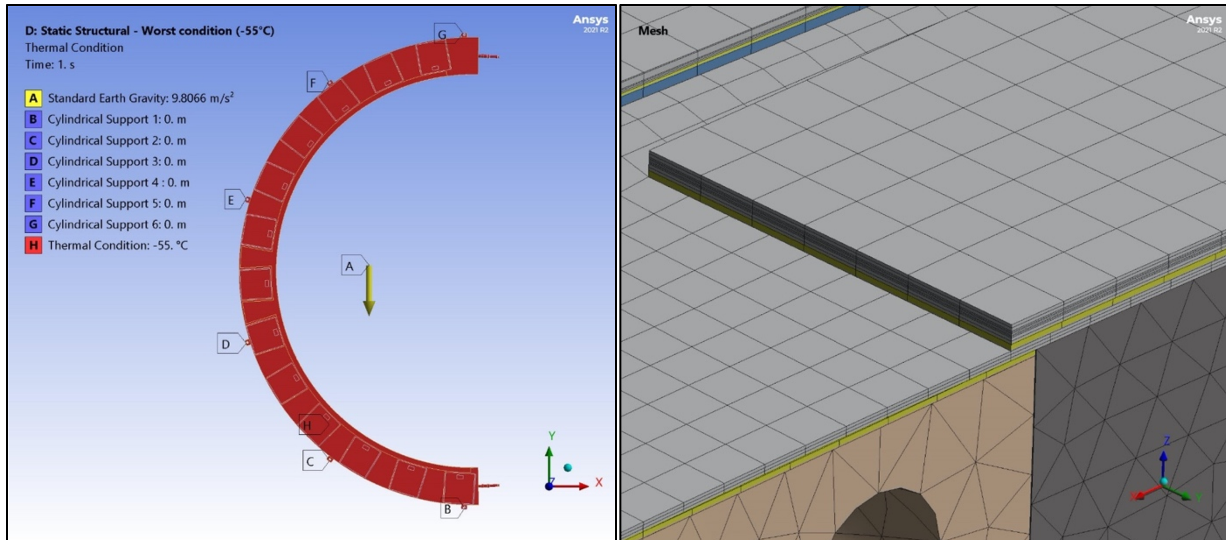

Figure 26: Left: Layer-4 half-ring thermo-mechanical FEA model. Right: Stack-up of the V6 bus tape implemented in FEA Model

All the inputs used for the thermo-mechanical FEA can be found in Reference [11] together with several presentations describing the work at various stages.

The mesh of the model is made up of 2.8 million quadratic solid elements, for a total number of about 9 million nodes. The FEA model is ideally constrained on the holes of the lugs, to simulate the final support conditions in the detector.

3.2.2.3 Engineering properties of the adhesive EA 9396

The glue layer underneath the bus tape, in the FEA model, is pure Epoxy Hysol EA 9396 adhesive[9], with a nominal thickness of 100 µm and 100% of coverage of the bus tape area.

The bulk resin properties of Hysol EA 9396 are drawn from the Henkel ® datasheet:

- Young's Modulus: E = 2.75 GPa @ +25°C
- Coefficient of Thermal Expansion: α = 70.7 µm/m°C @ +40°C
- Tensile Strength (UTS): = 35.2 MPa @ +25°C
- Density: ρ = 1.14 g/cm³

The values of the engineering properties are not known for a temperature range down to -55 °C, so the FEA has been performed with the values related to the temperatures +25°C/+40°C.

The Henkel datasheet also provides Lap Shear Strength values, according to ASTM D1002 and depending on the curing, also for a temperature of -55°C, as shown in Table 3.

[9] *Hysol EA9396 is a two-part, "low viscosity, room temperature curing adhesive system with excellent strength properties at temperatures from […] (-55°C to 177°C)." For more details see the product datasheet, which can be obtained, for example, at the following link:* https://twiki.cern.ch/twiki/pub/Main/AtlasEdinburghGroupMaterialStudies/Henkel_Hysol_EA_9396_epoxy.pdf.

Bond Strength Performance
Tensile Lap Shear Strength
Tensile lap shear strength tested per ASTM D1002 after curing as shown below.
Adherends are 2024-T3 bare aluminum treated with phosphoric acid anodized per ASTM D3933.

Test Temperature °F/°C	Typical Results Cure 5 days @ 77°F/25°C		Cure 1 hour @ 150°F/66°C		Cure 30 min @ 180°F/82°C	
	psi	MPa	psi	MPa	psi	MPa
-67/-55	3,300	22.8	3,300	22.8	3,500	24.1
77/25	3,500	24.1	4,000	27.6	4,000	27.6
180/82	3,200	22.0	3,300	22.8	3,300	22.8
300/149	1,800	12.4	1,800	12.4	1,900	13.1
350/177	1,250	8.6	1,200	8.3	1,200	8.3

Table 3: Lap Shear Strength of Hysol EA 9396 from Henkel ® datasheet

In addition, some measurements [12] of the Lap Shear Strength were performed by CERN on Epoxy EA 9396 adhesive, in the past, on unirradiated/irradiated samples, up to 15 MGy, as shown in Table 4.

Type	Single lap joint
Material	Loctite - Henkel EA 9396 AERO
Surface preparation	Acetone Cleaning
Material	AW6082
Mode of failure	Interfacial
Further comment	None
Irradiation	Cobalt 60 10 kGy/h

Dose (MGy)	Maximum shear strength (MPa)	Strain at break (mm)
0	3.964019515	0.629906803
0.2	6.191162077	0.44286262
0.5	5.205339301	0.341593335
1		
2.5	4.28127356	0.284709588
7	5.949880354	0.404698208
15	6.666174517	1.55217425

Table 4: Lap Shear tests performed at CERN on EA 9394 unirradiated/irradiated

The comparison between the Shear Strength of unirradiated EA 9396, given by Table 3 and Table 4, shows that the minimum value measured at CERN is significantly lower than the value given by the Henkel datasheet (4 MPa vs. 22 MPa), but the surface preparation of the samples is different. It's interesting to observe that CERN table reports the Shear Strength as 4 MPa for zero dose, while the related diagram indicates 6 ±1 MPa.

To be conservative, the Maximum Shear Strength of EA 9396 can be assumed equal to 4 MPa. However, the tests at CERN were carried out on a substrate of aluminium alloy, with acetone surface cleaning, so the results are strictly related to these conditions. In conclusion, it would be better to perform some lap-shear tests using samples of the half-ring's CFRP, with a defined surface preparation, to better define the limit in Shear Strength.

3.2.2.4 FEA results

FEA can calculate well the trend of the Shear stress, but the peak values calculated on the edges are fake. This because the peaks of Shear Stresses, in a real adhesive, occurring very close to, but not at the end of the overlap.

A simple FEA exercise can demonstrate that, increasing the mesh density, the peak values grow very fast on the last nodes. This statement explains why the maximum value of Shear stress, predicted by FEA, will be not compared to the minimum adhesive Shear strength: the average value of the Shear Stress is more significant.

Shear Stress

The analysis focus is on the Shear Stress lying in the plane parallel to CFRP/bus tape surface, taking as reference a local cartesian coordinate system, which has Y and Z directions in plane, X normal direction, and the origin coincident with the half-ring centre. Starting from the Shear Stress components τ_{XZ} and τ_{XY}, Ansys calculates the magnitude of in-plane shear stress, using the equation: $\boldsymbol{\tau_{in-plane}} = \sqrt{(\tau_{XZ}^2 + \tau_{XY}^2)}$. The result is shown in Figure 27.

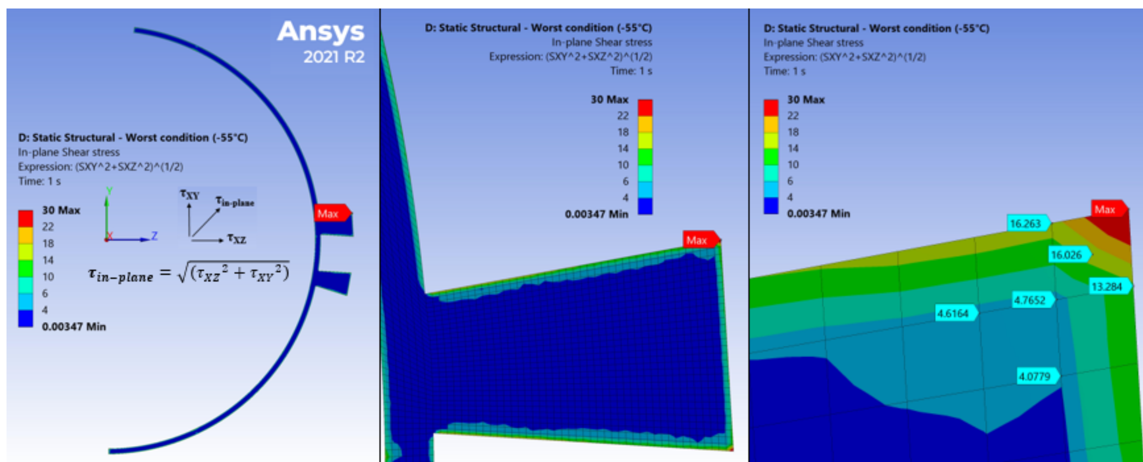

Figure 27 : In-plane Shear Stress in the glue layer

The peak of the in-plane Shear Stress, on the wing's corner of the glue layer, is not a real value, as explained at the beginning of this paragraph. Consequently, a high stress gradient within the last row of elements connects the peak to the light blue area, which has a Shear stress around 4 MPa. This effect, with lower stress gradients, occurs along all the edges of the glue layer.

The average value of the in-plane shear stress calculated by Ansy is τ in-plane,av = 3.08 MPa. The ratio between the Maximum Shear Strength measured at CERN (4 MPa), for unirradiated sample, and the average in-plane Shear stress gives a factor 1.3, lower than expected (good value: 3). However, the glue layer it's absolutely safe if the average Shear stress is compared to the reference value of Shear Strength given by the Henkel datasheet (22 MPa @ -55°C). This large variability of the Shear strength means that it is strictly related to the specific substrate material, the preparation of the bonded surfaces, and the curing procedure too.

Normal stress

Normal stress (σ_X, in the local coordinate system of Figure 28), in a glue layer, could be a concern close to the border regions, so we have to check it. As resulting by the FEA, the peak of Normal stress, $\sigma_{X,max}$ = 20.7 MPa, is located on the inner corner of the layer, as shown in Figure 28. It should be compared with the UTS (=35 MPa) of EA 9396, given by Henkel datasheet. However, it can be observed that this value is located on the last node, and the stress gradient reduces it very quckly to lower values on the subsequent nodes, so it doesn't affect a specific area. It has been verified that this effect persists increasing the mesh density, and the maximum value is depending on the mesh size.

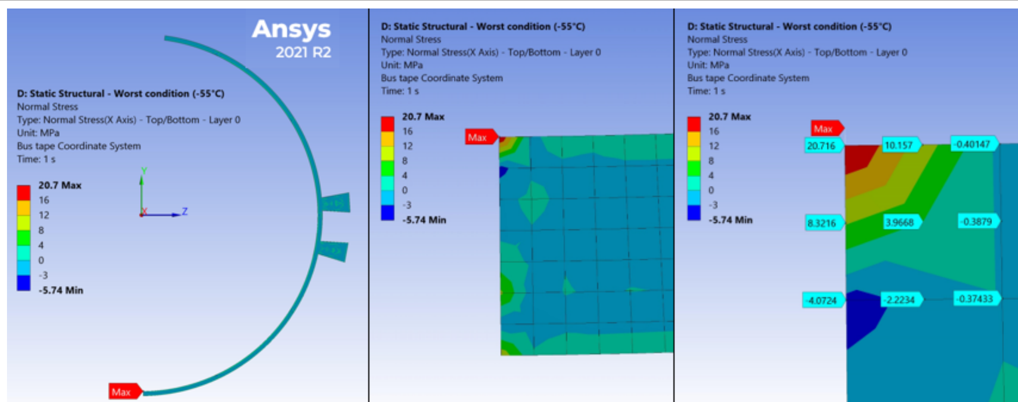

Figure 28: Normal stress in the glue layer

In conclusion, the Normal stress is below 4 MPa for almost the entire glue layer, also along the edges, with a few strongly localized exceptions. The average absolute value of the Normal stress is quite low, for both simulations with different mesh density (< 0.55 MPa).

Strain energy

Another interesting FEA result, to evaluate the strength of the glue layer, is the Strain energy (see Figure 29), that is the energy stored in the glue layer due to deformation during the cooling down. The Total Strain Energy of the glue layer, calculated by FEA at -55°C: E =7.1437e-2 J, divided by the bonding area A = 7.5586e-3 m^2, gives the average Strain energy value per unit area, E_{av} = 9.45 J/m^2.

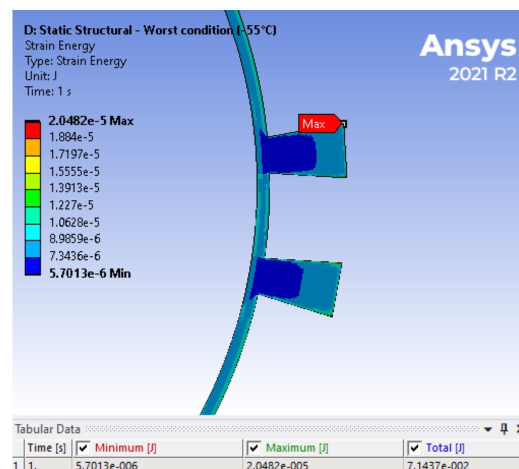

Figure 29: Strain energy stored in the glue layer @ -55°C

A measurement campaign was carried out at the Manchester University, to evaluate the adhesive's fracture energy of double cantilever beams samples, glued together with pure or doped Hysol EA 9396, before and after irradiation. The results of these measurements are very interesting, because the specimens were made of CFRPs, similar to those of the half-ring's faceplates.

The measurements of unirradiated EA 9396 samples provided two different values of Mode I adhesive Fracture Energy (G_{IC}), depending on the analysis method:

- G_{IC} = 250 ± 30 J/m^2 (method 1);
- G_{IC} = 320 ± 150 J/m^2 (method 2).

Considering the worst result of Fracture Energy given by the tests as G_{IC} = 170 J/m^2, it is much higher than the value of the Strain Energy stored calculated by the FEA at -55°C, E_{av} = 9.45 J/m^2, so the failure seems to be far away.

3.2.2.5 Conclusions

Premised that:

- the FEA works on ideal geometries, without local defects or lack of glue,
- the glue properties are partially unknown (e.g. Young Modulus, CTE, UTS at -55°C),
- substrate material, surface preparation and curing procedure can largely affect the strength of the glue layer,

the results of the thermo-mechanical FEA of the Layer-4 Half-ring at -55°C, focused on the analysis of the bus tape glue layer made of unirradiated Epoxy EA 939,6 with nominal thickness 100 µm, are:

- ➢ The average value of the in-plane Shear stress, resulting by the FEA ($\tau_{in\text{-}plane,av}$ = 3.08 MPa), is lower than the worst value of Maximum Shear Strength measured at CERN (4 MPa), by a factor 1.3. However, it must be considered that the samples used at CERN were different in material and surface preparation compared to the half-ring set-up. The peaks of Shear stress resulting by the FEA, on the edges of the glue layer, are not reliable so, a realistic safety factor cannot be calculated. In any case, this study is related to an extreme failure condition, the analysis repeated in nominal operating condition (temperature of the cooling fluid CO_2: -35°C) gives an average value of the in-plane Shear stress of 2.26 MPa.
- ➢ The Normal stress in the glue layer, resulting by the FEA, is lower than 4 MPa everywhere, except few locally exceptions on the edges, and the average absolute value is 0.55 MPa, while the UTS (@+25°C, by Henkel datasheet) is 35 MPa. The maximum value calculated by the FEA (20.7 MPa), on the outer vertex of the layer, can be considered a singularity, as demonstrated by a comparative analysis with a different refined mesh.
- ➢ The minimum Fracture Energy of unirradiated EA 9396 sample, measured by experimental tests (G_{IC} = 170 J/m^2), is much higher than the Strain energy per area calculated by the FEA (E_{av} = 9.45 J/m^2), during the cooling down from + 20°C to -55°C. This should mean that the failure condition of the glue layer is far away.

In conclusion, the FEA results can't exclude a local delamination starting from cracks generated by local defects or lack of glue, but a full delamination it's not a concern because the minimum Fracture Energy of the glue layer is much higher than the Strain energy due to the cooling down.

In any case, a good manufacturing procedure should consider having the full coverage of the bus tape surface, and a continuous fillet of glue around the bus tape edges.

3.2.3 Preliminary Bus-Tape Gluing trials

A trial gluing program was established to learn about glue coverage, thickness, and viscosity. As bus tape availability was limited, these trials were first performed on "fake bus tapes" (precision polymer shims prepared to known dimensions). These fake bus tapes were measured, then glued onto pre-measured Perspex slides (see Figure 30). Thickness analysis was performed using a Vernier calliper with a resolution of 10µm. Glue coverage and viscosity was initially visually assessed; ImageJ [13] software was later used to quantify glue coverage more accurately (see Table 5 at the end of this section).

Figure 30: Fake bus tape and shims prepared for gluing onto Perspex

The glue mass was calculated to determine the amount required to achieve 100% coverage at a thickness of 100µm: four lines of known length were drawn on cloth substrates, and glue was deposited on these lines using a pneumatic glue dispenser and different needle gauges (see Figure 31). The needle diameter was the visual reference for the glue bead width. Each substrate was weighed before and after depositing glue, to determine which needle gauge could create a glue bead that best matched the glue mass required.

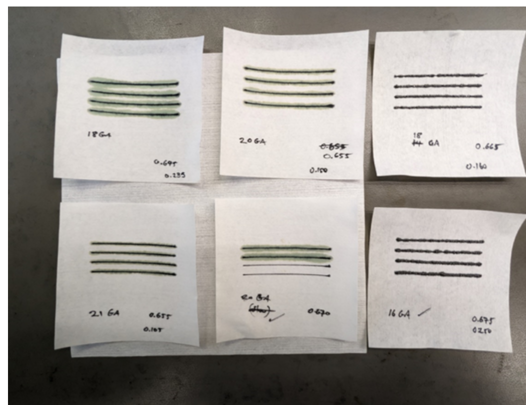

Figure 31: Glue-mass experiment to determine required needle gauge

To control glue thickness, two methods were trialled:

- Polymer precision shims equal to average bus tape thickness plus required glue thickness, and
- glass microspheres with 100 ± 10 µm diameter.

Mass was then applied during glue curing (see Figure 32).

Figure 32: Mass applied during glue curing

In the final stage of the trial, two bus tape coupons were glued onto Perspex slides (Samples 11 and 12 in Table 5). The thickness of the coupons was not as consistent as the fake bus tape, they measured between 0.4-0.45mm across their length. This resulted in an increased glue thickness range.

`

Sample	Glue composition	Target Thickness	Thickness	Needle Gauge (Brand**, Inner Diameter)	Coverage
1 (FBT)	Hysol	0.11mm	0.04-0.12mm	20 (Metcal, 0.61mm)	Breached borders, viscosity too low
2 (FBT)	Hysol + 30wt% Graphite	0.11mm	0.1-0.12mm	16 (Metcal, 1.19mm)	Excessive, needle diameter too large.
3 (FBT)	Hysol + 30wt% Graphite	0.1mm	0.07mm	18 (Metcal, 0.84mm)	~55%
4 (FBT)	Hysol + 30wt% Graphite	0.1mm	0.05-0.07mm	18 (Metcal, 0.84mm)	~55%
5 (FBT)	Hysol + 30wt% Graphite + 0.25wt% glass microspheres	0.1mm	0.06-0.12mm*	18 (Metcal, 0.84mm)	~65%
6 (FBT)	Hysol + 30wt% Graphite + 0.25wt% glass microspheres	0.1mm	0.06-0.12mm*	18 (Metcal, 0.84mm)	~75%
7 (FBT)	Hysol + 30wt% Graphite	0.1mm	0.1-0.13mm	17 (Weller, 1.14mm)	Excessive, needle diameter too large.
8 (FBT)	Hysol + 30wt% Graphite	0.1mm	0.09-0.12mm	17 (Weller, 1.14mm)	Excessive, needle diameter too large.
9 (FBT)	Hysol + 30wt% Graphite + 1wt% glass microspheres	0.1mm	0.09-0.1mm*	18 (Weller, 0.97mm)	~81%
10 (FBT)	Hysol + 30wt% Graphite + 1wt% glass microspheres	0.1mm	0.09-0.1mm*	18 (Weller, 0.97mm)	~77%
11 (Coup)	Hysol + 30wt% Graphite	0.1-0.14mm	0.03-0.14mm	18 (Weller, 0.97mm)	Glue breached border at minimum bus tape thickness
12 (Coup)	Hysol + 30wt% Graphite + 1wt% glass microspheres	0.1mm	0.05-0.17mm*	18 (Weller, 0.97mm)	~76%

* no shims applied during curing, thickness controlled by glass bead diameter.

** brands set their own needle diameter, there is no standard specifications.

FBT – Fake bus tape made from polymer precision shim

Coup – Rectangle coupon of real bus tape.

Table 5: Results from gluing trial

Conclusions

The combination of glass microspheres and the Weller 18-gauge needle achieves consistent glue thickness and good coverage.

3.2.4 Production Tooling and Method

Precision assembly tooling is required to accurately align the bus tape onto the half-ring. Figure 33 shows a CAD model of the tooling for Layer-2. A base tooling plate was produced from aluminium tooling plate with flatness better than 150μm/m, with threaded location pins for the half-ring and bus tape made to h6 tolerance (ISO 286-1), i.e. the diameter of the location pins is $3.2\text{mm}^{+0}_{-0.008}\text{mm}$ for a precise fit. Additionally, holes in the tooling plate base were specified to a positional tolerance of 50μm .

As can be seen in Figure 33, a populated bus tape has a number of surface-mount components on its wings. To avoid damaging these, a section of the plate in the wing area was machined out and 3D-printed inserts produced. These inserts were resurfaced flat to the top face of the base plate. Using this method eased the manufacturing of the base plate and allows for bus tape design changes without needing to machine an entire new plate.

The final piece of the tooling is a press plate to apply pressure during glue curing.

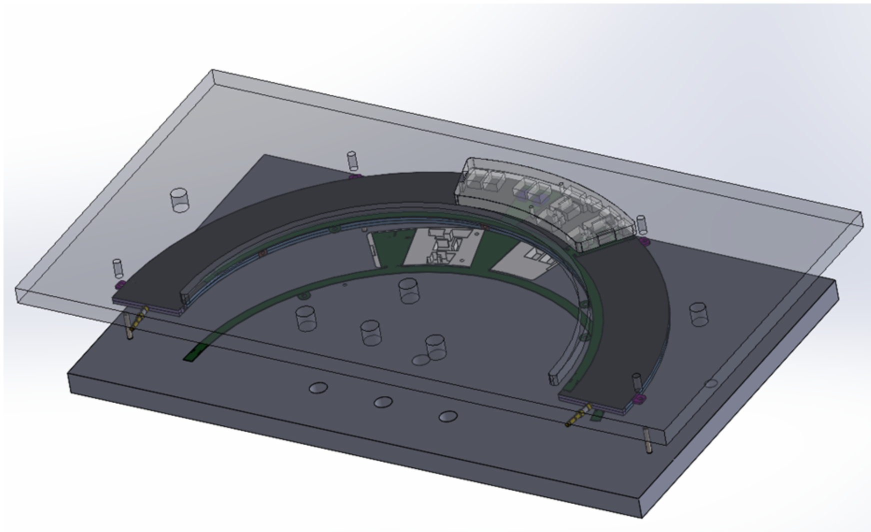

Figure 33: CAD rendering of the tooling for bus tape attachment to a Layer-2 half-ring.

Gluing procedure

Components

- Bus Tape
- Half-ring
- Hysol® EA9396
- Graphite Powder – 200 mesh
- Glass Microspheres 100μm diameter
- Conductive Silver Epoxy

Consumables and equipment

- P.P.E.: Gloves, safety glasses, face mask, laboratory coat
- Specimen polymer containers for Hysol mixing
- Dispenser syringes for Hysol application
- Clean-room wipes (lint free)
- Isopropanol

- PTFE mould release spray
- Automatic glue mixing machine, e.g. SpeedMixer DAC 150
- Pneumatic glue dispenser

The steps in the gluing procedure are as follows:

1. Clean all working surfaces and ensure tooling is clean (clean with isopropanol if required) and coated with PTFE (mould release spray).
2. Measure and map bus tape thickness using micrometre. Weigh bus tape and half-ring.
3. Clean bus tape and half-ring with isopropanol using lint-free clean room wipes.
4. Fit 3D printed inset, half-ring 3.2mm locator pins, polymer shims and bus tape using 3mm alignment pins (Figure 34a). As described in Section 2.2, the half-ring handedness is determined by the bus tape position on the half-ring; this is set by hole locations in the base plate.
5. Prepare the Hysol 100:30 (Part A:5g, Part B:1.5g) and load glass spheres at 1wt% (0.065g). Mix at 2000 rpm for three minutes.
6. Load mixed Hysol with 30wt% graphite powder. Mix at 3000 rpm for three minutes.
7. Fill syringe and dispense onto bus tape, wings first, using Weller 18-gauge needle (Figure 34b).
8. Mix conductive silver epoxy 1:1 ratio by hand, and load ~2mm bead onto grounding pads with swab.
9. Check spacers have not moved and place ring onto bus tape using 3.2mm locating pins (Figure 34c).
10. Secure press plate 3D printed insert with Kapton tape (Figure 34d) and place press plate onto half-ring (Figure 34e). Pull Kapton tape out from assembly. If insert is not secured by Kapton, it can fall onto half-ring and create damage.
11. Leave to cure for 24-48 hours.
12. Release ring by unscrewing 3.2mm locating and 3mm alignment pins, and visually inspect (Figure 34f).

The procedure is repeated to load second bus tape on opposite ring side. Alternatively, this design can be used to load bus tapes simultaneously on both sides of the half-ring.

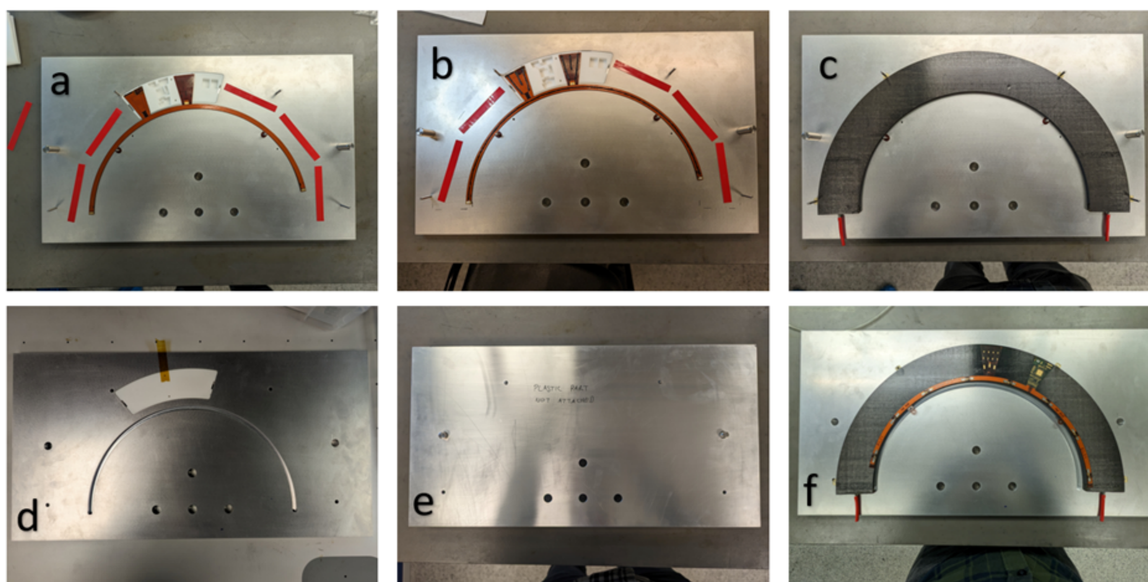

Figure 34: Key steps of the bus-tape loading procedure.

3.2.5 Qualification - metrology

Two prototype (Version-6) bus tapes were loaded onto a Layer-2 prototype half-ring.

Each bus tape was measured before loading using a SmartScope 300 [14] to check x and y geometry and to provide 'before loading' dimensions, in case they might prove useful in determining loading positional accuracy. During this initial measurement, each bus tape was taped (using Kapton tape) to the base plate of the SmartScope in a moderately-successful attempt to achieve flatness.

Additionally, the bus tapes' thickness was measured before loading using a micrometre in a number of positions along the tape, again to create a map for comparison to post-loading metrology.

After loading, the thickness of the half-ring plus glued bus tape was measured using a micrometre and compared to pre-loading measurements to estimate loading glue thickness; see Figure 35. All measurements except one are within the specification of 100^{+100}_{-50} µm.

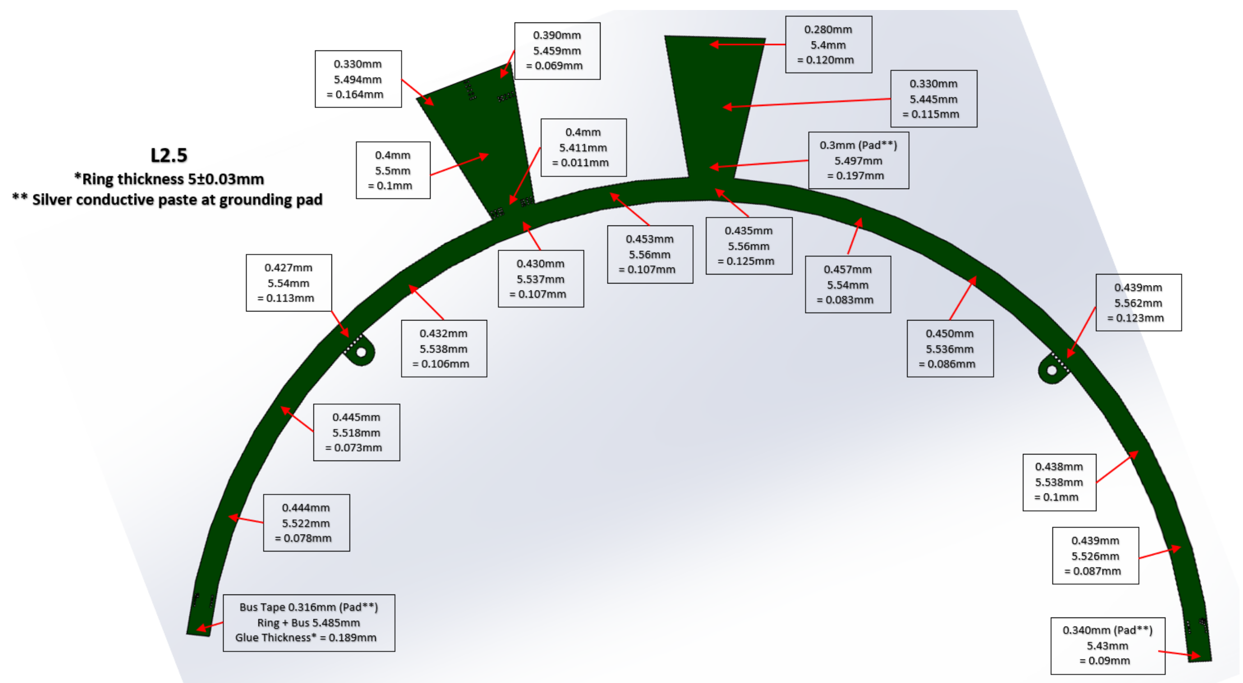

Figure 35: Comparison between pre-loading bus tape thicken and post-loading bus tape + half-ring thickness, to assess thickness of the glue layer.

<u>*Tasks remaining:*</u>

- The bus tape will be measured post-loading using a SmartScope, with reference to the half-ring (see Section 3.1.2), to analyse positional loading accuracy and glue thickness. The key positional measurements are the phi and radial positions of the groups of solder pads, which must meet the specifications listed in Section 3.2.1.
- A glue fillet will be added around the perimeter of the loaded tapes, as recommended from the FEA study above (see Section 3.2.2.5).
- At least one bus tape will be glued onto a Perspex half-ring using the tooling and method outlined above, to measure the expected glue coverage % from the planned production procedures.

3.3 Power Pigtails connection

3.3.1 Design Concept - Tooling

The soldering of the pigtails to the tape is done using a setup based on a soldering iron that has been customized with a rectangular aluminium head directly joined to the soldering tip. The tip is manually handled via a z-axis manipulator; a load cell allows control and measurement of the applied force during the process. The aluminium head has holes on the sides, hosting a PT100 to record the temperature of the head. A custom-made board allows automatic setting of the soldering temperature and monitoring of the applied load and the temperature of the head. A preliminary version of the setup is shown in Figure 36. This basic setup has been duplicated and sent to a second loading site for practice and to provide additional feedback.

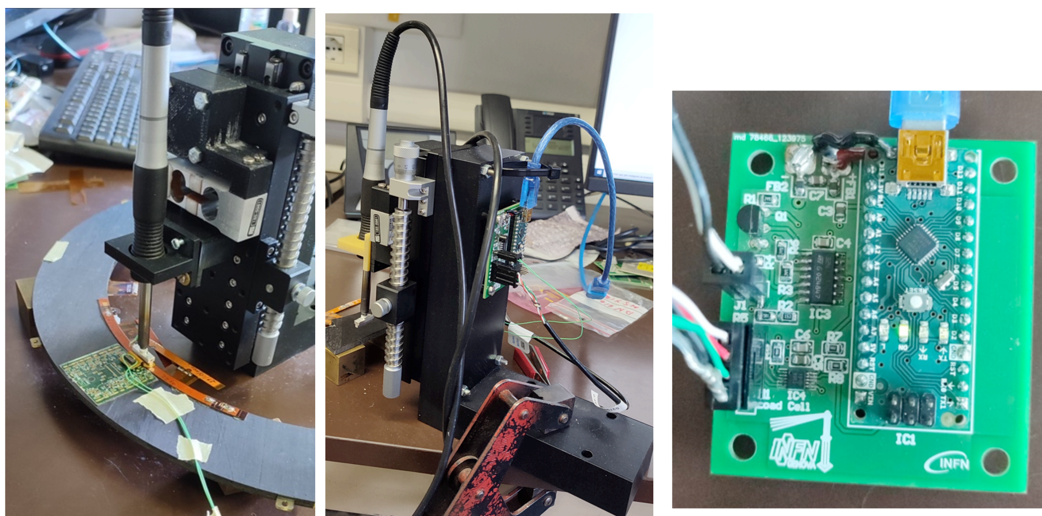

Figure 36: the preliminary soldering tool, with a customized aluminium head connected to a soldering station, and the card (on the right) allowing control and monitoring and pressure and temperature.

For production, the soldering setup has been improved: the soldering head can now be rotated to give safe access to the module pads once the modules are loaded on the half-ring. Unfortunately, due to the dimension of the half-ring frames, a single jig cannot accommodate all three half-ring flavours, so it is planned to have one jig for Layer-4 and Layer-2 half-rings, and one for Layer-3 half-rings. The design of the tool for Layers 2 and 4 is complete (see Figure 37) and a first prototype has been assembled (see Section 3.3.4). After more tests, the design will be adapted for the Layer-3 half-rings, and construction of final copies for the other loading sites will start.

3.3.2 Design Concept - Procedure

The pigtail-loading procedure consists of aligning and overlapping the bus tape and pigtail pre-tinned pads, then applying an initial force via the z-axis position, and finally starting the soldering. During this procedure the module pigtail is already connected on the module side (via a Samtec connector [15]), to minimize the stresses that the soldered pigtail could apply to the module if connected to it after having been joined to the tape with any misalignment. The area of the soldering head is 16.8mm long x 2.5mm wide, while the pads region is 16.5 x 2.0 mm^2: the alignment of the head to the pads is thus done by eye, without the need of additional

optical alignment. Alignment marks will be added on the version-7 bus tape and on the head to make alignment even easier.

During production the setup will be routinely calibrated using mini-tape coupons that are included in the production of the tape panel and pigtails.

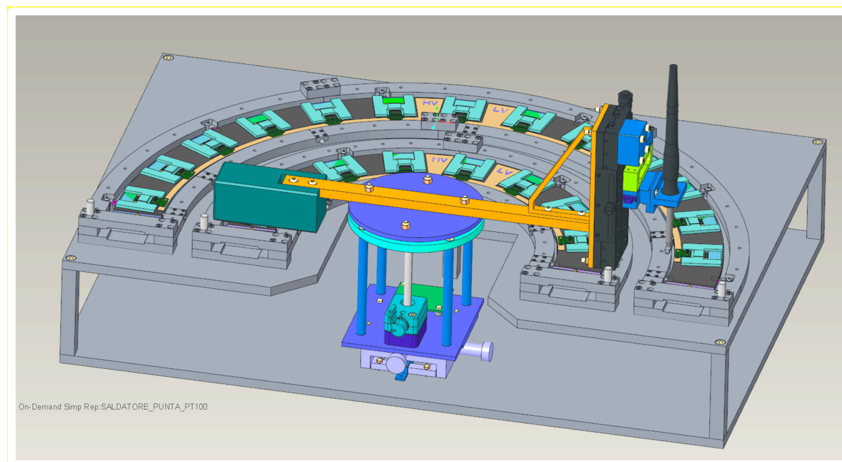

Figure 37: CAD rendering of the setup for soldering the pigtails on the tape after module loading. The soldering head can rotate to reach the module pads; once aligned in angle, the head is blocked. A photo of the tool is featured below in Section 3.3.4.

3.3.3 Preliminary trials

The soldering procedure was first optimized using mini-tape coupons and pigtails, produced specially for this purpose. The amount of pre-tinning, soldering time, and initial weight to apply are all parameters that have been qualified by measuring the electrical resistivity and the mechanical strength of the joint, as well as with x-rays to understand the uniformity of the paste once melted, see for example Figure 38. One important change we have implemented after preliminary tests on the Version-5 (V5) bus tape is the modification in the LV power pads from one single large pad in V5 to several narrower pads in Versions 6 and 7 (V6/V7), in order to have the pressure more balanced on the module pigtail pads.

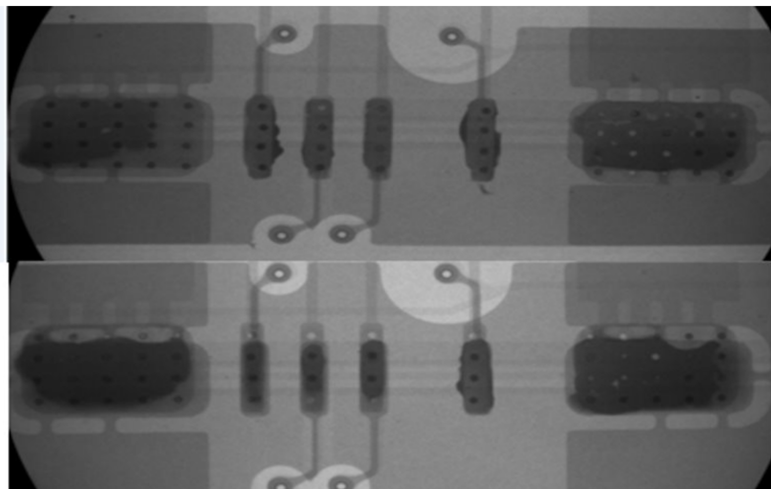

Figure 38: X-ray of soldering trials with a V5 bus tape.

The soldering is done in two steps: a pre-soldering for 45 seconds, and then the real soldering at higher temperature for 60 seconds. Typically, in the tests we have pre-tinned the pads on both surfaces by hand, and the soldering head temperature stays above 200 °C for almost 2 minutes with a maximum temperature of up to 240 °C, depending on the interfaces. The set weight applied is approximately 1N, but it increases up to about 5N during the soldering process, driven by the thermal expansion of the tip (see Figure 39). This force is not controlled, just monitored, but a good repeatability has been obtained.

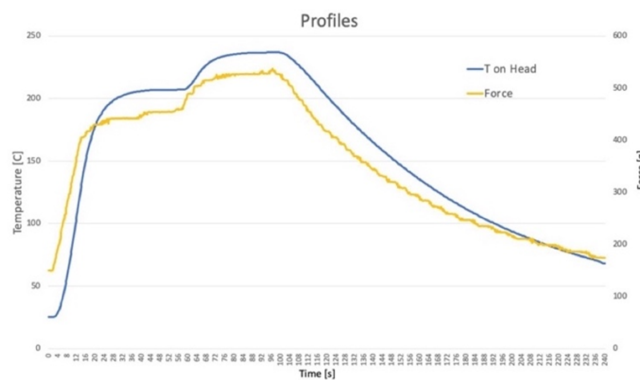

Figure 39: typical trends for the applied force and head temperature.

With dedicated samples, we have also measured the temperature on the half-ring surface close to the tape (up to 60°C) and on the module flex NTC which is very close to the Samtec connector (up to 53°C); this is shown in Figure 40. We therefore expect that the module temperature may reach up to 55°C for a short time, see Figure 41. Further tests will be done with real modules, but overall this does not raise a concern[10].

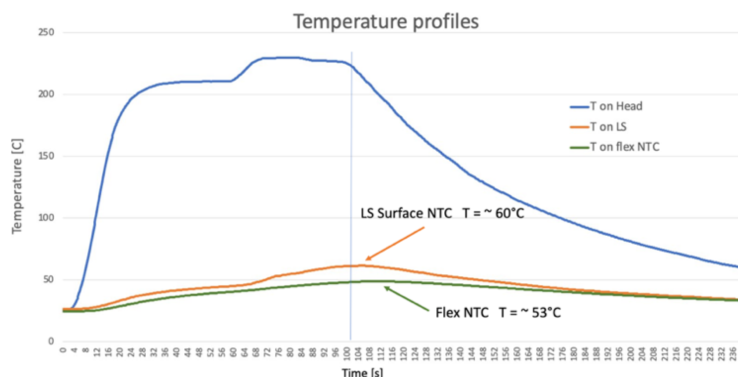

Figure 40: Temperature trends for the sensors on the soldering head, on the surface, and on the flex module.

[10] Note that the modules have been qualified to withstand temperatures as high as 60°C without negative effect.

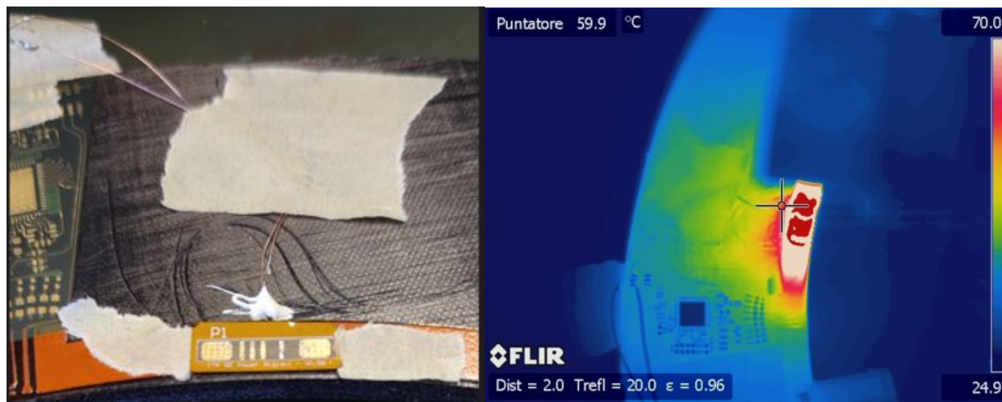

Figure 41: Left: photo of the temperature measurement on the half-ring surface. Right: thermal image while soldering.

To validate the design of the short "I-shaped" pigtails connecting modules and bus tapes without a connector, but with soldering as in the current baseline finalized in tape V6, a realistic sample was prepared and tested. The main concern is that the I-shape pigtail is very short and its length may be not enough to absorb the CTE mismatches between the interfaces. To run a first test, realistic as much as possible at that stage, we used a Layer-2 half-ring, pigtails and custom connectors, a V6 tape cut in two parts with three module pads each, and two dummy modules (300µm-thick silicon, V1 flex hybrid, and a custom Samtec FMT connector). Two samples were prepared on the half-ring, each of which was composed of a module-pigtail-tape combination, using a part of the tape rather the full one to ease the mechanical placement, not having yet final jigs for the alignment.

The flex modules were glued to the silicon tiles using preliminary quad jigs. The modules were then glued to the local support using the module-loading gantry system and SE445 adhesive (see Section 3.6): the glue layer thickness was confirmed to be within the specification. Finally, the tapes were glued to the local support in front of the modules – notice this is not the standard sequence but without final jigs this was the best way to guarantee the nominal distance between the module and the tape. To glue the tapes, first a controlled quantity of Hysol was deposited using a mask, and then the tape was placed using preliminary alignment jigs. The local support with the two modules and tapes is shown in Figure 42.

Figure 42: Left: Sketch of the Layer-2 half-ring with the two test samples done with a module connected to a piece of tape. Right: picture of one of the samples.

After the gluing, tests have been performed: optical inspection, resistive measurements and thermal performance when biased. The sample was cycled fifteen times (over the course of about thirteen hours) between -55°C and 60°C. Tests have been repeated and results do not spot significant changes. Some more details are given below.

For the optical inspection, some reference distances between the tape and the flex were measured: no relative displacement was observed after the cycles, as shown in Figure 43. The resistivity measurement was done exploiting the power pads of the neighbouring modules that are located on the tape (see Figure 44) and shortening V_{in} and V_{out} on the module flex. No changes have been observed in the resistivity after the cycles. Thermal performance has been checked while a current of 6A is flowing in the samples using an IR camera. Minimal differences have been noticed, most probably due to the room temperature variation during the set of measurements (see Figure 45).

These tests validate the mechanical/electrical connections in the interfaces. The next step will be to validate with real modules, in order to check the effect on the pixel bumps.

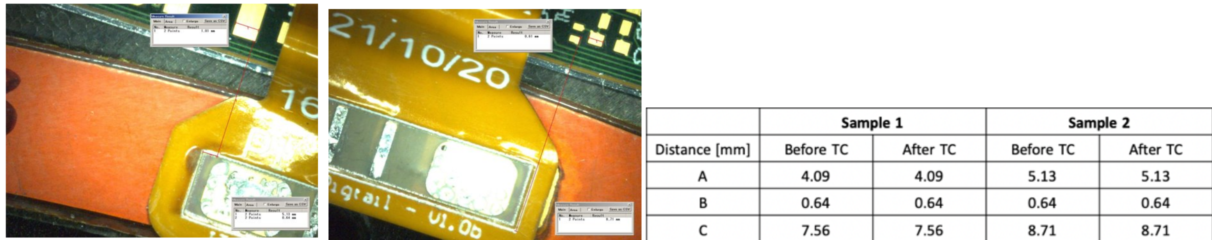

	Sample 1		Sample 2	
Distance [mm]	Before TC	After TC	Before TC	After TC
A	4.09	4.09	5.13	5.13
B	0.64	0.64	0.64	0.64
C	7.56	7.56	8.71	8.71

Figure 43: (Left and Center) zoom in pictures of the region between the tape and the module. (Right) A summary table for the measurements done before/after the cycles.

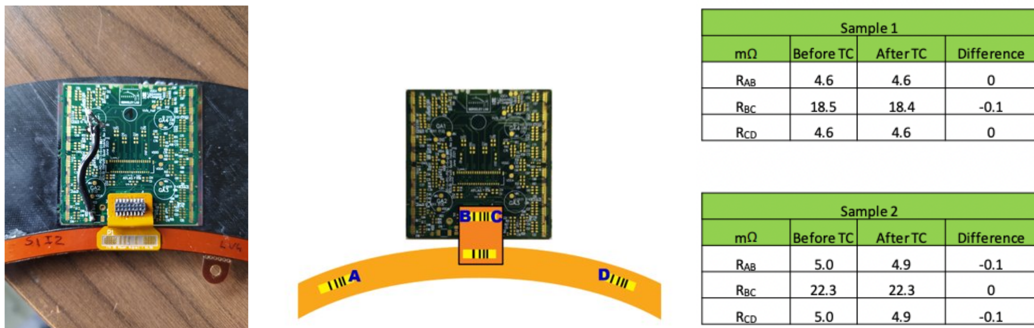

Sample 1			
mΩ	Before TC	After TC	Difference
R_{AB}	4.6	4.6	0
R_{BC}	18.5	18.4	-0.1
R_{CD}	4.6	4.6	0

Sample 2			
mΩ	Before TC	After TC	Difference
R_{AB}	5.0	4.9	-0.1
R_{BC}	22.3	22.3	0
R_{CD}	5.0	4.9	-0.1

Figure 44: (Left) picture of the shortcut within Vin and Vout on the flex module. (Center) sketch of the points where the resistivity has been measured. (Right) A summary table for the measurements done before/after the cycles for the two samples – absolute differences between the two samples depend on the different shortening between Vin and Vout on the flex module.

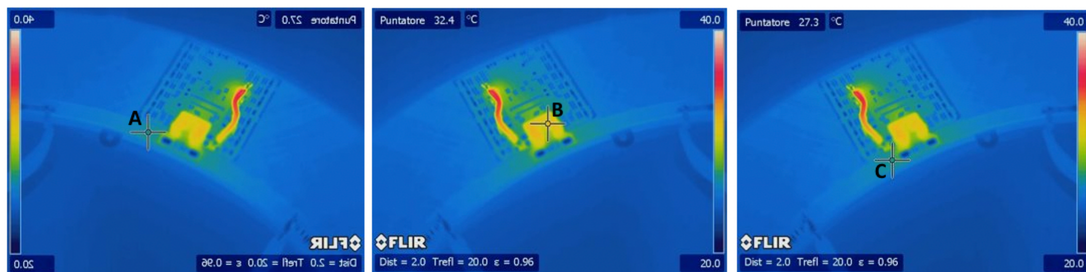

	Sample 1		**Sample 2**	
Temperature (°C)	Before TC	After TC	Before TC	After TC
A	27.0	27.1	27.7	27.8
B	32.4	32.3	34.6	34.6
C	27.3	27.2	28.2	28.1

Figure 45: (Top) Thermo-images of the modules when current is on and measurement in three locations. (Bottom) A summary table for the temperature measured before/after the cycles for the two samples. Small differences may be related to the tiny difference in the room temperature.

3.3.4 Trials with realistic components

Further validation of the soldering procedure was done with a V6 bus tape with components loaded by the CERN workshop, which is the baseline for services production. As pictured in Figure 46 and described further in Section 0, a Layer-4 half-ring was assembled with a V6 bus tape, two ITkPixV1.1 digital modules, and two RD53A modules; pigtails were loaded for the ITkPixV1.1 modules, while the serial-powering chain was closed in the other module pads positions via ad-hoc shortening pigtails to allow serial powering.

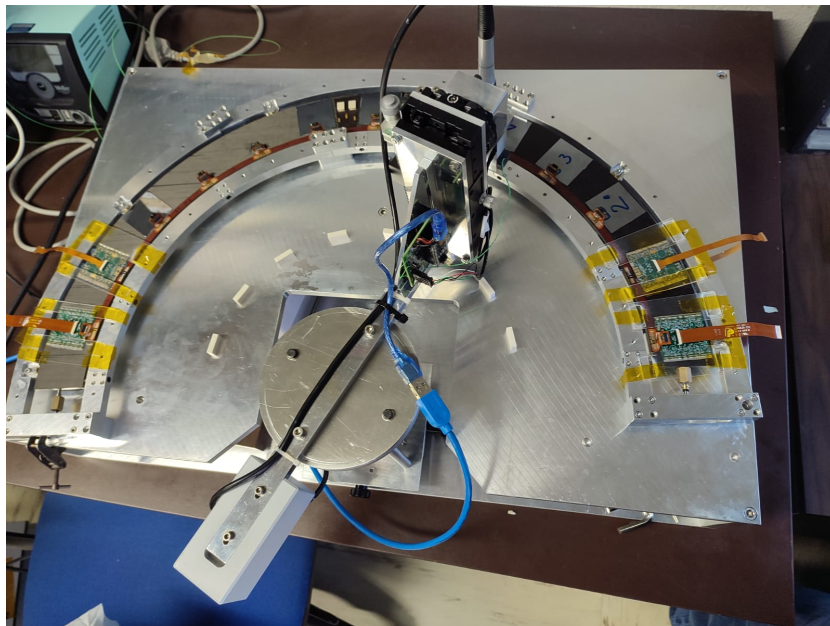

Figure 46: The pigtail-soldering setup being used while soldering a Layer-4 half-ring with a V6 bus tape, two RD53A quad modules, two ITkPixV1.1 digital quad modules, and a number of dummy Silicon tiles.

Figure 47 shows the temperature and applied force trends for a few positions during the soldering of the pigtails. In general, the temperature of the head is very well reproducible, while a larger range of forces is applied, depending on the pre-tinning material and distribution. During the SMD loading of the bus tape, the tape pads were also pre-tinned. As the paste used is lead-free, the melting temperature was about 40°C higher than we used in our previous tests. This fact implies the need for higher temperature during the soldering, where the maximum temperature on the soldering head is 300-330°C. The expected temperature reached by the modules was evaluated by placing an NTC on one of the dummy Si tiles very close to the soldering area. The NTC reached 60°C while the local support surface was warmed up to 50°C, see plots and images in Figure 48. For this V6 bus tape, the choice of lead-free paste was driven by the very small 0201 SMD components, which are no longer present in the latest bus tape version (V7). The lead-free paste is more suitable to place such small components as it flushes less, but if required a paste containing lead can be used in pre-production.

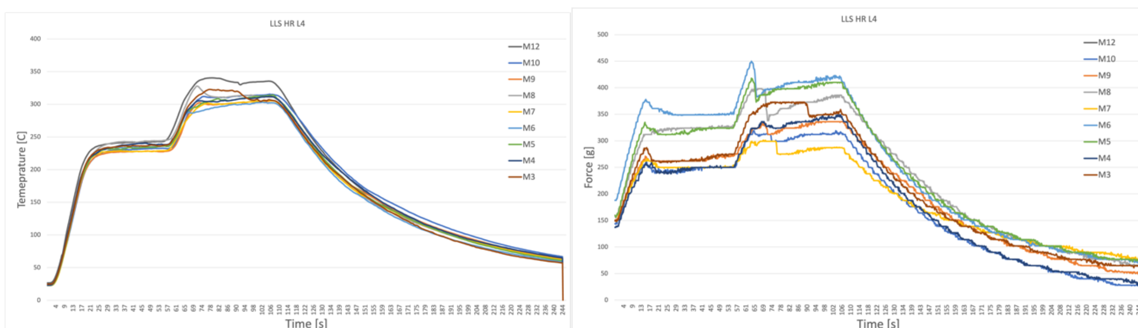

Figure 47: Temperature of the head (left) and force applied to the power pads (right) during the soldering process, on several power pads on a Layer-4 half-ring.

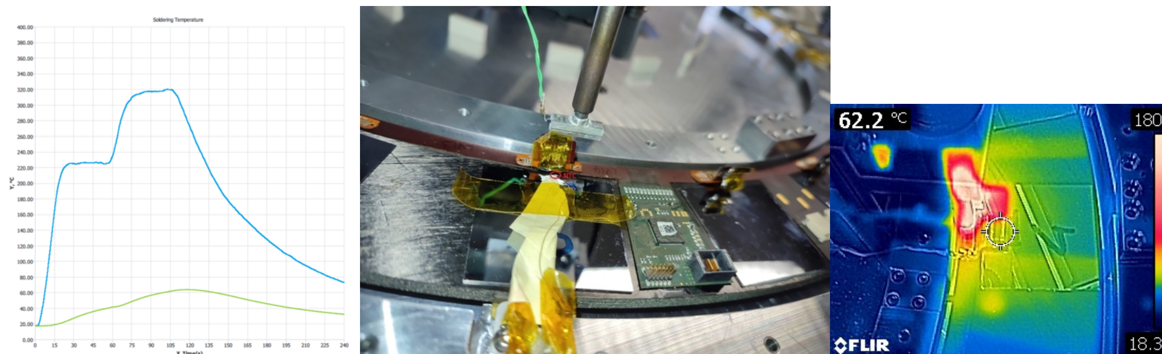

Figure 48: Temperature trends for the sensors on the soldering head and on the Si tile (left). Picture of the temperature sensor on the Si tile surface (centre) and thermal image while soldering (right).

3.3.5 *Irradiation QA*

Four samples were irradiated in November 2022 at the IRRAD facility [16] at CERN, up to a fluence of 7.6×10^{15} protons/cm^2. These samples are mini-tapes glued to a prepreg-and-foam support structure and soldered to pigtails (see Figure 49), thus mimicking the real interface of the tape with the local support and the modules. Two types of glues have been used: SE4445 and Hysol. After irradiation the mechanical shear was measured by pulling the pigtail: the applied load was larger than 2kg for all the samples and the pigtails were not detached, see Figure 50.

Figure 49: Sample with mini-tapes and pigtails glued on a bespoke mini-structure of prepreg and carbon foam. The carbon foam layer is minimized under the irradiation region to avoid possible irradiated powder to be missed and to minimize the material.

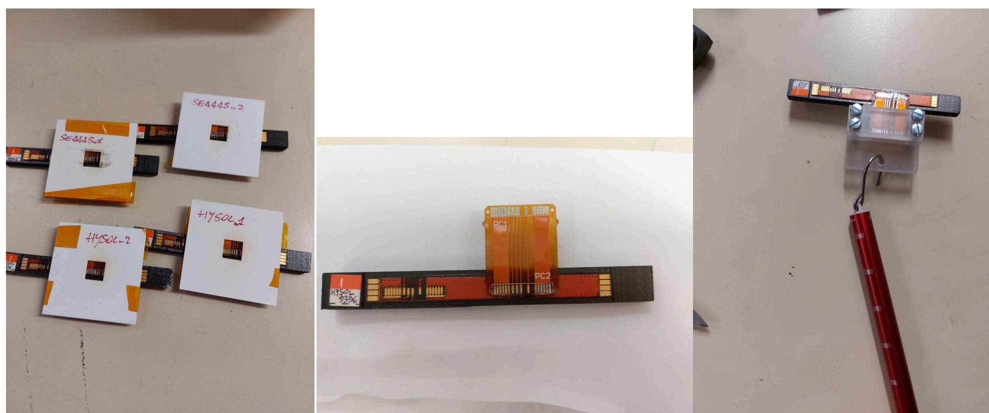

Figure 50: samples after irradiation; setup for shear test.

3.4 Module Loading technique – RAL

This section describes the equipment and methods used to load pixel end-cap half-rings at RAL, and which have been used as described to produce the "Ring-1" Outer Endcaps demonstrator.

As described earlier in this document, Outer Endcap half-rings are supplied to the loading sites in their own aluminium handling frames. The half-rings stay in their handling frames for the duration of loading and testing at RAL. The mounting lugs of the half-rings contain small holes which are used as fiducials, allowing optical alignment of modules.

A brief overview of the RAL loading process is given in Section 3.4.1.

The equipment used during loading is described in section 3.4.2

Glue deposition is described in section 3.4.3.

The loading procedure is described in section 3.4.4.

3.4.1 Description of the loading process

The RAL loading process uses manually-adjustable bespoke 'bridges' to pick up modules and place them in the correct places on half-rings under a gantry equipped with an optical metrology system to guide the placement.

3.4.2 Description of the tooling and equipment

3.4.2.1 Aerotech gantry

A custom Aerotech linear motor gantry is used (see Figure 51). It has a working area of 500mm by 700mm, and an original positioning accuracy of ± 10µm. After custom calibration at RAL, a positioning accuracy of ± 5µm has been achieved.

A tooling plate is mounted to the gantry, forming a bed plate with dowels and tapped holes for mounting loading tooling plates.

The gantry is equipped with a camera (Basler Ace 1920-40um) and optics based on a Mitutoyo x5 telecentric objective. The long working distance (55mm) of this arrangement allows the camera to be used to observe the positions of the module corners from above the loading bridges, without risk of collision.

A Keyence LT9030M laser displacement head can be mounted on the gantry, coupled to a LT9501 laser displacement meter, allowing precision height measurements to be made on the gantry.

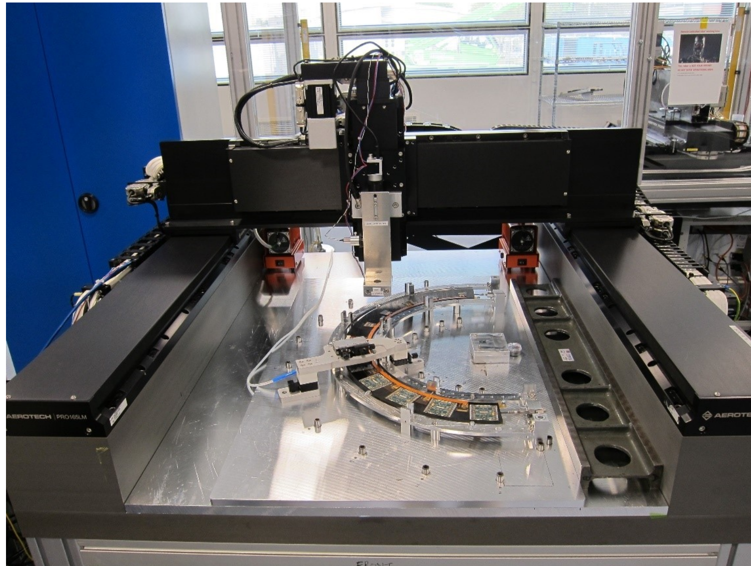

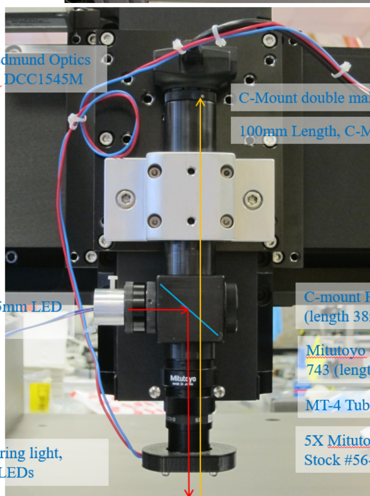

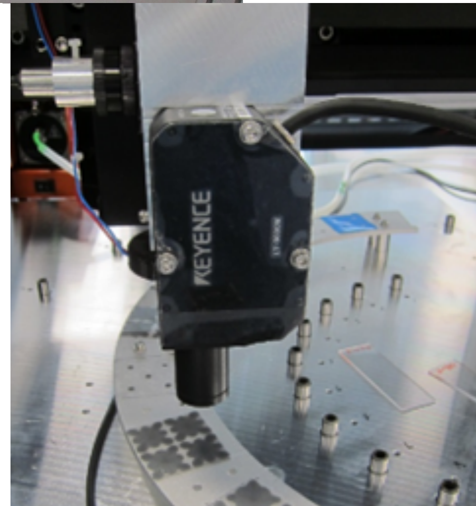

Figure 51: Top: the RAL loading gantry. Bottom left: the gantry optics and camera. Bottom right: the Keyence LT9030M laser displacement head.

3.4.2.2 Loading tooling plate

For each flavour of pixel end-cap half-ring, a tooling plate has been made with dowels and tapped holes to allow a half-ring handling frame and loading bridges to be fixed to it; see Figure 52.

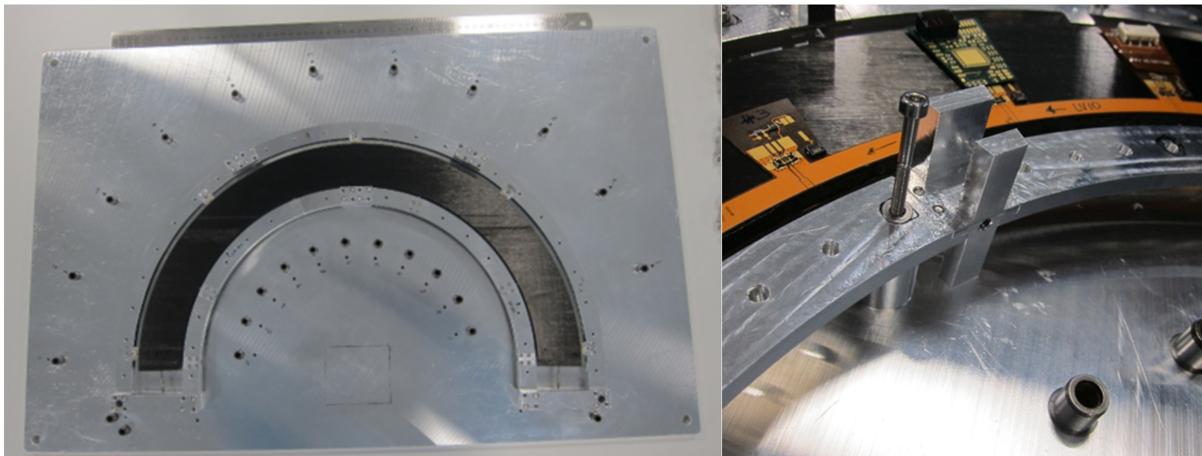

Figure 52: Left: the Layer-2 tooling plate. Right: fixation of the handling frame to the tooling plate.

3.4.2.3 Loading bridges

Loading bridges (Figure 53) are used to hold and position the modules on the half-ring surface. A vacuum chuck is built in to pick up the module. This chuck is designed to be rigid under torsion and translation, to allow positioning of the module. It is designed with vertical springing, using spring pressure to push the module down onto a bed of wet adhesive. The vacuum cups are intended to be coplanar, but the lower part of the chuck can tilt to follow half-ring surfaces which are not absolutely horizontal. The bridges are dowelled into position on the tooling plate but have their own adjustments in the radial and tangential directions, to allow fine placement of the module. There is also a rotational adjustment, which changes the module rotation angle.

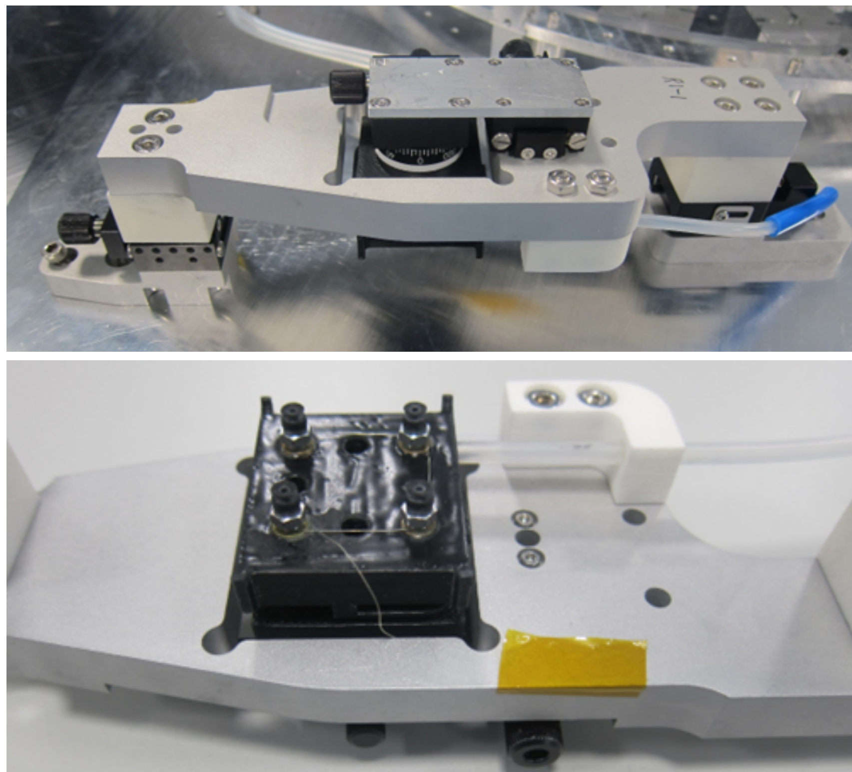

Figure 53: Top and bottom views of a loading bridge.

3.4.2.4 Pickup jig

The pickup jig (Figure 54) allows initial placement and initial alignment of a module. A module is removed from its handling frame, and placed on the pickup jig vacuum chuck, with its position defined by dowels. A loading bridge can then be placed over it, aligned by dowels on the pickup jig. This allows the loading bridge vacuum cups to engage with the module pickup points. Vacuum is applied to the loading bridge vacuum cups and removed from the pickup jig vacuum chuck. The loading bridge can then be removed from the pickup jig with the module attached, ready to be placed over a half-ring.

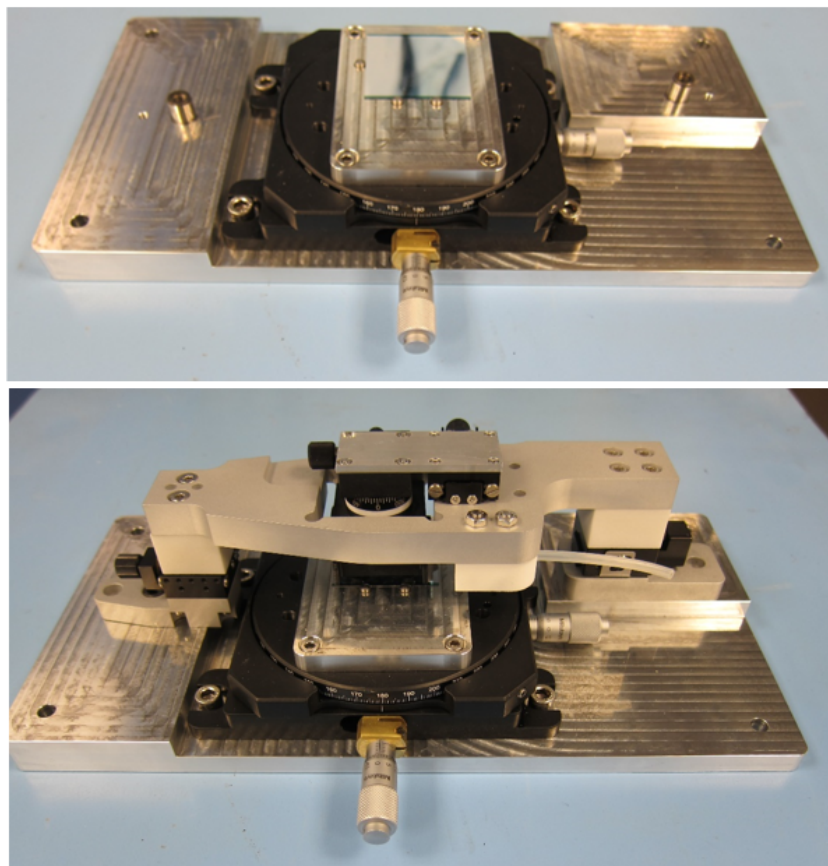

Figure 54: Top: a dummy silicon module on the pickup jig. Bottom: a loading bridge picking up a module.

3.4.2.5 Vacuum pen

A custom vacuum pen has been made, with four vacuum cups, for manual handling of modules.

3.4.2.6 Gantry calibration plate

A machine calibration plate, 508mm by 609mm, is used for periodic gantry calibration. It is a glass plate with an array of chrome features, allowing optical calibration using the gantry camera (Figure 55, left photo).

3.4.2.7 ESD blower

As an extra precaution against static charge build-up, an ionised air blower has been mounted above the gantry (Figure 55, right photo).

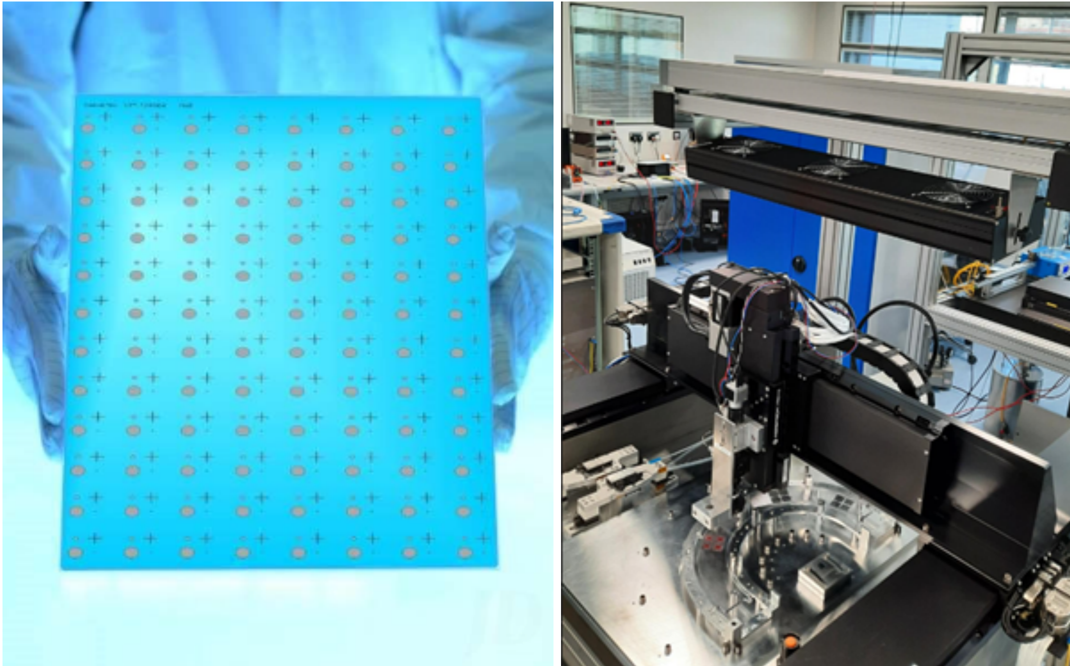

Figure 55: Left: gantry calibration plate. Right: ESD blower.

3.4.2.8 OGP SmartScope

The SmartScope allows modules and half-rings to be surveyed and compared to CAD models. It is used for module thickness measurement as well. It can perform optical alignment in X and Y, and incorporates a laser for height measurement. Use of the SmartScope for metrology will allow loading on the gantry to be performed in parallel, speeding up production.

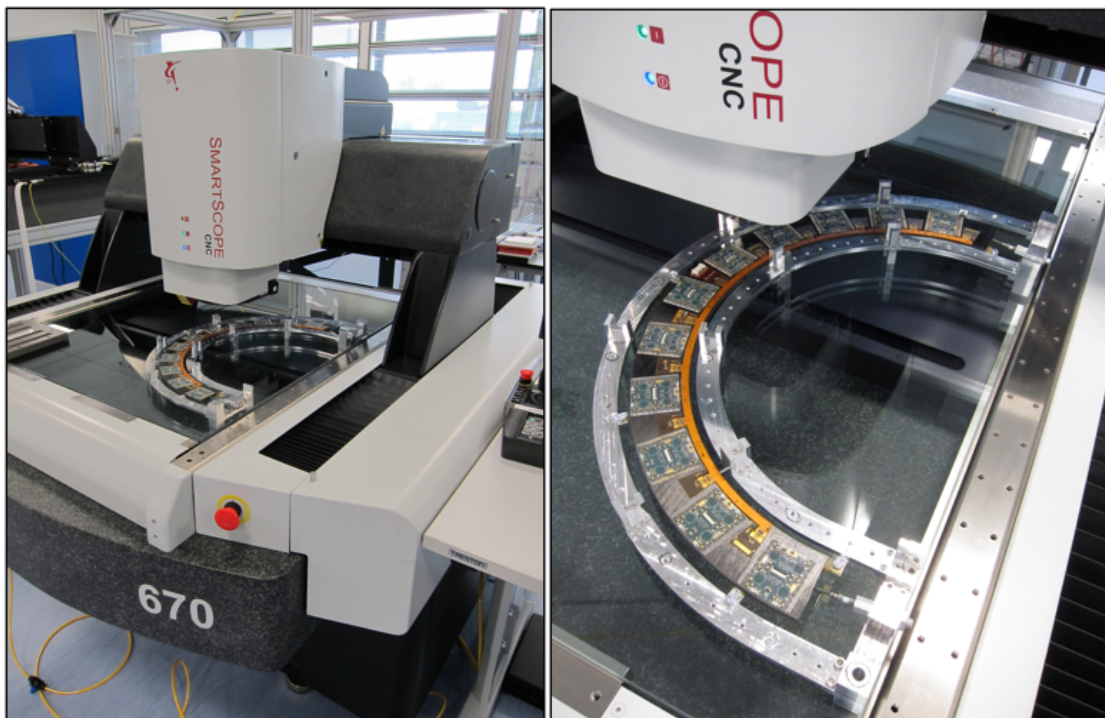

Figure 56: A loaded Layer-3 half-ring undergoing metrology on the SmartScope.

3.4.2.9 Planetary mixer

Glue for mounting modules is mixed in a SpeedMixer planetary mixer. It allows for glue to be mixed in 5g pots, for one syringe-worth of glue. A custom adapter was 3D-printed to allow syringes containing glue to be mounted in the mixer, and spun, to expel any air bubbles introduced into the glue when it was loaded into the syringe.

3.4.2.10 Gantry syringe mount

Glue is dispensed from a syringe mounted on the gantry (Figure 57, left photo). A custom syringe-holder is fitted to the gantry for this. Gas pressure from the Nordson fluid dispenser, applied to the syringe, dispenses glue.

3.4.2.11 Nordson EFD Ultimus V fluid dispenser

The Nordson fluid dispenser (Figure 57, right photo) provides gas pressure to the glue syringe to dispense glue. It allows for gas pressure to be adjusted to account for glue viscosity, to control the volume of glue dispensed.

Figure 57: Left: gantry syringe mount. Right: Nordson fluid dispenser.

3.4.3 Glue Deposition

Glue for module loading is prepared by mixing SE4445 glue with 100-micron glass spheres (to constrain the glue thickness during module loading) in the SpeedMixer. The glue is then transferred to a syringe. A needle is added to the syringe, and the syringe is then attached to the gantry. The Nordson gas pump is also connected to the syringe to provide pumping pressure to the syringe, to dispense glue.

With each new needle, the needle XY offset must be determined. This is done by depositing a small dot of glue in a certain location on the gantry. The gantry camera is then moved to this location, and optical alignment with image recognition is used to align the camera with the dot. From there the needle offset can be calculated.

With a new syringe of glue, a test pattern of glue is first printed onto a glass slide. The glass slide is weighed before and after this printing, and the gas pressure of the Nordson gas pump is adjusted to ensure a constant mass of glue is dispensed with each pattern printed.

The gantry is then moved to the desired module location, and a star pattern of glue is printed at the location of each FE chip.

3.4.4 Module placement

The loading process can be broken down into the following stages:

1. Perform metrology on the bare half-ring.
2. Determine the position of the half-ring on the the gantry using the the half-ring fiducials, allowing the ideal module locations to be determined, (done once per half-ring side).
3. Place and attach a module to the pickup jig.
4. Measure module thickness.
5. Transfer module from the pickup jig to a loading bridge.
6. Place bridge over half-ring and use gantry optical alignment and loading bridge adjustments to move module to ideal location. Then remove bridge with module.
7. Mix adhesive, fill the syringe, and mount it on the gantry.
8. Measure the syringe needle offset and print a test pattern.
9. Print glue on half-ring at desired module location.
10. Place bridge back over half-ring, placing module on glue.
11. Check/adjust the module position.
12. Perform metrology after all modules have been loaded and the adhesive has cured.

These steps are described in more detail below.

Step 1:

The bare half-ring is measured on the OGP Smartscope, to determine surface height at module locations, for future glue-thickness determination.

Step 2:

The half-ring in its loading frame is bolted to the loading tooling plate on the gantry (Figure 58. The gantry camera is used to identify the half-ring fiducials to determine the half-ring position, and from that the ideal module locations.

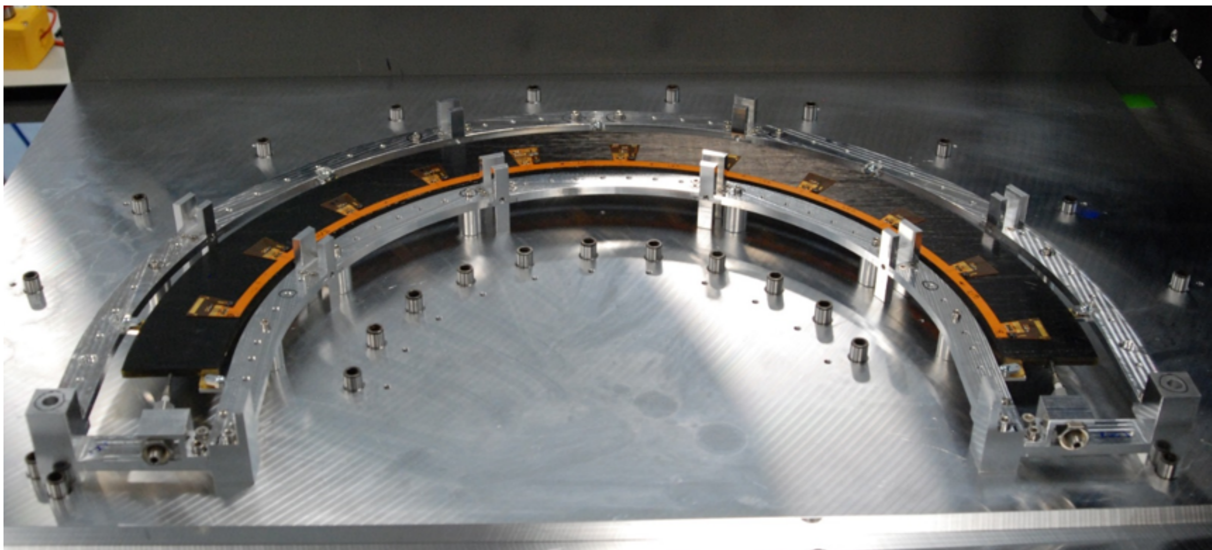

Figure 58: A Layer-3 half-ring placed on the loading tooling plate on the gantry.

Step 3:

A reception-tested module is removed from its handling frame using the vacuum pen, placed on the pickup jig, aligned against dowel pins, and held there by the pickup jig vacuum chuck.

Step 4:

Module thickness is measured with the OGP SmartScope while the module is vacuumed onto the pickup jig.

Step 5:

A loading bridge is placed over the pickup jig. Vacuum is applied to the bridge and removed from the pickup jig.

Step 6:

The loading bridge is placed, with the module attached, over the half-ring, in the position where the module will be mounted (Figure 59). The bridge is screwed to the loading tooling plate. The gantry camera is moved so that crosshairs on the camera view are aligned with the ideal module corner positions (Figure 60). The loading bridge adjustments are then used to bring the module corners to the ideal positions, within required tolerances. The bridge with module is then removed and placed to one side.

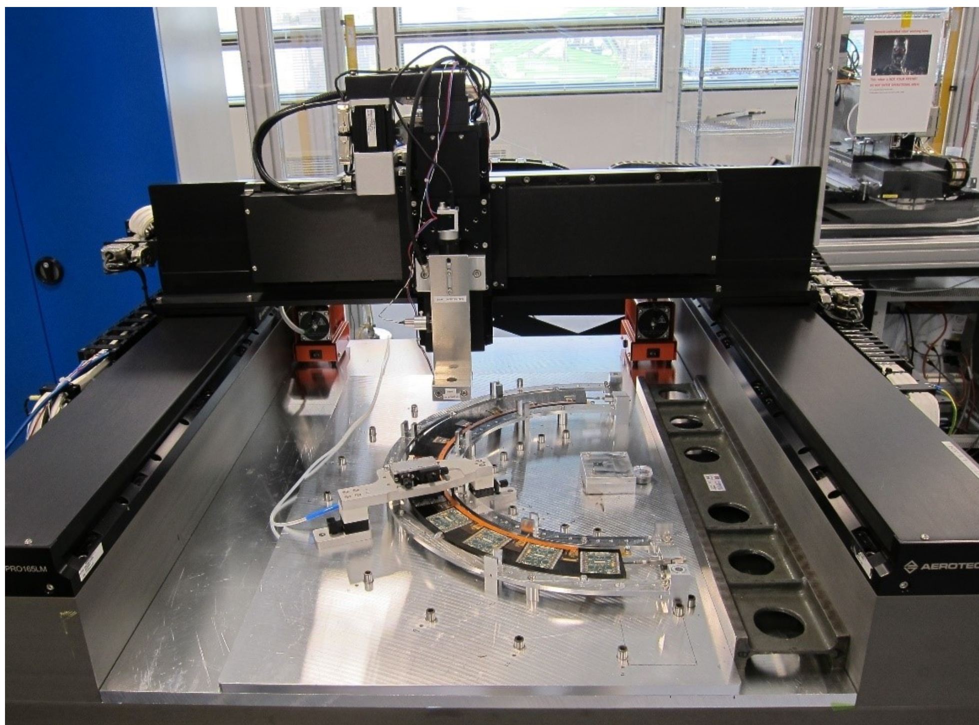

Figure 59: A module being positioned on the gantry.

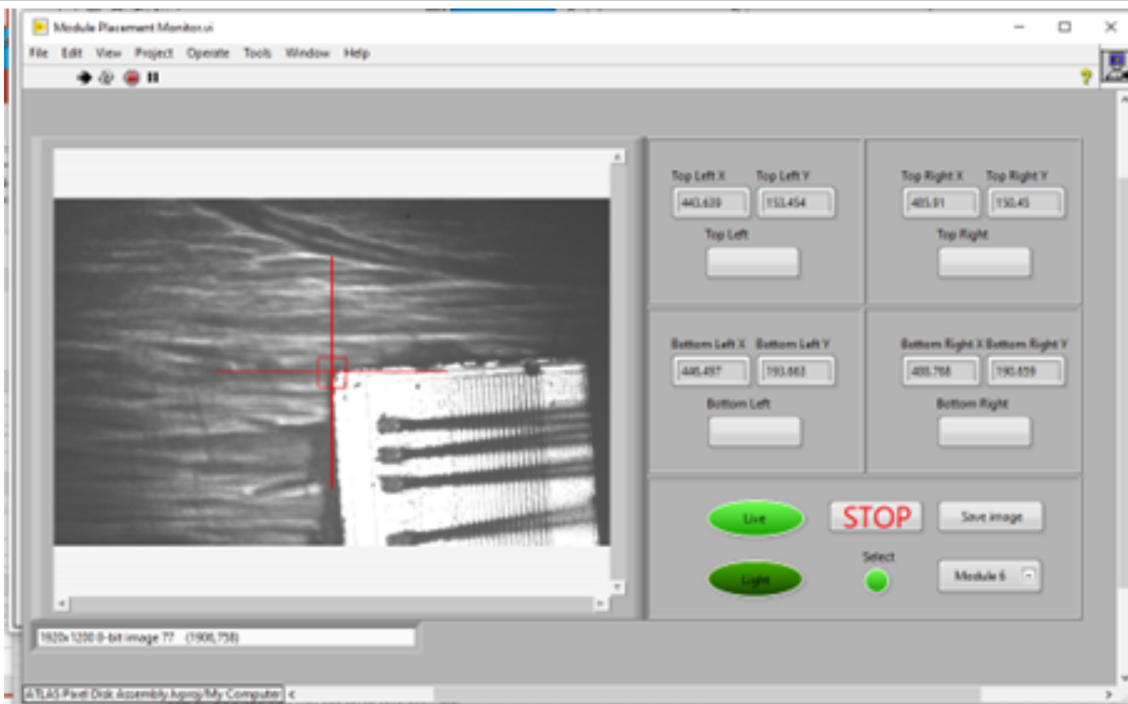

Figure 60: Gantry camera finding the ideal module position.

Step 7:

Glue is mixed with 100-micron glass spheres (to constrain the glue thickness during module loading) and loaded into a syringe which is then mounted on the gantry.

Step 8:

The syringe needle offset is determined, and a glue test-pattern is printed (Figure 61, left photo) and then weighed to determine required gas-pressure adjustment.

Step 9:

The gantry is moved to the desired module location, and a star pattern of glue is printed at the location of each FE chip (Figure 61, right photo).

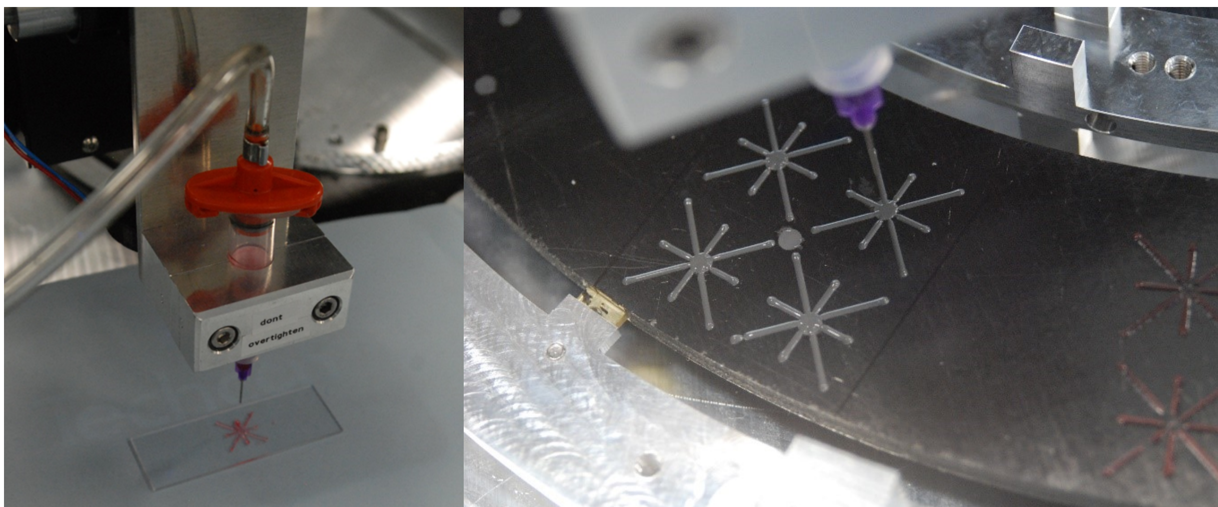

Figure 61: Left: printing a glue test pattern. Right: printing glue on the half-ring.

Step 10:

The loading bridge with module is then placed back over the half-ring and screwed down, pushing the module onto the wet glue (Figure 62).

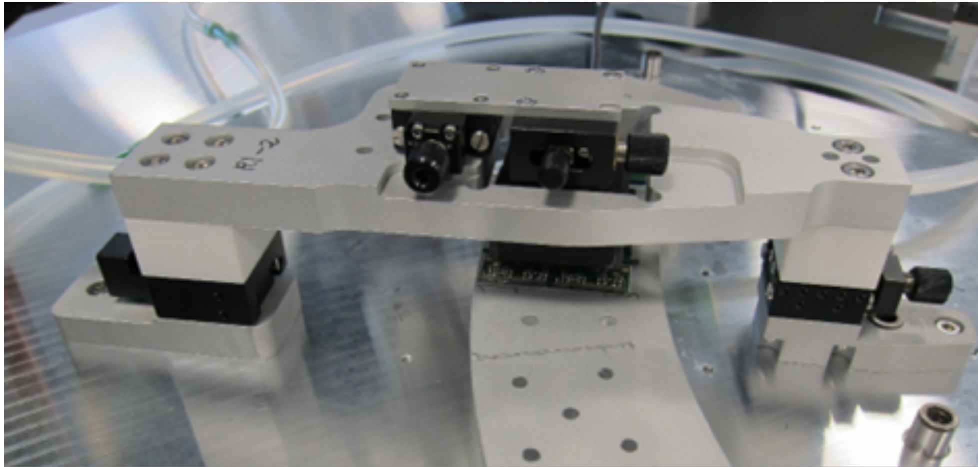

Figure 62: A module being pressed into the glue patterns on a test half-ring.

Step 11:

The gantry camera is used to check the locations of the corners of the module. If required, the loading bridge adjustments are used to bring the module corners to the ideal positions, within required tolerances.

Step 12:

Once all modules have been loaded, and all glue has cured, the half-ring in its handling frame is moved to the OGP SmartScope to be measured, to determine glue thicknesses and module XY positions, as discussed for Ring-1 in sections 4.1.1 and 4.1.2 respectively.

3.5 Module Loading technique – Oxford

3.5.1 Description of the loading process

The loading technique at Oxford is similar in principle to that employed by RAL but involves greater integration of the module pick-and-place with the gantry. The general philosophy is that the gantry picks up so-called bridge tools, with which it will lift and place modules on a half-ring. These will stay with the positioned module until the glue cures and can then be released and used to place further modules. This approach exploits the equipment and method employed by Oxford for the production of ITk quad pixel modules, where much tighter placement tolerances are required. Details of the gantry can be found in Reference [17].

3.5.2 Description of the tooling

The bridge tool schematic can be seen in Figure 63. On the side facing the module there are four aluminium pillars milled from a single block of metal, which form a planar surface to pull the module to. These match the pick-up areas of the module intended for this purpose. Within the pillars are routed vacuum channels, which pull the modules against the pillars when their vacuum is engaged. The interface is a flexible suction cup mounted on a barb inside the pillar. Further to the features designed for module pick-up, the bridge tool also features three thrust screws which can be used to set the height of the module when placed upon the half-ring. This was necessary before the adoption of silica spheres to control the glue layer thickness and are no longer strictly needed. Current loading trials have been performed by setting the thrust

screws such that the resulting glue thickness would be thinner than the spheres if the spheres were not present.

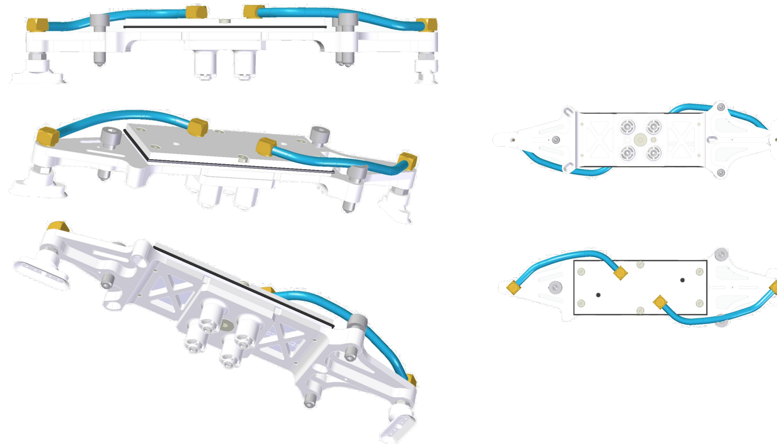

Figure 63: Oxford bridge tool.

The bridge tool is picked up by the gantry head via an intermediate vacuum spreader. Two iterations of this can be seen in Figure 64. All of the results below were performed using type A, which was observed to have insufficient vacuum force to prevent the bridge tool from slipping during placement. This resulted in precisions worse than that those seen during the module construction and should be corrected by the new design (B). This is in the process of being validated.

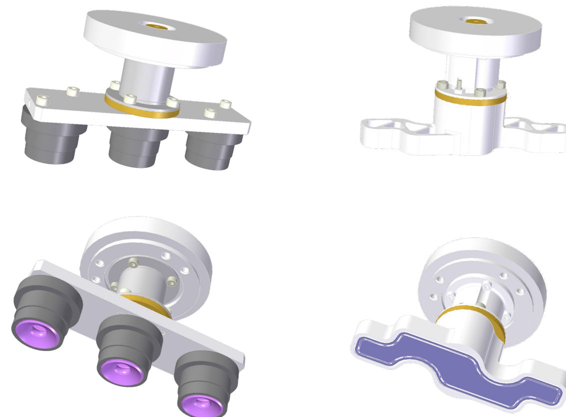

Figure 64: Intermediate vacuum spreader iterations.

A schematic of the complete loading tooling mounted on the Oxford gantry can be seen in Figure 65. There are three distinct base plates: the ring loading plate (1), the module park position plate (2) and the gantry tool rack (3). The ring loading plate serves as a mounting point for the handling frame holding a half-ring and contains stainless steel blocks on which the bridge tools will rest during module placement (and where they can be parked beforehand). The module park position is simply a series of vacuum channels and mechanical dowels used to place the modules in preparation for loading. The gantry tool rack contains the vacuum spreader tools.

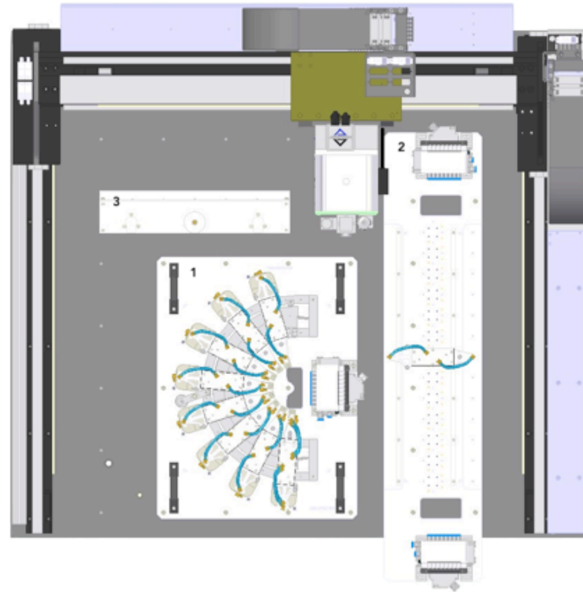

Figure 65: A schematic of the loading tooling mounted on the Oxford gantry showing the ring loading plate (1), the module park position plate (2) and the gantry tool rack (3).

3.5.3 Glue Deposition

Glue is deposited in the sixteen-spoke star pattern shown in Figure 66 which has been optimised for sharp corners in the final pattern after loading has been performed and the glue has set.

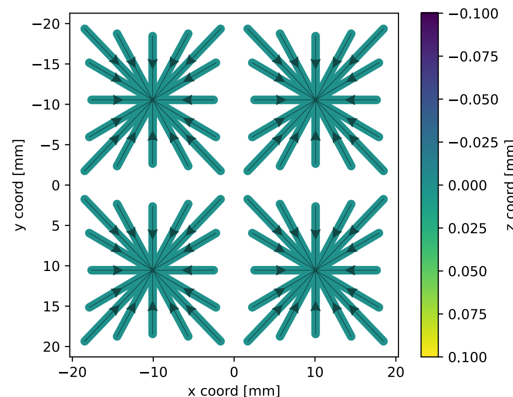

Figure 66: Schematic view of the glue pattern used for quad-module loading at Oxford.

A linear model was developed for glue deposition. The model specifies a line speed v; inputs are target mass m, the total line length of the glue pattern l, and the massflow rate of the glue f:

$$v = \frac{lf}{m}$$

The massflow rate must be measured for each new mixed batch of glue as a calibration step. The target mass was optimised by visual inspection of deposited patterns of varying masses. A sample of these is shown in Figure 67, and a preliminary recommended target mass of 80-85mg has been determined. An automated calculator has been implemented for the model, which is used during loading runs.

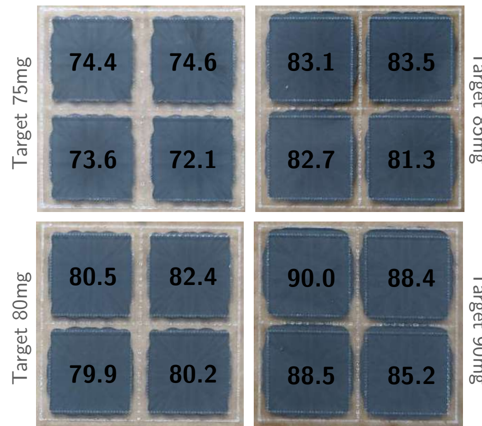

Figure 67: Results of an example deposition attempt (sample S09) with four different target glue masses, used for optimisation of the target mass used with the linear model during loading.

A tendency for the glue patterns deposited later in time to exhibit a deficiency of up to 5% of the target mass was observed, and the model was extended to a second-order correction for the viscosity change over time:

$$\frac{\partial v}{\partial t} = \frac{l\frac{\partial f}{\partial t}}{m}$$

Linear fits to several glue mass flow rate evolution curves determined from depositions performed at 20-30psi with a 23AWG needle measured $\frac{\partial f}{\partial t}$ as $(3 \pm 0.3) \times 10^{-5}$ mg/s^2. However, the implementation of this correction within the loading program is still outstanding.

Through several depositions on glass microscope slides, the model was verified to constrain the final deposited mass within a 5% tolerance range on both the Nordson Pro4 development setup and on the Aerotech gantry which will be used for loading, given a dispense pressure in the range of 20-30psi (chosen prior to flow rate measurement and kept constant after) and a 23AWG needle gauge. Deviations from the target mass for patterns deposited for three glue mix batches are shown in Figure 68.

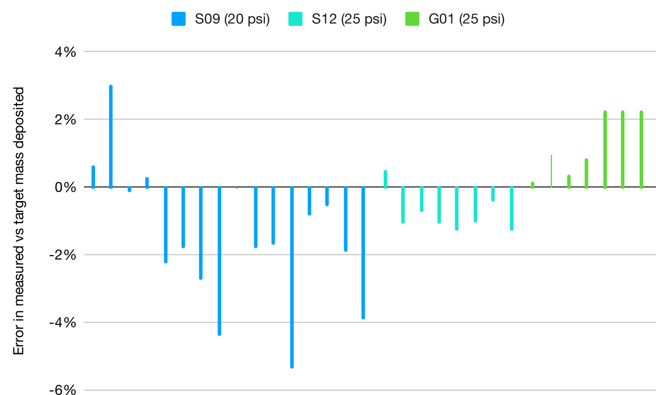

Figure 68: Deviations of deposited mass from target mass for three glue mix batches. S09 and S12 were deposited using the Nordson Pro4 development setup, whilst G01 comprises a verification run on the Aerotech gantry after porting the glue deposition scripts.

The mixing procedure for the glue is summarised in Figure 69, and involves the separation of the SE4445 cartridge into separated syringes to allow for more accurate measurement of each component during mixing. Equal masses of the two components are combined with CoSpheric Soda Lime 94-100 um spacer spheres at a ratio of 0.25% by volume to control layer thickness.

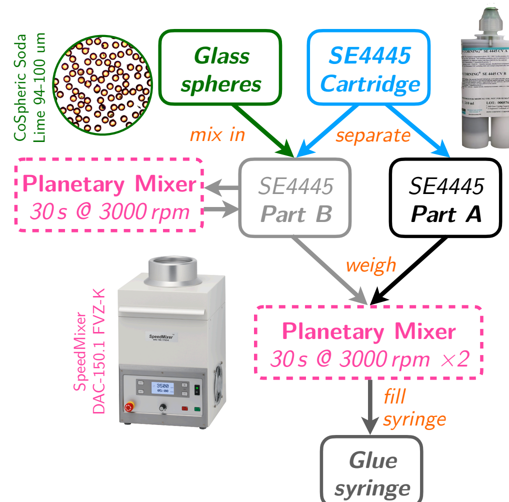

Figure 69: Glue-mixing procedure used during verification pattern depositions and loading trials at Oxford.

3.5.4 Module placement

The concept for the module placement is demonstrated in Figure 70. After performing an initial metrology of the half-ring and module alignment fiducials, the gantry deposits SE4445 via a mounted syringe and pressure dispenser over the desired module position. The line speed is tuned based on a measurement of the glue flow rate to control the mass of glue deposited, using the linear model described in Section 3.5.3. The gantry then picks up a bridge tool via the vacuum spreader tool and positions it over a module. The bridge tool is lowered onto the module and vacuumed to the module parking plate before the gantry head releases it. The gantry head can then be retracted, and the spreader tool rotates so that when it is lowered again it will be able to pick up both the bridge tool and the module underneath it. Vacuum can then be released on the module and the bridge tool, allowing both objects to be raised above the module parking plate. The bridge tool can now be positioned correctly over the half-ring and lowered onto the glue patterns deposited earlier.

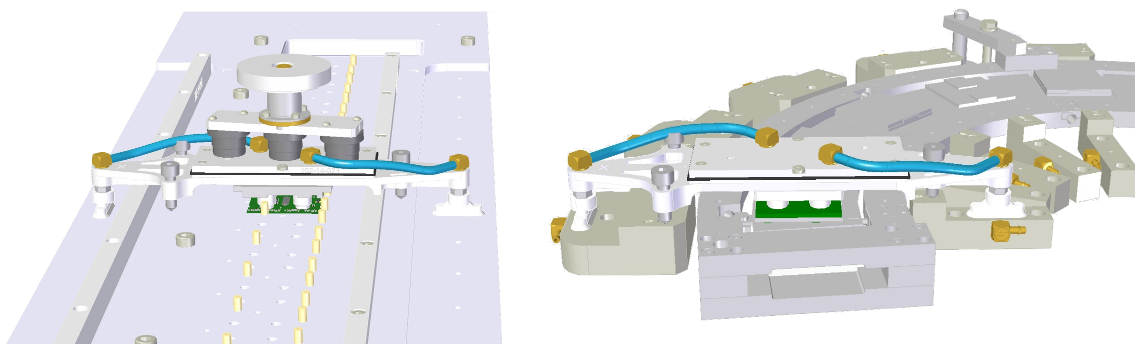

Figure 70: The concept for the module placement at Oxford.

A visualiser has been developed to allow verification of loading scripts prior to loading; a trace of a full loading procedure for a Layer-2 half-ring is shown in Figure 71.

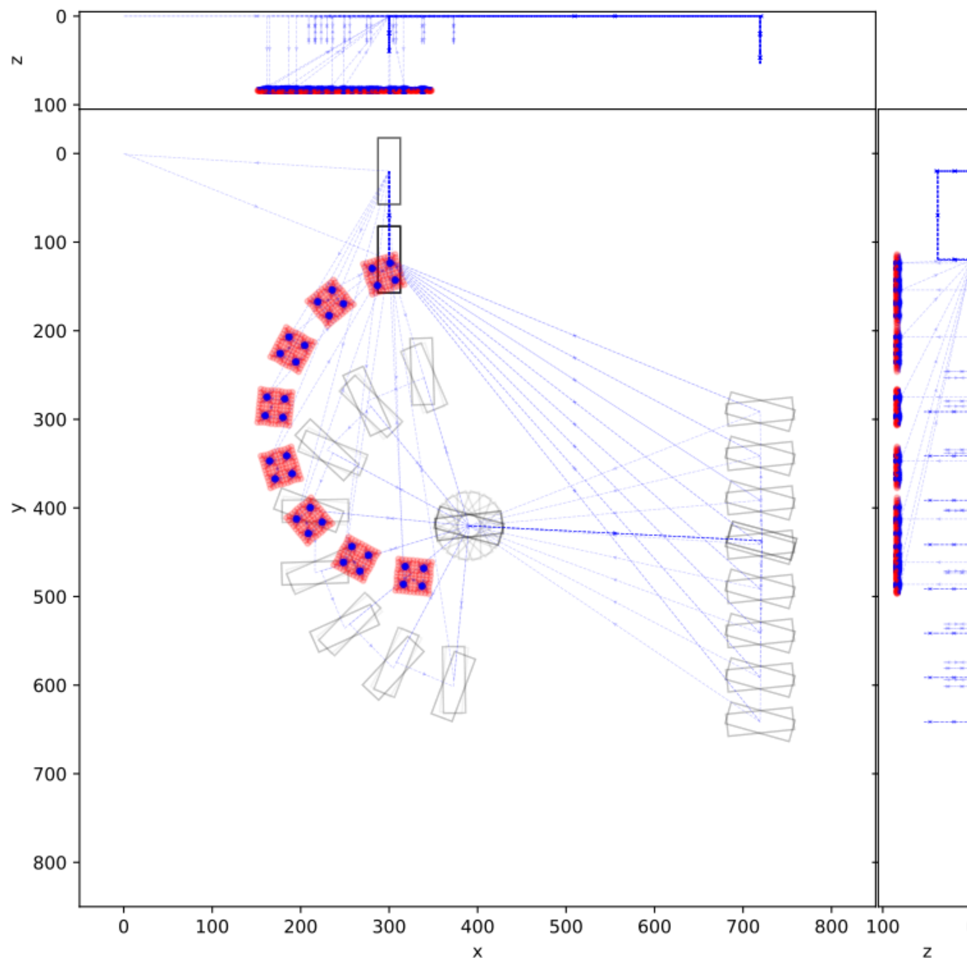

Figure 71: Visualiser trace of a full loading process, including deposition of glue patterns (note here that the syringe is offset from the spreader tool attachment location on the gantry head), and loading of modules held by bridge tools pre-placed on the half-ring.

Further information, along with a detailed operating manual for the gantry and software framework for generating loading scripts, can be found in Reference [17].

3.6 Loading technique – Genova and Lecce

The loading technique of the two Italian sites is based on a fully automatic "pick-and-place" strategy performed by a precision robot. The idea derives from the experience with the module loading for the legacy ATLAS Pixel detector. For the ITk Pixel Endcaps however, instead of a custom robot, the idea is to use a general-purpose precision gantry equipped with a custom head holding the tools needed for loading and programmed to perform the full module loading procedure with a minimum of manual human intervention.

Compared to the manual or automatic bridge technique, the drawback of the pick-and-place approach is that only one module at a time can be loaded and during the glue curing no other modules could be loaded or metrology performed because the gantry head is used to keep the module in position. The experience accumulated in the last year shows that thirty minutes after the deposition of the glue the pressure on the module can be safely released and the pick-and-

place head moved. In this sense, the dead time seems to be acceptable and possibly compensated by the overall speed of the automatized procedure.

3.6.1 Description of instrumentation and tooling

Both sites purchased the same gantry from **PI** (Physik Instrumente) with x, y, z and theta stages and honeycomb optical breadboard of 1m x 0.8m working area. The repeatability of the gantry movements has been measured to be of the order of 5μm. The absolute precision is obviously dominated by the mechanical deformations of the gantry and head components. However, a large fraction of these imperfections is systematic and can be corrected with an appropriate calibration. The resulting absolute precision over the full working area after calibration is of the order of 25μm. Some improvement in the calibration procedures is still possible, therefore slightly better results could be achieved in the future.

A key point of the loading-head design is that the suction cups handling the module are mounted on the theta stage with a load cell allowing a continuous measurement of the force exerted during pick-up and placement on the half-ring. In particular, during placement above a patterned glue layer, the correlation between load cell weight reading and final glue layer thickness can be used, together with the position of z stage, to ensure that the module is properly placed. Pressure control is also useful when the glue is doped with silica spheres of precisely controlled diameter to enforce a minimum glue thickness, because it can prevent excessive forces to be applied on a limited surface of the FE chip.

The z-stage of the gantry head holds the syringe of a volumetric glue dispenser used to deposit a precise SE4445 glue pattern on the half-ring surface. The geometrical precision of the pattern is guaranteed by the gantry while the uniformity in volume is guaranteed by the volumetric dispenser. The volume and shape of the deposited glue can be checked after each 4-fold pattern deposition by scanning it with the confocal z-profilometer held by the gantry's head (see below).

Finally, the z stage holds a camera with a microscopic telecentric lens, allowing precise (2μm) measurements on the x-y plane and a chromatic confocal profilometer providing contactless measurements of the z coordinate with a precision of 1μm.

Two vacuum parking tools are located on the periphery of the gantry boards. The primary function of these tools is to hold modules in position during metrology and pick-up. The tools are also used to perform tests of glue deposition and tests of placement, with or without glue, and for other measurements or calibrations (e.g. compensation of mechanical errors during rotation of the theta stage or measurement of the exact position of the syringe needle).

3.6.2 Schematic description of the loading procedure

In this section we describe the steps that are performed for gluing a module on a half-ring. We assume here that the half-ring is mounted on its handling frame and that bus tapes have already been glued on both sides.

1) The handling frame is fixed on the gantry's breadboard with an orientation such that the handling frame's platforms designed for holding each of the half-ring's fixation lugs are facing upwards.
2) A height map of the half-ring is measured to ensure global and local (in each module site) planarity within specifications and co-planarity with the gantry table (Figure 72). In general, the loading procedure can compensate inclination of the local support relative to the table in the module area up to 150μm. Calibrated shims below handling frame links and end pieces could be used to improve the half-ring co-planarity if needed, but this is not expected to be necessary if all the parts are within specifications and correctly assembled.

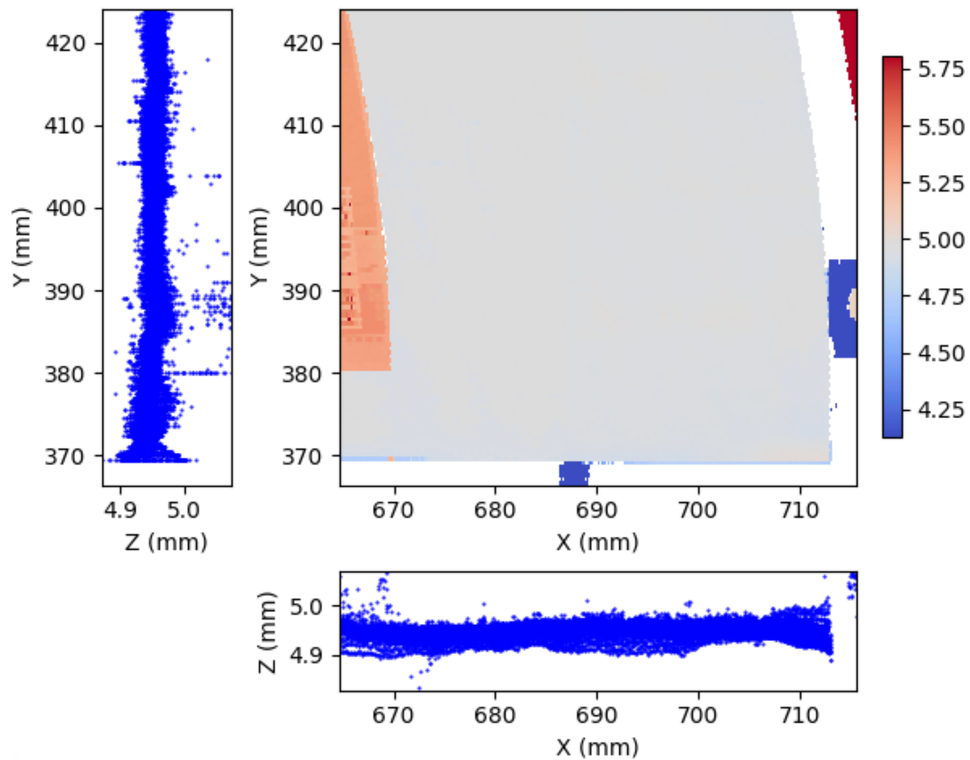

Figure 72: Example of a half-ring profile measurement in a module region.

3) Using the gantry's microscope, the x-y positions of the half-ring fiducial points are measured and the half-ring reference frame with respect to the gantry's reference frame is calculated as illustrated in Section 3.1.2.
4) The position of the bus tape pads in the half-ring reference system is measured with the microscope and verified to be compliant with the specifications (Figure 73). The conformity of the inner rim after tape gluing is also verified.

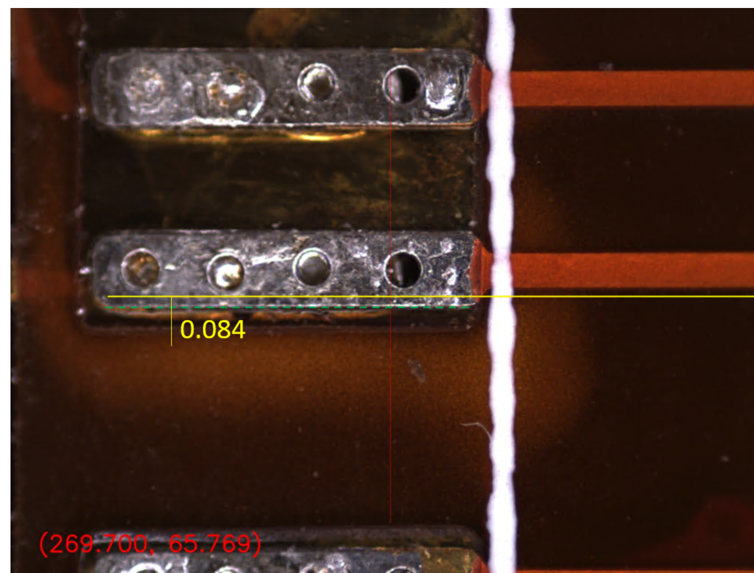

Figure 73: Measurement of the offset between power tape reference pad (in green) and module nominal position (in yellow).

5) The module is prepared for loading. This procedure implies the extraction of the module from the carrier, the removal of testing pigtails, and the removal of the flex frame with an appropriate tool. This is a delicate operation that must be executed in a clean environment, possibly under a microscope. After preparation, the module is placed in a gel pack, moved to the gantry area and placed on the gantry's parking tool using a vacuum pickup pen.
6) Using the gantry's microscope, the x-y position of the module's fiducial points is measured and the module's central position and orientation before pick-up are calculated. The shift between the flex and the bare module is measured and verified to be in spec. A compensation for a possible shift of the flex pick-up points with respect to the module centre is calculated.
7) Using the gantry confocal optical pen, the module height around the four flex pick-up circles is measured (with vacuum on and off) and verified to be within specifications.
8) The pick-up head is placed on top of the module and lowered until the force measured by the load cell is 300g. At this point the vacuum is removed from the parking tool and opened on the pick-up tool. The module is picked-up the from the parking tool and placed on the half-ring in the pre-calculated position. This deposition without glue ("dry run") is useful to verify the correct positioning and to measure the assembly profile (half-ring + module) without glue.
9) The x-y position of the module's fiducial points and z profile of the module's upper surface are measured in dry-run placing conditions (Figure 74). The module is then picked from the half-ring and placed back on the parking tool. Position and rotation are re-measured.

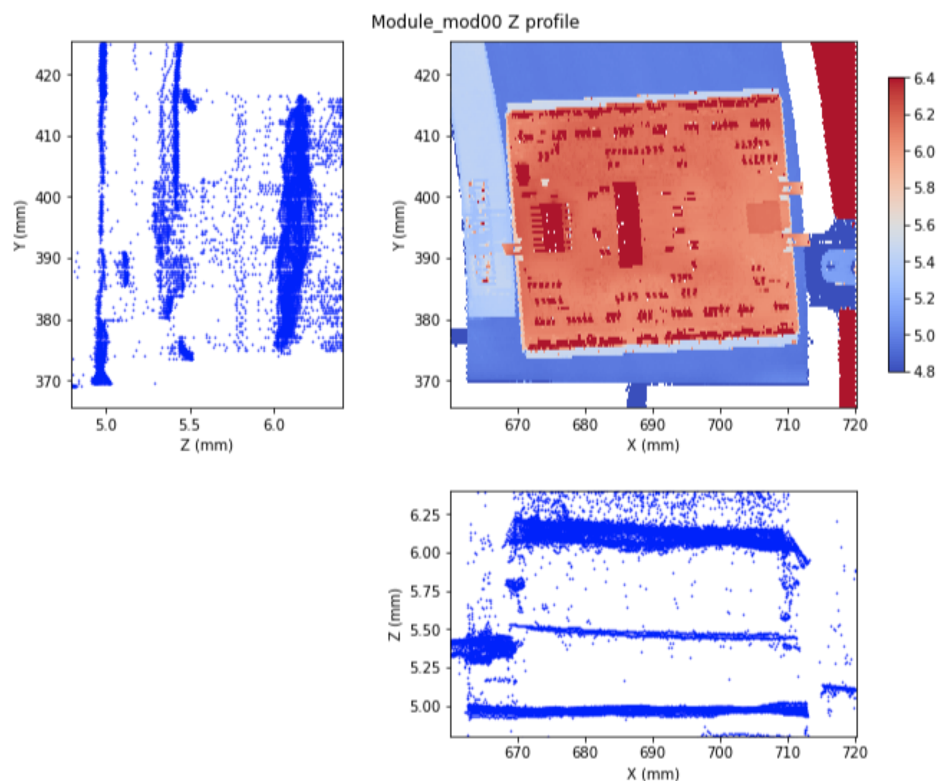

Figure 74: Example of a z profile with a module placed on the half-ring without glue (dry run).

10) A disposable syringe (prepared as illustrated in Section 3.6.3) is placed on the gantry's glue dispenser. The x-y-z position of the syringe needle is measured using a precision jig or with the help of external USB cameras.
11) (optional) A complete glue pattern made of four snowflakes with eight radial rays is deposited on a 41cm x 42cm x 0.044cm glass placed on the auxiliary parking tool. The weight of the glue is measured, to ensure it's in the expected range (0.40 +- 0.01 g). Additional measurements can be performed, if needed: the volume of the individual flakes can be measured using the confocal pen and a deposition of a second glass on top of the glue pattern can be performed to verify the glue coverage after a compression of 200 g for 30 minutes.
12) The syringe needle is moved on the half-ring surface where the module should be placed, and a complete pattern of glue is deposited on the half-ring. The syringe is then removed from the glue dispenser.
13) The module is picked up from the parking tool applying a 300 g force and placed in the nominal x-y position and with the nominal angular orientation on the half-ring above the glue pattern. Corrections to take into account the shift between the bare module and the flex are applied if needed. The module is then slowly lowered onto the glue pattern while continuously monitoring the global applied vertical force by measuring the calibrated unbalance of the loading cell strain gauges' Wheatstone bridge. Once the target total applied force (typically 200g) is reached, the lowering of the module onto the glue pattern is stopped, and the module is kept in position by the gantry's head for the time needed for sufficient curing of the glue (~30 min). The position of the z stage and the pressure applied are continuously monitored and the force is always kept below 200g.
14) The vacuum on the head pick-up tool is then released and the gantry's head is moved away from the module.
15) Using the gantry's microscope, the x-y position of the loaded module's fiducial points is measured, and x-y position residuals calculated.
16) Using the gantry's confocal optical pen, the z profile of the loaded module's upper surface is measured, and the achieved glue thickness X-Y distribution is calculated by subtracting the dry-run module's z-profile measured at point 9 (Figure 75).

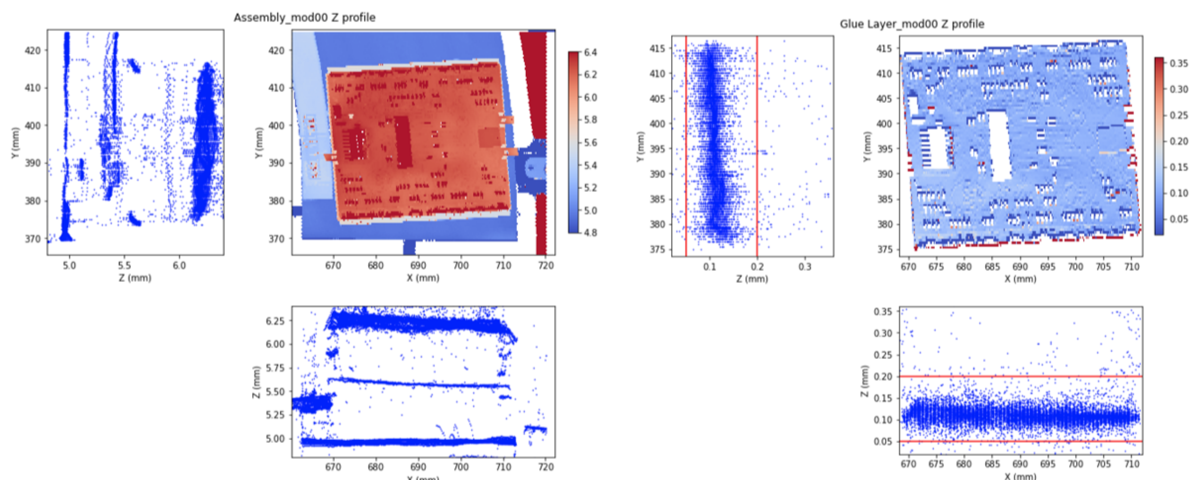

Figure 75: Example of a z profile of a module glued on the half-ring and corresponding glue profile obtained subtracting the dry-run profile in Figure 74.

All the steps are fully controlled via software, and the intervention of an operator is only needed to confirm the readiness for each step and at points 9 and 12 to mount and dismount the syringe.

Steps 5-16 are repeated for each module on a half-ring face. Then the handling frame is flipped, and the procedure is repeated for the other half-ring side.

If needed (e.g. to perform tests on a sub-set of modules), the handling frame can be removed from the gantry and then repositioned to complete the loading. In this case, steps 1-3 must be repeated.

The typical duration of a module loading procedure, including glue preparation and module specific metrology is of the order of two hours. Two more hours per side are needed for positioning and global metrology. Some improvement in the timing could perhaps be achieved by improving the control software and dropping some test(s) that may turn out to be redundant after the pre-production phase.

The module placement precision relies on the gantry precision and on the calculated transformations between the different reference systems (gantry, camera, z profilometer, half-ring). As discussed in Section 3.6.4, we are confident that this approach is sufficient to meet the specifications (150 µm precision in module positioning). Nonetheless, we are considering installing a micro-camera close to the pick-up tool to be able to monitor (and possibly fine tune) the module position during placement and initial curing.

3.6.3 Glue preparation and deposition

The glue is prepared starting from a 220 ml cartridge of the two-component SE4445. The cartridges are rotated slowly for 24 hours before being dumped in two cups which fit the glue planetary mixer. The white component is mixed with 106 um diameter silicon spheres for a 2% concentration in weight, resulting in a 1% concentration in the total glue weight when mixed with the gray component.

Each syringe of glue is prepared by mixing the two components with the mixer for four seconds. About 2cc of each component are extracted using two different 3cc syringes (without needles but with plunger). The two parts are poured in a small cup in equal weight and mixed with a stick. When the two parts are well mixed a third 3cc syringe without needle is used to pick-up the glue. In this last operation is important to avoid air bubbles in the syringe. A dispenser syringe of 3cc, without needle but with a piston all the way down, is filled by glue from the tip side. In this operation the syringe tip is coupled to the tip of the syringe with glue by a pierced tip cap and the glue is poured from one syringe to the other by slowly pushing the plunger. After this the tip cap must be removed and replaced with a needle.

3.6.4 Gantry calibration for metrology

The XY metrology of the loading is provided by the microscope placed on the gantry z-stage and the gantry XY encoders readings. The gantry native software and firmware allow to load correction maps for the XY encoders readings. The correction maps were measured in-situ using a 24-inch by 28-inch machine-calibrated plate with a screen-printed array of 25mm x 25mm squares.

After gantry calibration the microscope defines the XY gantry reference systems and every additional instrument or tool position must be referred to the microscope. Specific procedures were put in place in order to provide X, Y, and Z coordinates shifts for the z-profilometer, glue syringe, and suction cups barycentre.

The glue syringe coordinates shifts are corrected each time a module is loaded because the syringe is replaced with a new one. The suction cups' barycentre coordinates shift depending on the angle of the gantry theta stage, because the suction cups barycentre doesn't lie on the theta stage rotation axis. In order to correct automatically for this, it is necessary to measure the

suction cups’ barycentre coordinates shifts and the distance from the theta stage rotation axis for a default angle. In fact, from these four parameters it is possible to calculate the suction cups’ barycentre coordinates shifts for every theta angle.

3.6.5 Safety Considerations

The adoption of a fully-automated pick-and-place approach create concerns about safety during operation that must be seriously addressed. The main risk is to accidentally touch the half-ring or a module as a consequence of an improper movement of the gantry head. In the past year of intense development, we actually had several accidents where the gantry head was improperly driven by the controlling software and collided with some part of the setup. With one exception, the accidents were without any consequence. However, in one case the surface of a half-ring was seriously damaged by the syringe holder. A similar accident during production would have caused the loss of a half-ring and of all the modules already loaded. We clearly have to work hard to mitigate this risk. We have identified the following strategies:

- Implementation of position-dependent checks directly in the gantry controller. It is possible to implement low-level functions running continuously on the gantry hardware controller and check that potentially dangerous regions are not accessed at all (even following high level software malfunction) or only accessed at very low speed and performing micrometric movements.
- Use of a unique software framework to control all the steps of the loading procedure and provide software assistance for the few manual interventions needed. Manual editing of configuration files must be avoided. Any dynamically-computed parameter (e.g. half-ring reference system or module pickup position) should be verified with automatic measurements and validated by an operator before starting loading procedures.
- Strict software qualification process: each new version of the controlling software must be certified with extensive tests on non-production items before being used in production.

4 Results of Loading Design Validation

4.1 Loading Validation at RAL

Twenty-two RD53a quad modules were loaded onto the Pixel Outer Endcap demonstrator "Ring-1". Modules were first loaded onto side B, then onto side A.

The first module loaded onto Ring-1 was tested after loading and found to be performing as it had before loading. It was later damaged by a lab-equipment malfunction, which, while unfortunate in light of the scarcity of modules at the time, did provide us with an excellent opportunity to test the re-workability of SE4445: the module was removed by simply sliding a pallet knife carefully through the SE4445 layer between the module and the half-ring. This proved straightforward, and the module came off in one piece. Remaining SE4445 was removed from the half-ring surface with isopropanol and another module was successfully mounted in the same place.

4.1.1 Glue thickness

The thickness of each module is measured before loading using the OGP SmartScope. The module is vacuumed down onto the pickup jig, and the thickness is measured at four points on the module PCB – at the centre of each of the four circles provided for pickup vacuum cups.

The surface height of the half-ring is measured before loading using the Aerotech gantry equipped with the Keyence laser displacement meter, at each of the locations where the centre of a module pickup circle will be located.

The thickness of the adhesive is then measured after loading using the Aerotech gantry equipped with the Keyence laser displacement meter. The height of each module is measured, at the the centre of each of the four circles provided for pickup vacuum cups. From each of these heights the corresponding module thickness is then subtracted, to give the glue thickness.

Glue thicknesses for all modules on Ring-1 are listed in Table 6, and plotted with the mean and standard deviation in Figure 76. All glue thicknesses are found to be within the required range of 50 to 200 microns, and averaging close to the target thickness of 100 microns.

Position	TL	TR	BL	BR	Mean
1	100	123	104	116	111
2	101	101	81	98	95
3	116	111	89	92	102
4	112	120	98	109	110
5	111	108	100	101	105
6	107	111	100	103	105
7	102	103	94	99	100
8	93	93	91	97	94
9	95	97	100	107	100
10	104	114	94	98	103
11	85	108	91	116	100

Position	TL	TR	BL	BR	Mean
1	110	107	101	104	106
2	100	112	103	110	106
3	107	94	94	96	98
4	115	129	109	137	123
5	107	129	109	138	121
6	90	117	96	105	102
7	100	128	108	107	111
8	92	90	87	79	87
9	86	84	86	100	89
10	111	113	108	97	107
11	107	105	104	107	106

Table 6: Measured glue thicknesses for all modules loaded on Ring-1. Left table: side A. Right table: side B.

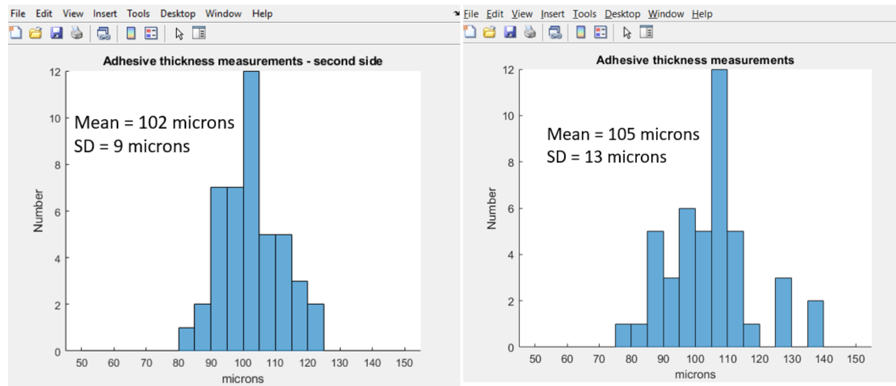

Figure 76: The glue thicknesses for the modules loaded on Ring-1 side A (left plot) and side B (right plot).

4.1.2 Placement accuracy

Loaded module locations are measured on the OGP SmartScope.

The location of the half-ring is measured in reference to the two fiducials at the ends of the half-ring. This defines the ideal module locations.

The XY positions of each corner of each module are measured at the corner of each corresponding FE chip. Due to this, the following module placement measurements are a conservative estimate of loading accuracy, as they include module construction and FE chip dicing accuracy.

Figure 77 and Figure 78 show the deviation from the ideal location for module corners respectively for side A and side B of Ring-1.

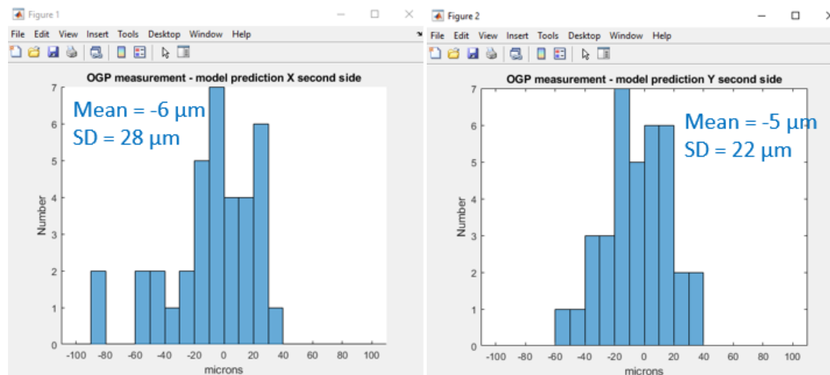

Figure 77: X (left) and Y (right) deviation from the ideal location for modules corners for modules on side A of Ring-1.

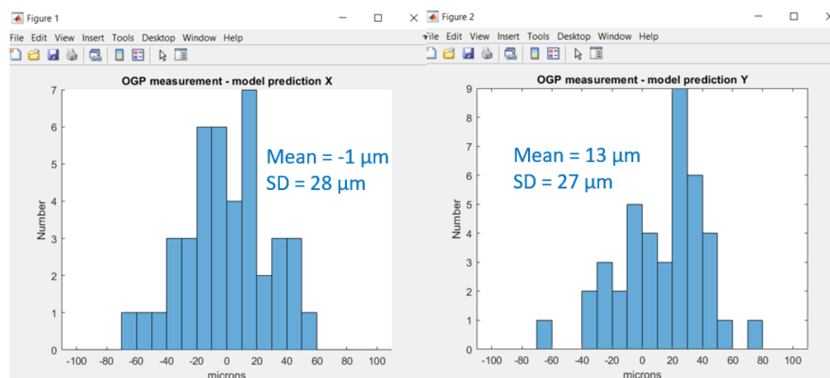

Figure 78: X (left) and Y (right) deviation from the ideal location for modules corners for modules on side B of Ring-1.

The RMS of the distribution is 28 microns in X, and 25 microns in Y, averaging over both sides.

For side A, two modules are omitted from the plots. Module MPP6 (position 4) was known to be significantly non-standard in size. Module LivThick10 (position 1) was omitted as a time saving measure, being the final module to be loaded. Module 6108-20 (position 11) shows the effect of a cut error: the RH corners of this module are placed within 47 microns in X of the predicted points, however the LH corners show an error of 87μm, indicating a dicing error of 40μm from the nominal size.

For side B, three corners are omitted from the plots, as these were damaged and could not be used for alignment.

4.1.3 Loaded modules functionality check

This topic is covered in Section 5.

4.1.4 TFM cross-check

The Thermal Figure of Merit (TFM) of a local support structure quantifies the worst-case thermal resistance along the path between the cooling pipe and the module. The TFM is defined as the ratio between the temperature difference (ΔT) between the hottest point on the face of a structure and the evaporation temperature of the coolant, and the module's power per unit of area. The measurement of the TFM on prototype half-rings loaded with silicon heaters has been covered extensively in previous reviews [1] [18].

It would be extremely interesting to measure the TFM (Thermal Figure of Merit) on Ring-1 as it is the only Outer-Endcap local support structure so far to be fully loaded with real modules (as opposed to silicon heaters); it is well known that the power distribution across the surface of real modules is non-uniform, in contrast to the uniform power distribution in silicon heaters.

It should be possible to run Ring-1 in the large (room-size) climate chamber at Liverpool and take a thermal image of the surface during operation. While it is difficult to measure absolute temperatures with a thermal camera due to calibration issues, temperature sensors could be fixed to the surface of the half-ring and these, together with the temperature sensors built into the modules, ought to provide the required calibration.

4.2 Loading Validation at Oxford

4.2.1 Glue thickness

Studies of glue-layer thickness have been performed both on a Nordson Pro4 dispense system, and on the Aerotech gantry. Oxford uses 94-100um CoSpheric-brand silica spacer spheres within the glue mixture for layer-thickness control.

Results from depositions between glass slides on the Nordson Pro4 with deposited masses between 75mg and 90mg demonstrated a thickness of 114.5um on average, with a tolerance range of 7.5um (6.7%) observed either side of this, measured using a micrometer to determine the thickness of the slides and pattern before and after deposition and glue setting. These results are shown in Figure 79, and were gathered across a range of samples, and depositions with clear issues (for example, needle drippage) that would be rejected and re-run during production were marked as outliers and excluded from this study. It was also observed that significant over- or under-deposition of glue (i.e. above 90mg or below 75mg) resulted in pattern thicknesses outside this range.

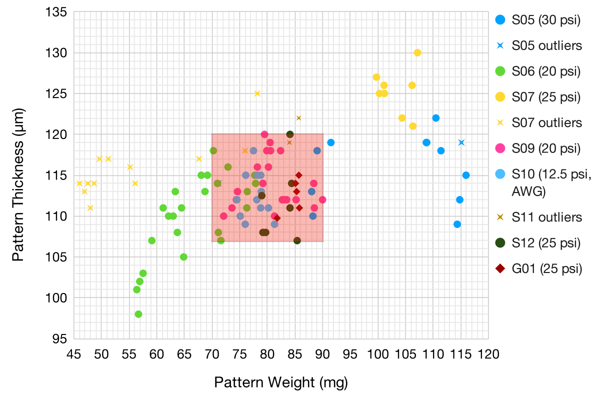

Figure 79: Pattern thickness vs. pattern weight for test depositions performed on the Nordson Pro4 glue robot (samples S05-S12), and the Aerotech gantry (sample G01).

A small series of test depositions were also performed with glass slides on the Aerotech gantry – these are marked in Figure 79 as sample G01 and exhibit the same behaviour as was observed on the Nordson Pro4.

Layer heights were also checked during initial loading test runs on the Aerotech gantry with the complete tooling setup and a prototype aluminium half-ring. Glass pieces were loaded onto aluminium, and the layer heights measured using a Keyence SmartScope, with an estimated accuracy somewhat lower than that for the micrometer. The results are shown below in Table 7. They show greater variability than was observed for the glass-glass depositions, but are still within the specification of 100^{+100}_{-50} µm. An increase in layer height from over-deposition of glue was observed for alu5 and alu6 due to user error during flow rate calibration – this issue was solved for later loading attempts, and the solution (purging the needle prior to the flow rate measurement) has been integrated into our internal documentation.

Loading Position	Glue Thickness (µm)
alu5	146
alu6	166
alu7	109
alu4	118
alu3	125

Table 7: Glue layer heights for preliminary loading runs of glass slides onto an aluminium dummy half-ring. The positions on the half-ring are given in chronological order of loading.

4.2.2 *Placement accuracy*

The placement accuracy has been measured for the first seven loading trials performed on the Aerotech gantry, with six glass slides and one mechanical dummy module loaded onto an aluminium dummy half-ring. The physical results are shown in Figure 80, and the figure shows the chronological progression of loading trials. Initial loading tests in positions alu5 and alu6 were subject to an initial learning process and show problems with the glue deposition as a result; later positions showed good quality of the glue deposition. The loading of alu1 with a

mechanical dummy was performed with no damage to the wire bonds or SMD components during loading, verified by the comparison of images taken using the SmartScope before and after loading.

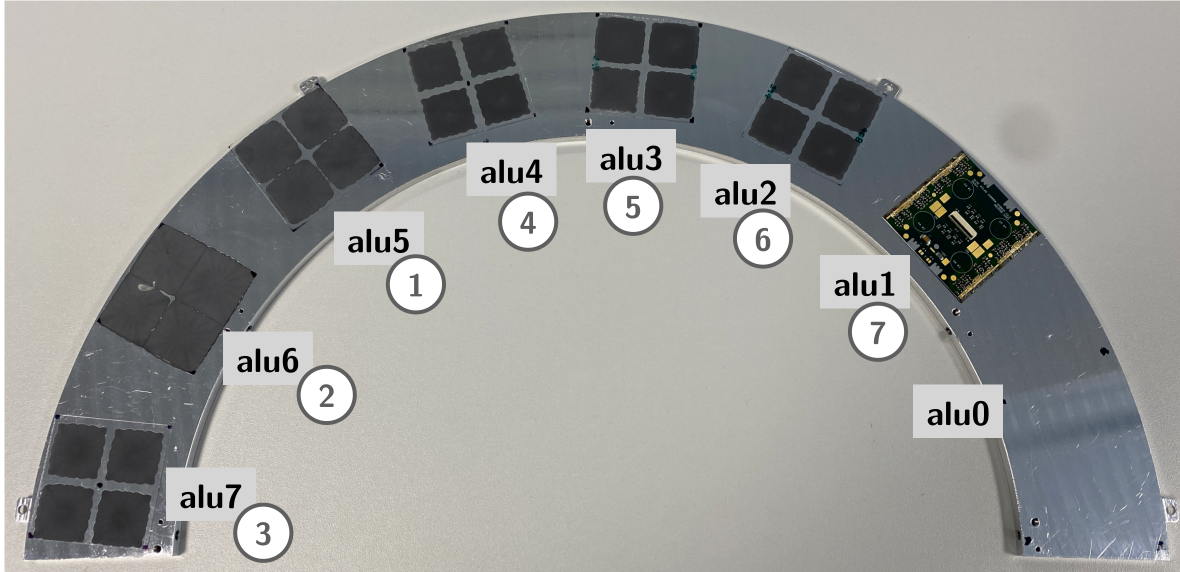

The placement accuracy for the seven loaded positions is summarised in Table 8 and does not meet the expected performance based on experience using the gantry for module loading. The accuracy of the gantry calibration was assessed by cross-checking measurements of module positions using the SmartScope. Module positions and rotations after loading were determined using the same fiducial fitting method used during placement in order to factor out effects from small variations in the size of the loaded glass slides.

	Aerotech Gantry Offset			**SmartScope Offset**			**Agreement**		
	X (µm)	**Y (µm)**	**Phi (°)**	**X (µm)**	**Y (µm)**	**Phi (°)**	**X (µm)**	**Y (µm)**	**Phi (°)**
alu5	-2085	-102	89.733	-2114	-112	89.833	28.25	9.72	-0.100
alu6	-743	-694	0.217	-747	-712	0.349	3.64	18.96	-0.132
alu7	-1163	-351	-0.030	-1190	-333	0.048	26.36	-18.24	-0.078
alu4	-126	-166	-0.194	-142	-163	-0.047	15.69	-3.04	-0.147
alu3	-46	111	-0.245	-50	107	-0.098	4.02	3.50	-0.147
alu2	-229	310	-0.315						
alu1	-130	574	0.029						

Table 8: Loaded module offset from nominal position, given in chronological order of loading. Equivalent fiducial measurements on the SmartScope were used to cross-check the gantry calibration, and confirmed the significant inaccuracies observed during gantry loading. Comparison of the two datasets shows a gantry calibration accuracy within about 30um.

Significant deviations of several hundred microns were observed from the nominal position during loading. Careful observation of several dry loading runs showed potential slippage within the vacuum interface between the spreader tool and bridge tool during the loading

process. As a result, the spreader tool was redesigned (see Figure 81)to have a larger effective vacuum area and better hold vacuum on and through the bridge tool. Results for the placement accuracy using the new tooling are still outstanding.

Figure 81: Original (left) and redesigned (right) spreader tool in use at Oxford.

4.3 Loading Validation at Genova

Based on module-loading experience for the legacy ATLAS Pixel Detector, the Genova team designed and realized a multifunctional gantry's head (Figure 82) which, in addition to accomplishing the task of vacuum picking and placing the quad modules from/onto any suitably horizontal support under controlled vertical position, speed and total applied force, also provides the possibility of constantly monitoring the absolute X-Y position of one edge of the placed module in real time during its own placement. In addition, the head is instrumented with a chromatic confocal profilometer for accurate measurement of z-profiles over large surfaces (almost as large as the whole operational surface of the gantry's breadboard), and with a (currently pressure-operated, but asymptotically volumetrically controlled) glue dispenser for accurate glue pattern deposition. The continuous optical control of one edge of the module being placed is achieved by cleverly placing relative to the pick-and-place load cell a telecentric optical microscope. The same microscope, when the load cell is not holding a module under itself, has a free field of view that allows it to be used for accurate optical metrology of all objects (the half-ring, its handling frame and the modules, both before picking and after placing) involved in the precision module loading task. The main pick-and-place functionality of the gantry's head is accomplished by a load cell whose load force is continuously monitored by reading the calibrated unbalance of a Wheatstone-bridge configuration of four strain gauges glued inside the deformable cavity of the cell. The load cell is equipped with four suction cups, carefully equalized in their relative vertical position such that their four mouths, when relaxed, lie on a plane parallel to the plane of the gantry's breadboard, and whose relative X-Y position under the load cell matches that of the four round areas designed for module picking on the upper surface of the module's flex. The shape and elasticity of each suction cup are suitably chosen to allow the suction cup to maintain a sufficient residual flexibility after the basic deformation due to vacuum picking: the goal is to exploit this residual flexibility during the module placing phase, in interplay with the compression resistance of the silica-spheres-loaded glue, to compensate for possible initial non-parallelism of the two surfaces to be glued and eventually reach the desired glue thickness uniformity over the whole module's surface. An extensive set of tests, only partially illustrated in the following paragraph, has proved that this goal is indeed achieved even when the initial non-parallelism (or non-flatness) of the two surfaces amounts to few hundreds μm along each side of the whole module's surface.

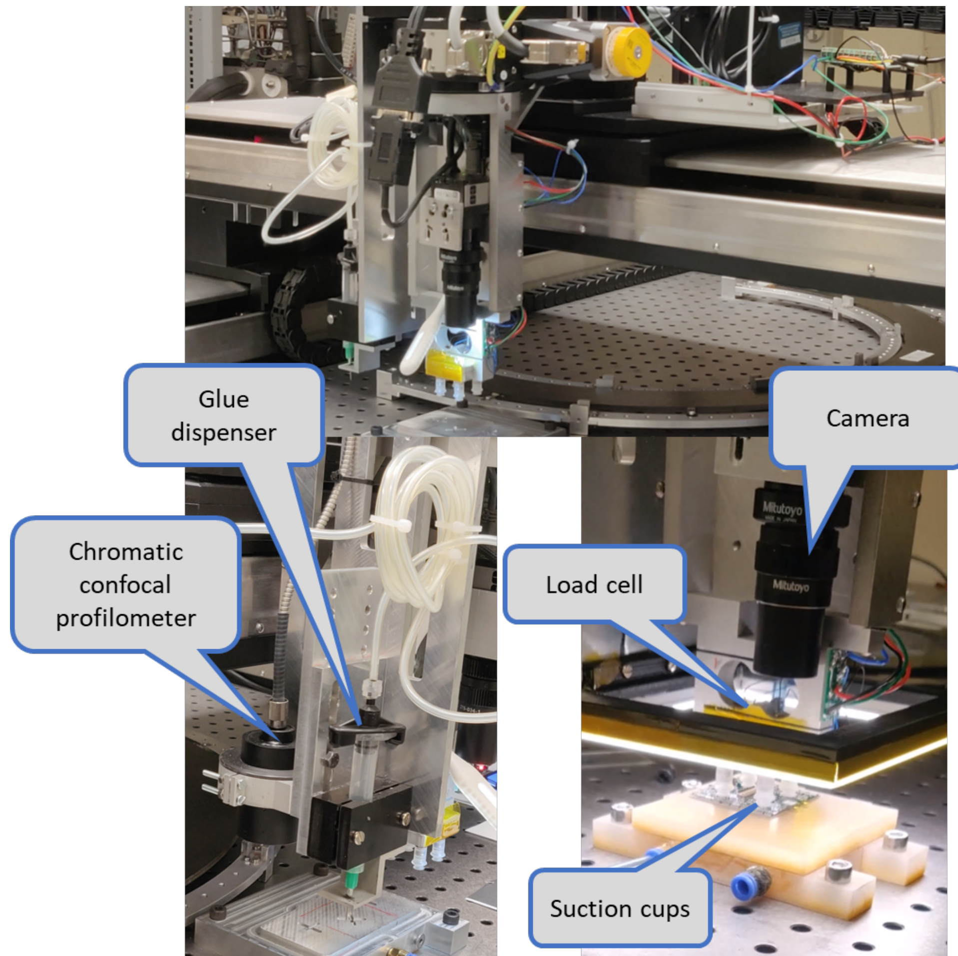

Figure 82: The multifunctional Genova Gantry's head.

4.3.1 *Glue thickness*

Glue thickness uniformity after curing is estimated for each loaded module by subtracting the z-profile of the module's upper (flex) surface measured at dry-run (i.e.: no glue) placing from the z-profile of the same surface measured after gluing. Figure 83, Figure 84, Figure 85, and Figure 86 show the X-Y glue thickness distribution and its X and Y projections for all four modules loaded on a production-grade Layer-4 Half-Ring: ITkPixV1 digital modules placed in position #00 and #12 respectively, and sensor-equipped RD53A modules placed in position #01 and #11. All measured glue thickness values have been found to be everywhere within the design (50 µm, 200 µm) range, displayed in both projections by two limiting red lines. The same compliance with the design specifications was obtained on a larger sample of "dummy-module" loading operations performed by gluing a set of flat and thick (650 µm) 4cm x 4cm silicon slabs either on the same production-grade Layer-4 half-ring or on other supports.

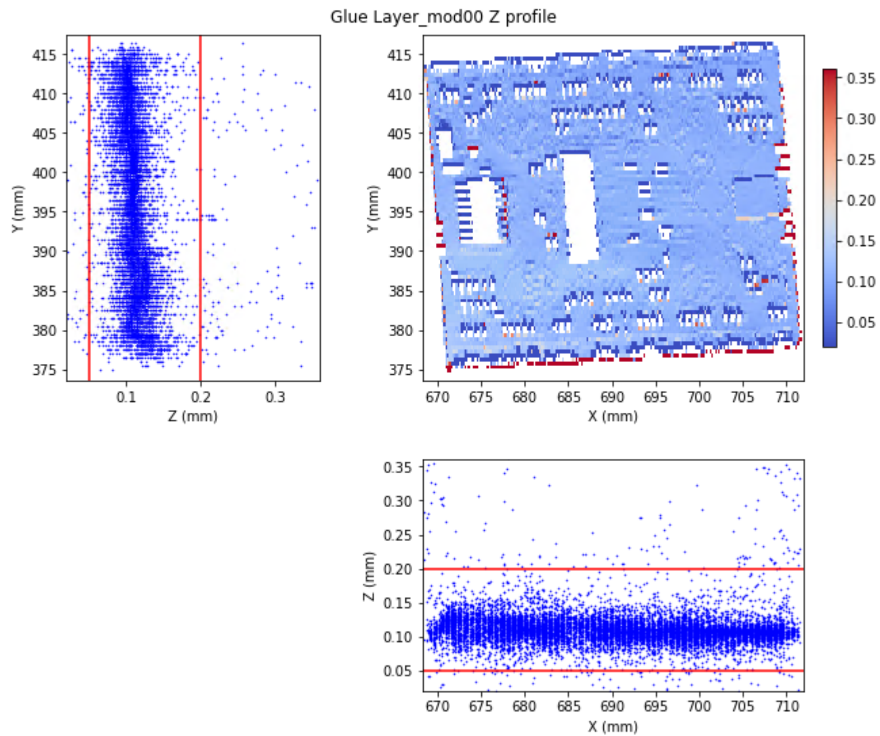

Figure 83: Glue thickness XY distribution measured for the digital ITkPixV1 module glued in position #00 on the Layer-4 half-ring

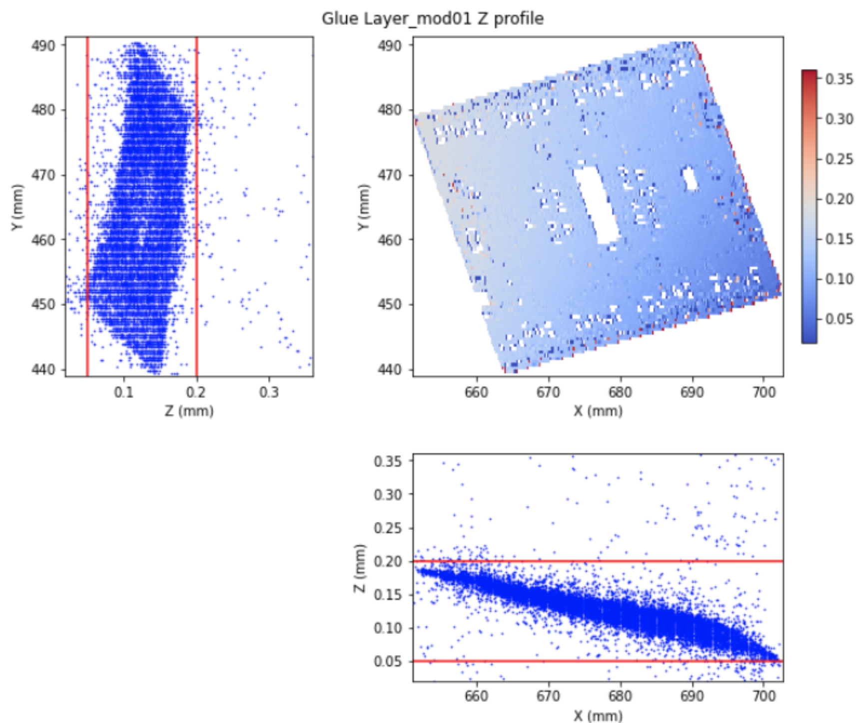

Figure 84: Glue thickness XY distribution measured for the sensor-equipped RD53A module glued in position #01 on the Layer-4 half-ring.

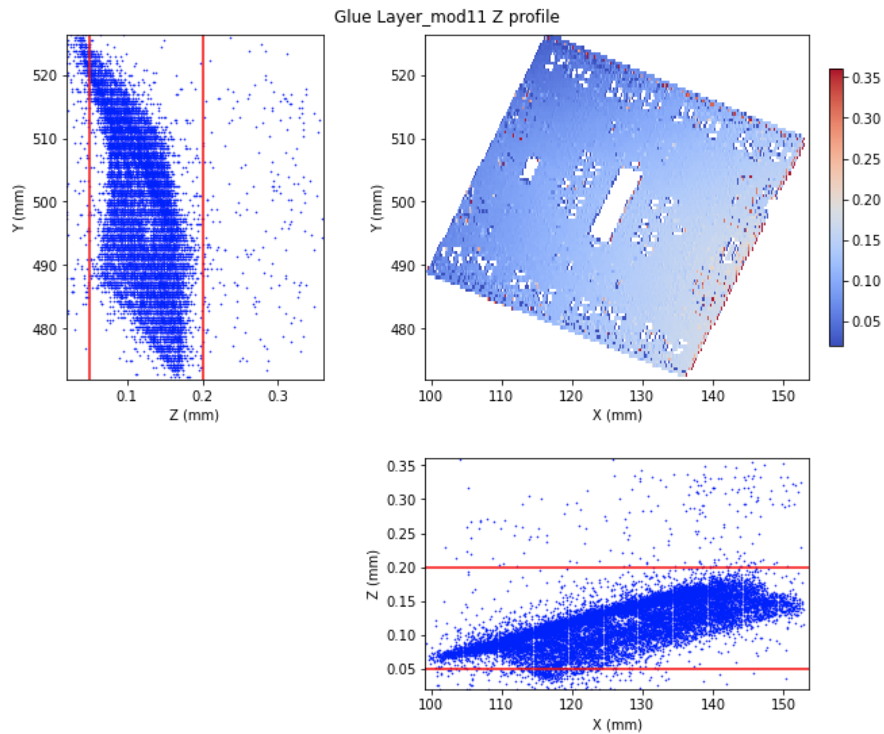

Figure 85: Glue thickness XY distribution measured for the sensor-equipped RD53A module glued in position #11 on the Layer-4 half-ring.

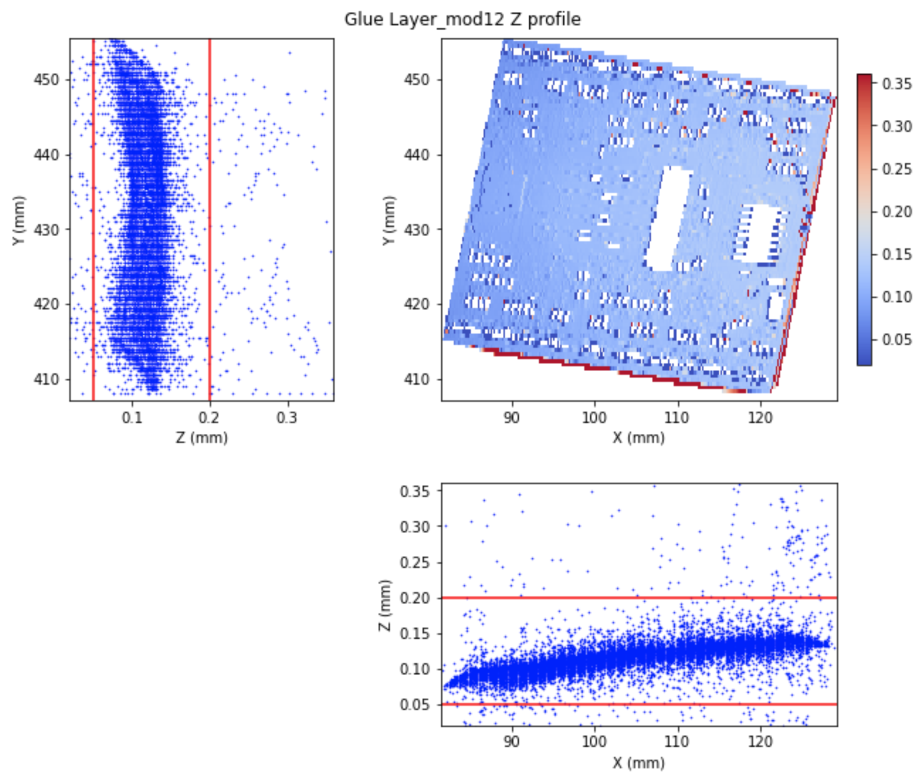

Figure 86: Glue thickness XY distribution measured for the digital ITkPixV1 module glued in position #12 on the Layer-4 half-ring.

4.3.2 *Placement accuracy*

Following the X-Y calibration of the Genova gantry using the telecentric optics equipping the gantry head and a high precision 2D crystal mask, the residual intrinsic X and Y inaccuracy were measured as a function of the X-Y position on the gantry's breadboard. The results are displayed in Figure 87 (X residuals) and Figure 88 (Y residuals). The measured absolute residuals on each coordinate are everywhere well within a ±20 µm band. Even though this, combined with a measured repeatability of ≤ 5 µm, is well within the requirements, we plan for the future to further correct for at least part of this residual inaccuracy.

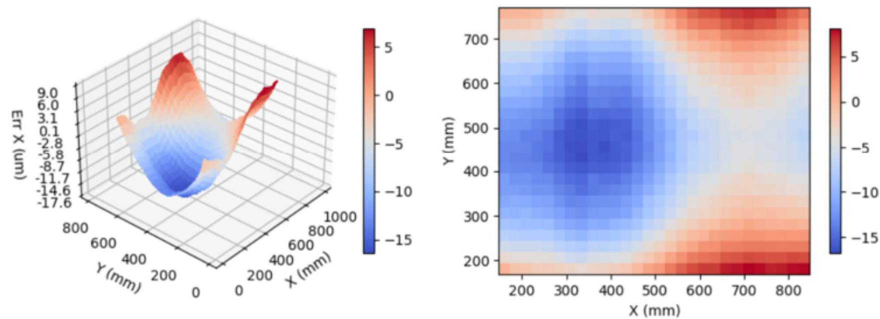

Figure 87: Residual X inaccuracy as a function of the XY nominal coordinates as measured after Gantry's on-site calibration.

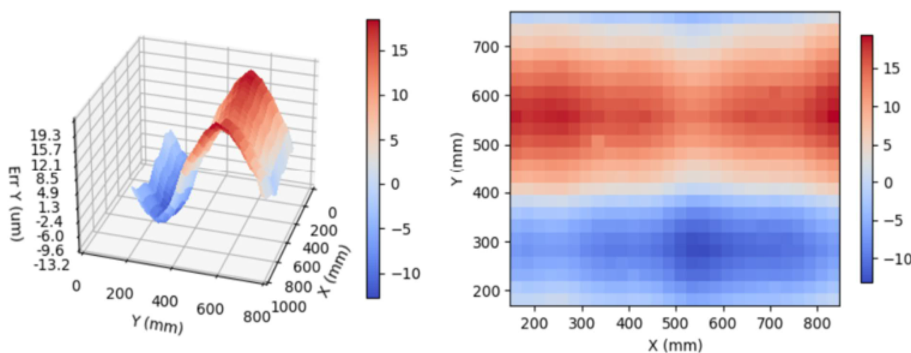

Figure 88: Residual Y inaccuracy as a function of the XY nominal coordinates as measured after Gantry's on-site calibration.

An example of the placement accuracy and precision obtained when placing a module in a given position and at a given orientation (in "dry-run" mode: i.e., without glue) on a half-ring after having picked it from the parking position is shown in Figure 89, which shows the distribution of the residuals in the module's centre position and in the module's azimuthal orientation in the XY plane relative to the target position and orientation respectively. The measured inaccuracies (~ 37µm in position and ~0.11° in orientation) are attributable to the non-perfect, but tolerable, correction for the non-coincidence of the gantry's rotation axis and the axis parallel to it and passing through the centre of the picked-up module. This introduces a theta-dependent inaccuracy which, albeit within specs at a fixed angle, we plan to further address before starting the production phase. The theta-dependence of this systematic effect is the most probable justification of the much wider distribution of residuals that is obtained when performing the same kind of study on modules placed in the same position but at many different ideal orientations spanning the whole range covered by a single half-ring (-90°, +90°): see Figure 90.

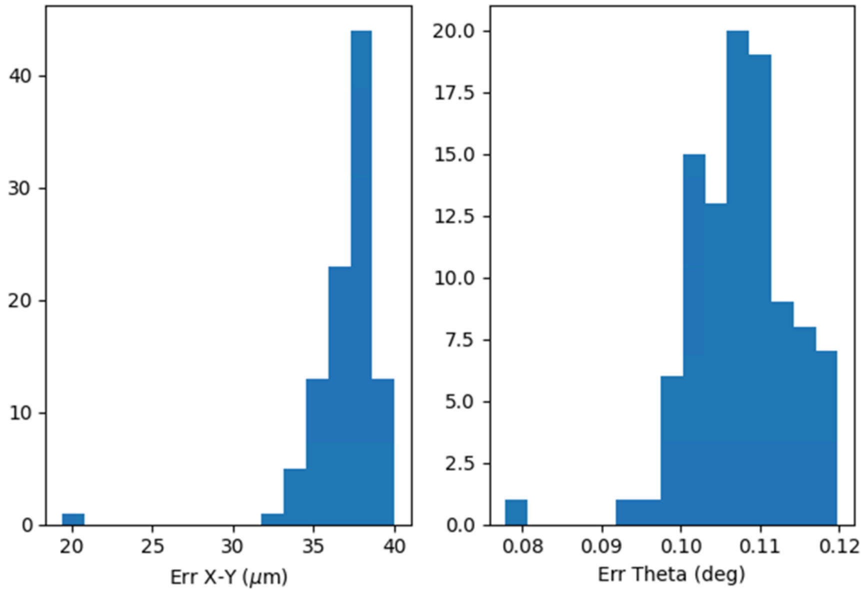

Figure 89: Assessment of the intrinsic (not attributable to the local support non-horizontality and/or glue/spheres effects) module placement accuracy and precision at a given orientation: residuals in the module's center position and in the module's azimuthal orientation in the XY plane relative to the target position and orientation in a large sample of repeated module's pick-and-place operations in "dry-run" mode at a fixed placement angle (70°)

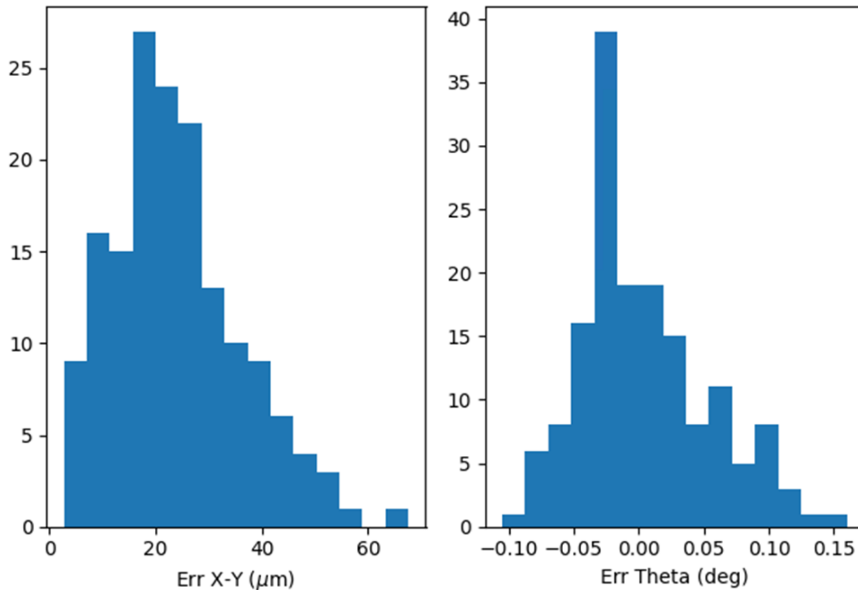

Figure 90: Assessment of the intrinsic (not attributable to the local support non-horizontality and/or glue/spheres effects) module placement accuracy and precision on a full range of orientations: residuals in the module's centre position and in the module's azimuthal orientation in the XY plane relative to the target position and orientation in a large sample of repeated module's pick-and-place operations in "dry-run" mode at placement angles ranging between -90° and 90°.

Figure 91 and Figure 92, finally, show two examples of module placement accuracy in "real life" conditions. They show two corners' position of the flex of the ITkPixV1 module glued in position #00 on the Layer-4 half-ring and compare them with the ideal target position for each of them (displayed as the nearby edge of the yellow shape in each figure). One corner ("corner 3") is almost perfectly placed on target, while the other is located ~110 µm from it.

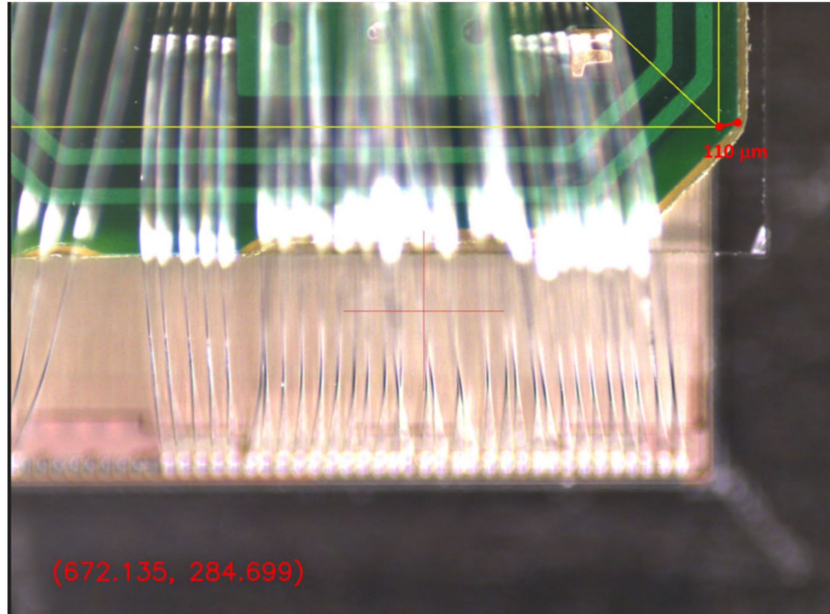

Figure 91: Assessment of the achieved accuracy of placement when gluing ITkPixV1 module in position #00 on the Layer-4 half-ring: flex corner 0.

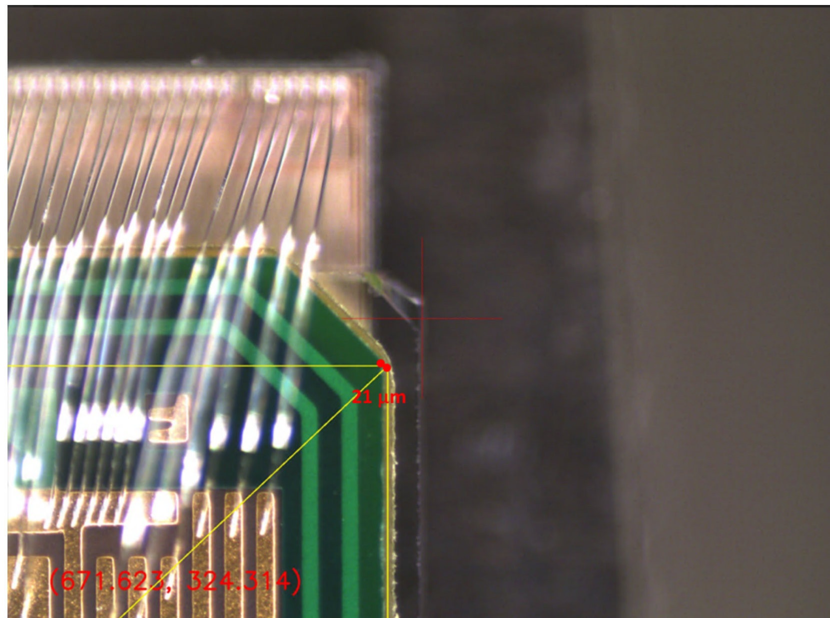

Figure 92: Assessment of the achieved accuracy of placement when gluing ITkPixV1 module in position #00 on the Layer-4 half-ring: flex corner 3.

4.3.3 Loaded modules functionality checks

After having loaded four modules (ITkPixV1 digital placed in position #00 and #12 respectively, and sensor-equipped RD53A placed in position #01 and #11) on the production-grade Layer-4 half-ring, and before connecting them to the bus tape previously glued on this half-ring, each of them was checked to be functional and with a performance comparable to that observed on it before loading. Powering and data readout, at this stage, were performed by connecting one module at a time to the power supply and to the YARR [19] readout system respectively using the standalone testing power and data pigtails that equipped the modules in their carrier before loading. Both testing pigtails were connected at the other end to an ad-hoc single-module powering and data transmission PCB, respectively, with the power one providing also monitoring functionality of the module's temperature. Before and then during module powering, the half-ring was cooled by circulating chilled water (T_{water} = 15°C) in the half-ring titanium pipe. During the tests, the loaded half-ring was kept in controlled humidity conditions (dew point ~1-2°C) within a properly interlocked lead shielded box which allowed us to also perform X-Ray scans with a mini-X tube. All functionality tests (threshold, digital and analogue scan, as well as readout of the module's hit pattern in an X-Ray scan for the 2 sensor-equipped RD53A modules) showed results that match very well the performance of each module before loading, proving that the loading process had no adverse effect on any of them. The same set of functionality tests was then repeated, in the same experimental conditions, after having connected each of the two ITkPixV1 digital modules to the bus tape by means of a V2 power pigtail, by soldering the latter to the V6 bus tape with the soldering tool described in section … In this second set of tests, the two ITkPixV1 modules were serially powered through their power pigtail / bus tape connection, which provided also monitoring of the modules temperature through the MOPS chip loaded on the bus tape itself. The results of these tests, which were again all successful, are illustrated for each of the four modules in Figure 93, Figure 94, Figure 95, and Figure 96, where the thresholds pattern resulting from a threshold scan is shown for each of the four modules; and in Figure 97 and Figure 98, where the hit pattern resulting from an X-Ray scan of the 2 sensor-equipped RD53A modules is shown.

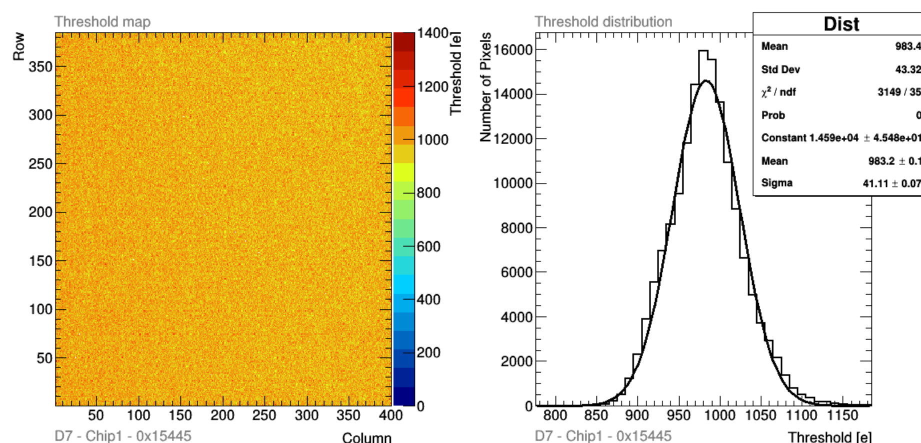

Figure 93: Thresholds pattern and distribution observed on the digital ITkPixV1 module glued in position#00 on the Layer-4 half-ring after loading and V2 power pigtail soldering on the V2 bus tape; both loaded ITkPixV1 modules were serially powered through the bus tape during this test.

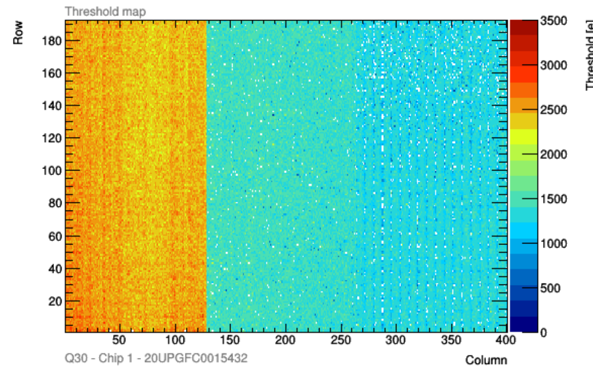

Figure 94: Thresholds pattern observed on the sensor-equipped RD53A module glued in position#01 on the Layer-4 half-ring after loading; both loaded RD53A modules were individually powered during this test.

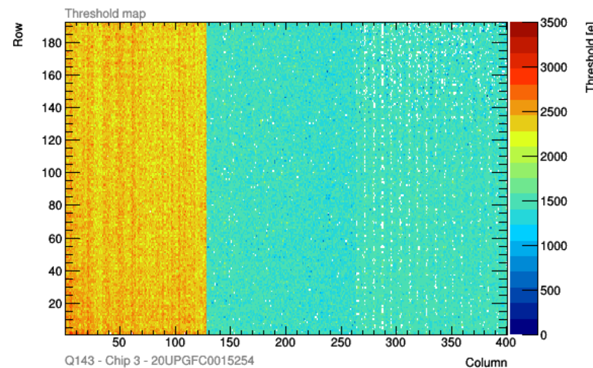

Figure 95: Thresholds pattern observed on the sensor-equipped RD53A module glued in position#11 on the Layer-4 half-ring after loading; both loaded RD53A modules were individually powered during this test.

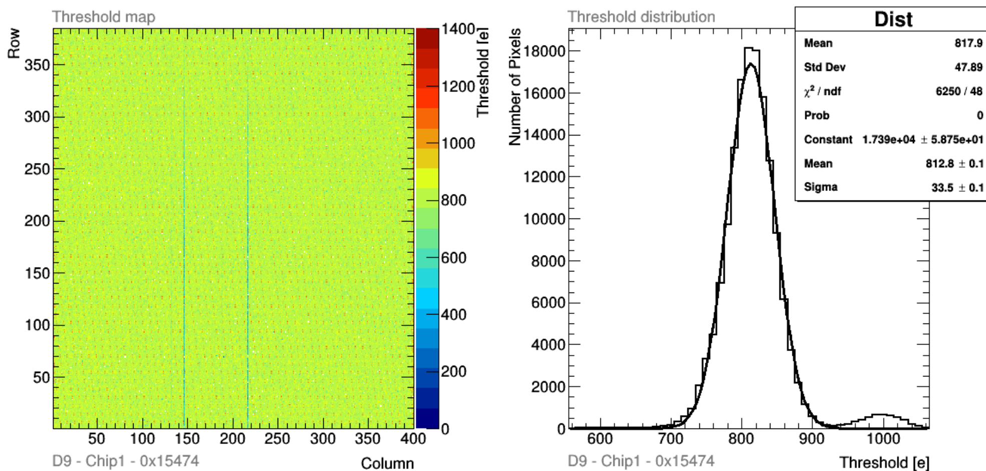

Figure 96: Thresholds pattern and distribution observed on the digital ITkPixV1 module glued in position#12 on the Layer-4 half-ring after loading and V2 power pigtail soldering on the V2 bus tape; both loaded ITkPixV1 modules were serially powered through the bus tape during this test.

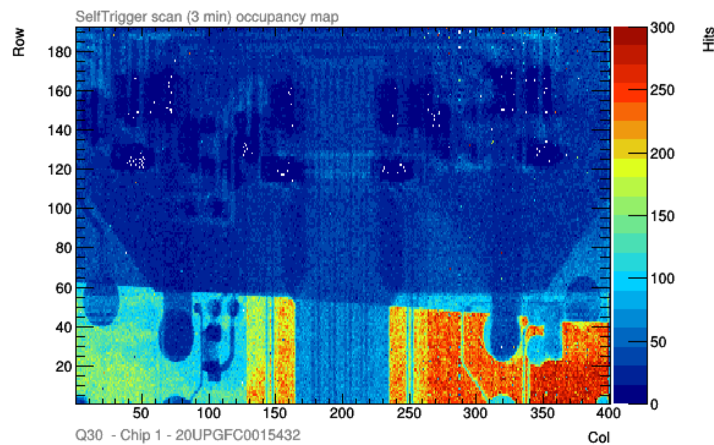

Figure 97: Hit pattern observed during an X-Ray scan on the sensor-equipped RD53A module glued in position#01 on the Layer-4 half-ring after loading; both loaded RD53A modules were individually powered during this test; the XY features observed in the hit pattern reflect the metallization of the module's flex superimposed to the partial shielding of a glass slab placed above the module to protect its wire bonds; also, the irradiation is not uniform over the module's surface due to the relative position of the module and of the X-Ray gun.

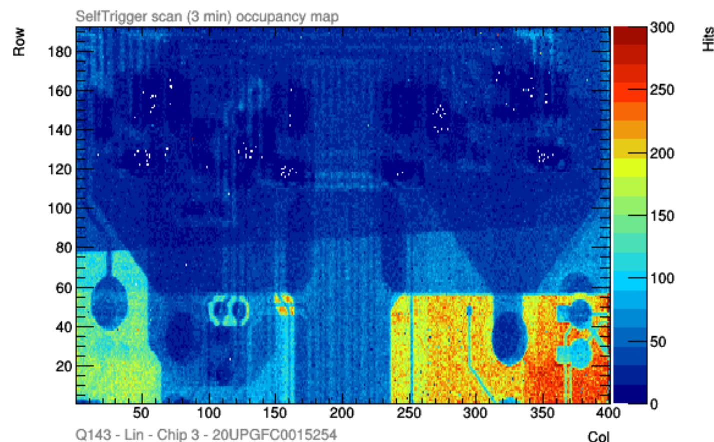

Figure 98: Hit pattern observed during an X-Ray scan on the sensor-equipped RD53A module glued in position#11 on the Layer-4 half-ring after loading; both loaded RD53A modules were individually powered during this test the XY features observed in the hit pattern reflect the metallization of the module's flex superimposed to the partial shielding of a glass slab placed above the module to protect its wire bonds; also, the irradiation is not uniform over the module's surface due to the relative position of the module and of the X-Ray gun.

4.4 Loading Validation at Lecce

The loading technique in Lecce is pick-and-place as in Genova, and uses the same gantry, the same microscope and the same brand of confocal optical pen for z metrology, and a very similar glue dispensing system.

In Lecce the confocal optical pen is fixed on the y-stage and not on the z-stage like in Genova because it is bulkier, with the direct consequence that the measuring height is limited to 1cm in a fixed interval.

The microscope is fixed on the z-axis and during pick-up and loading the module is outside the microscope field of view (unsupervised pick-and-place). This was done for simplicity and to increase the microscope magnification by a factor of two, adding a 10cm tube extension between camera and telecentric objective.

The pick-and-place head has a load cell to measure the applied weight force, as in Genova. In addition, in Lecce, the pick-and-place head has three micrometric vertical linear stages to adjust the pick-up plane orientation defined by the four suction cups (see Figure 99). The pick-and-place head is the only tool placed on the gantry rotational stage. Python code was developed to automatically calculate the vertical position of the three micrometric stages to optimize the relative planarity between the bottom surface of the picked-up module and the local half-ring surface of placement, knowing the orientation of the two. In this work the micrometric stage positions were adjusted only once to have the best pick-up planarity and calibrated shims were used to reach a parking tool and half-ring local planarity better than 50μm.

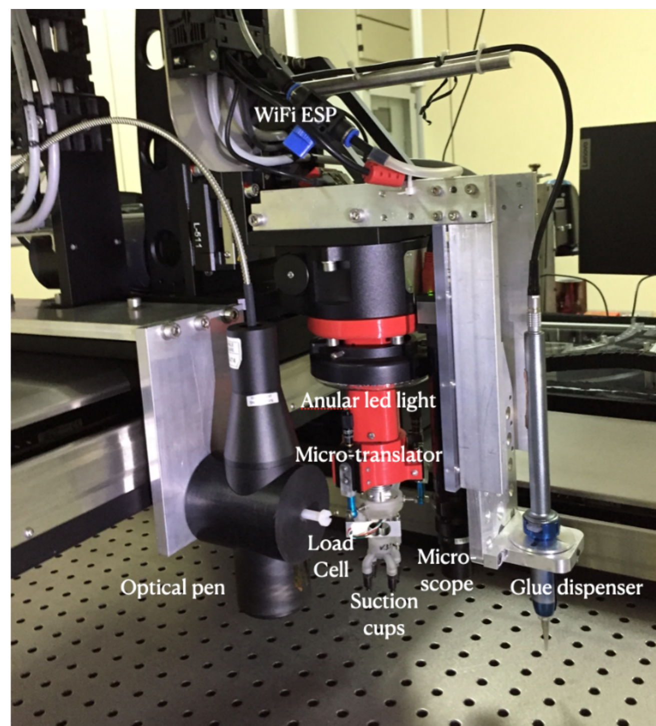

Figure 99: Lecce's gantry pick-and-place head with instrumentations and tools.

The Lecce site exercised its capability by fully loading one side of a dummy Layer-2 half-ring made of Perspex and one side of a prototype Layer-4 half-ring, provided by Genova. Both half-rings were equipped with prototype handling frames made in Lecce (see Figure 100).

The Layer-2 half-ring was loaded with eight dummy glass tiles with area 41mm x 42mm and thickness of about 420μm. This allowed verification of the capability to load modules with realistic geometry and procedure - in particular, to deposit glue in a reproducible way and within specifications, to reach the required placement accuracy, to verify all the loading procedure and to demonstrate an adequate loading speed.

Before loading the half-rings the full process was tested and tuned by gluing silicon and glass dummy tiles on the parking tool (see Figure 100a).

The Lecce site was provided with one RD53a digital quad and two RD53a quad modules. The modules were loaded in one day on the Layer-4 half-ring in the three left-most slots after ten dummy glass tiles were loaded in two days.

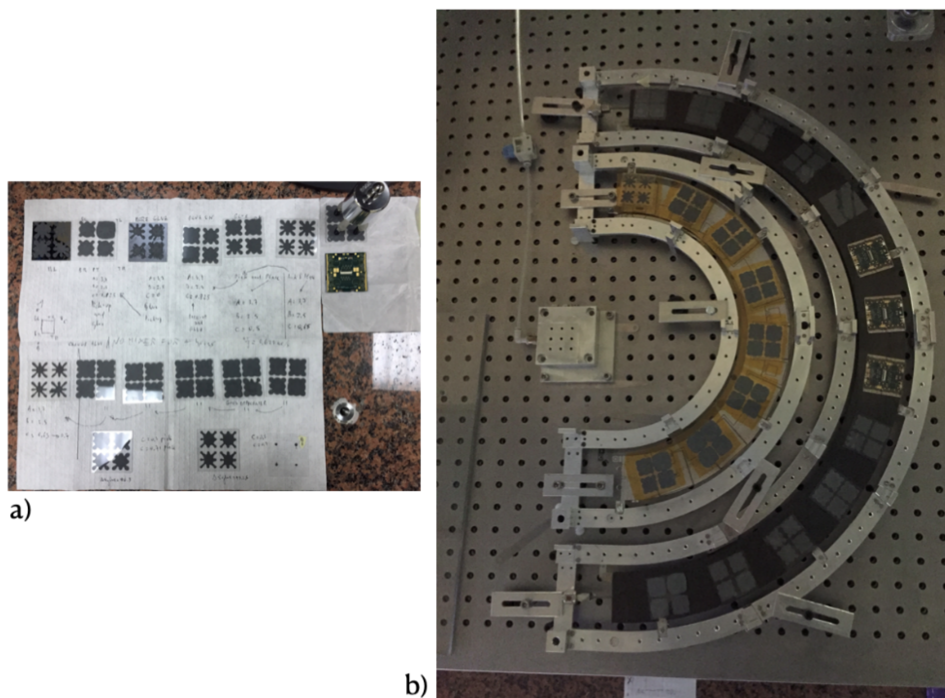

Figure 100: a) Gluing on parking tool of silicon and glass dummy tiles to tune the loading procedure. b) Dummy Layer-2-size half-ring and prototype Layer-4 half-ring loaded with glass tiles and RD53 quad modules at Lecce site.

4.4.1 Glue thickness

The final thickness of the adhesive underneath the module after loading and glue curing is obtained by subtracting, from the heights of the module after loading, the height of the half-ring before loading and the module height (measured again by subtraction on the parking tool before pick-up). In the measurements shown in Figure 101a and Figure 101b the heights are measured in correspondence of the four pick-up circles, but a complete height map could be easily obtained with the chromatic confocal optical pen placed on the gantry (see Section 3.6).

The measured distribution of the glue coverage is reported in Figure 101c. It is obtained from the image color bit map of the loaded glass tiles (see Figure 101cd) extracting the fraction of points with a color code corresponding to the glue inside a Region of Interest.

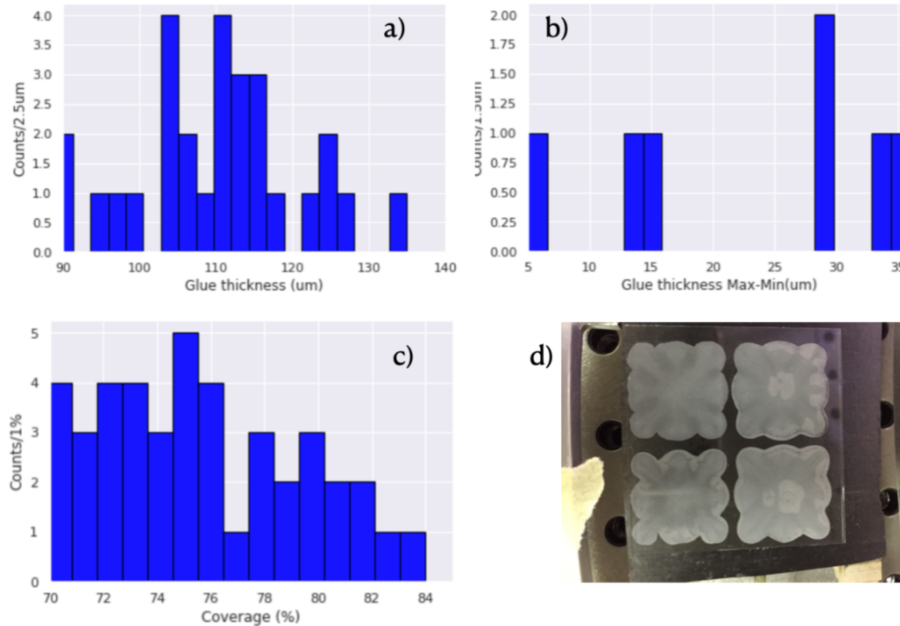

Figure 101: Glue thickness measurements after loading in correspondence to the module pick-up circles (a) the difference between maximum and minimum glue thickness for a module (b), glue coverage distribution) and a typical glue shape after loading starting with t the snow flake pattern described in section 3.4 (d).

Table 9 reports the measured thickness of the glue for the three loaded modules on the Layer-4 half-ring. It is important to stress that the Layer-4 half-ring is an old prototype with large deviation of the local planarity and the weight applied during glue curing is about 200 g.

	Glue thickness [µm]			
	Point 1	Point 2	Point 3	Point 4
Digital Quad	150	120	130	140
Quad Module A	110	150	160	120
Quad Module B	115	155	145	125

Table 9: Glue thickness measurements obtained in correspondence of the module pick-up circles (a) the difference between maximum and minimum glue thickness for a module (b), and glue coverage. Measurements are from glasses tiles and SE4445 glue with 106µm silicon spheres of 1% in weight.

The reproducibility of the amount of glue deposited for each module was checked several times by weighing the glue dispensed on glass tiles in exactly the same conditions. The volumetric glue dispenser showed always a good reproducibility independently of the glue viscosity conditions. Figure 102 shows one of these distributions obtained from the same syringe over the course of about two hours.

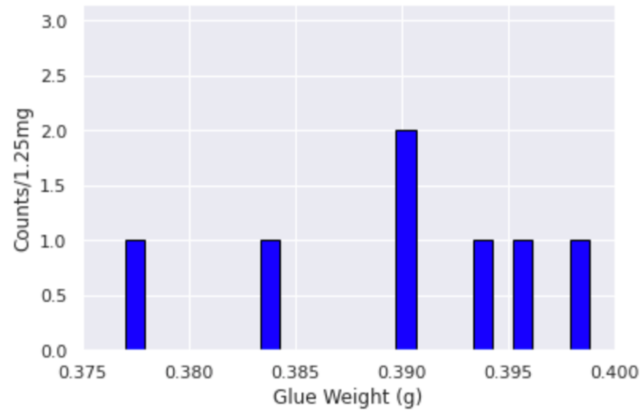

Figure 102: Glue weight distribution for several trials of glue patterns from the same syringe in about two hours' time using a volumetric glue dispenser.

4.4.2 Placement accuracy

The placement accuracy was estimated from the reproducibility of the module position after pick-up and placement on the vacuum parking tool. The residuals of the x and y coordinates of the four corners were never higher than 100µm in any direction (see Figure 103). As already said in Section 3.6, the observed placement accuracy is dominated by a systematic effect due to the placement angle which could be eliminated once measured. These distributions were similar to the distribution of the residuals of the loaded glass tiles and modules, where the final position of the placement is due to the glue curing and not to vacuum pick-up tools.

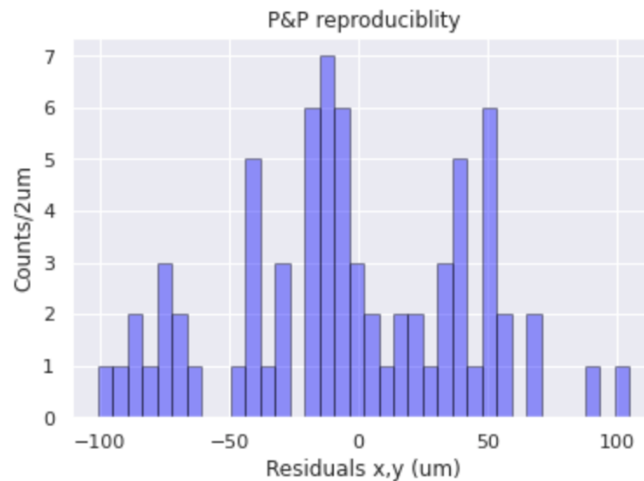

Figure 103: Pick-and-place position reproducibility after pick-up and module placement on the parking tool for different placement angles.

Figure 104 shows a photo of a loaded-module corner taken from the gantry microscope. In the picture the wanted position and the real position of the corner are added to extract the XY loading misalignment (as reported in Table 10). The microscope field of view is H=1.47 mm (2048 pixels) and V=1.1 mm (1536 pixels) which corresponds to 0.716µm/pixel for both views H and V.

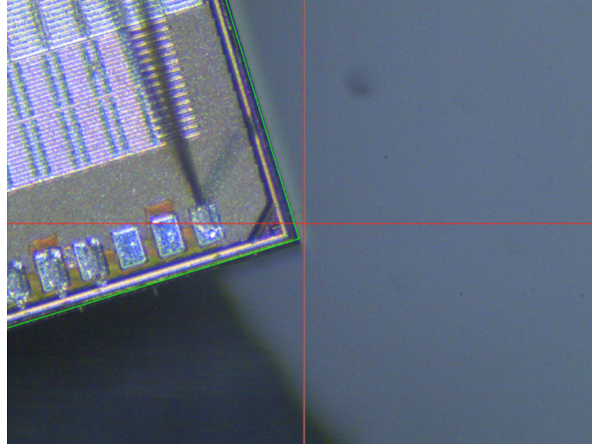

Figure 104: Target position (red cross) and placement position (green corner) of a loaded module as shown by the gantry microscope.

	X and Y Residuals (µm)			
	Corner 1	Corner 2	Corner 3	Corner 4
Digital Quad	-	-	-	-
Quad Module A	45, -10	40, -20	45, -5	45, -5
Quad Module B	40, -20	40, -35	40, -20	55-40

Table 10: Measured X and Y position residuals of the modules four corners after loading with respect to the predicted position as calculated by the module metrology on the parking tool before pick-up and Gantry XY shift and theta rotation before loading. A systematic shift in X of about 40µm is apparent from these measurements.

4.4.3 Loaded modules functionality checks

The modules were tested before loading by a typical reception test setup. The reception test DAQ is based on the PileUp board [20] and YARR Software and Firmware [19]. The DCS uses WinCC Software to supervise instrumentations and monitor environmental parameters (temperatures, humidity and light) by dedicated OPC[11] servers. The instrumentations were controlled by the GPIB interface and the corresponding OPC server, developed by the Genova group [21]; the sensors were read out by the ELMB board using ANAGATE device and the corresponding OPC server developed by the CERN group [22].

The Lecce group is also able to test modules with Felix board using VLDB+ interface but the YARR test system is currently more advanced in producing module performance plots and automatic comparison between different runs.

The loaded modules were tested one by one with the same setup (Figure 105) inside the test box (see Section 6.2.2). The tests were done cooling the half-ring with CO_2 provided by MARTA [23] and dry air was flushed. The internal environmental conditions were monitored together with the module temperature. In the test box a relative humidity of about 2-3% was reached

[11] Open Platform Communications; see for example [28].

with a dew point of about -42.5°C and no light. The MARTA temperature set point was fixed at 5°C achieving a MARTA local box inlet/outlet temperature of 4.8/5.4°C.

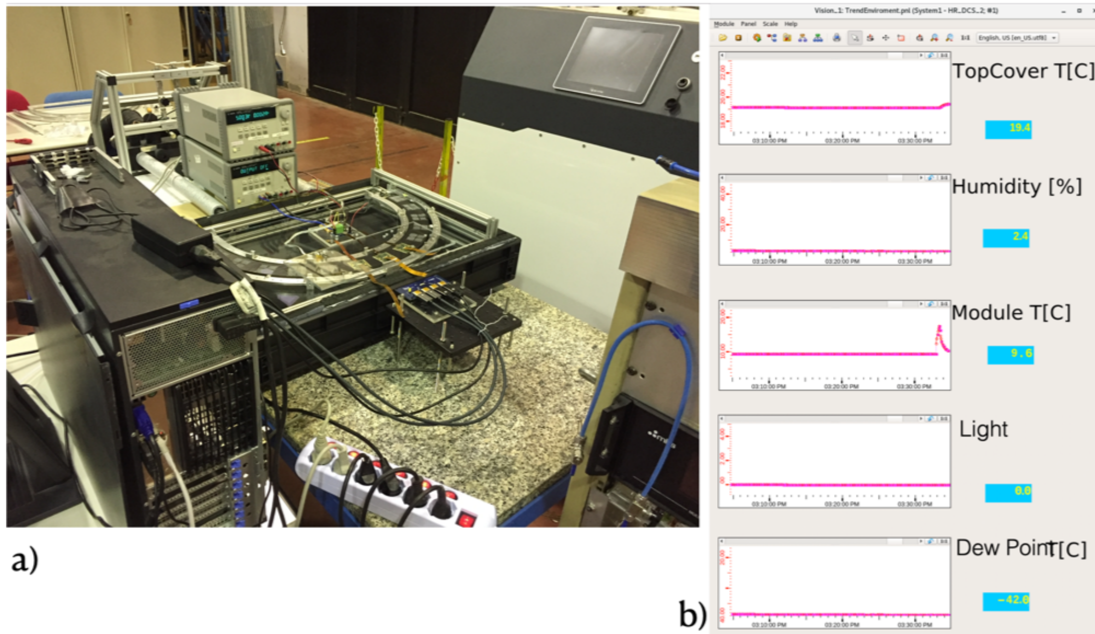

Figure 105: a) Setup in Lecce used to test one by one the loaded quad modules. The upper shell BOX is removed in this picture to show the setup. b) The WinCC GUI used to monitor the Test Box environment parameters.

A comparison of the distribution plots and maps of the three modules before and after loading didn't show any significant statistical difference. The tests consisted of: digital scans, analogue scans, threshold scans and disconnected bumps scans. Figure 106 shows typical examples of these comparisons.

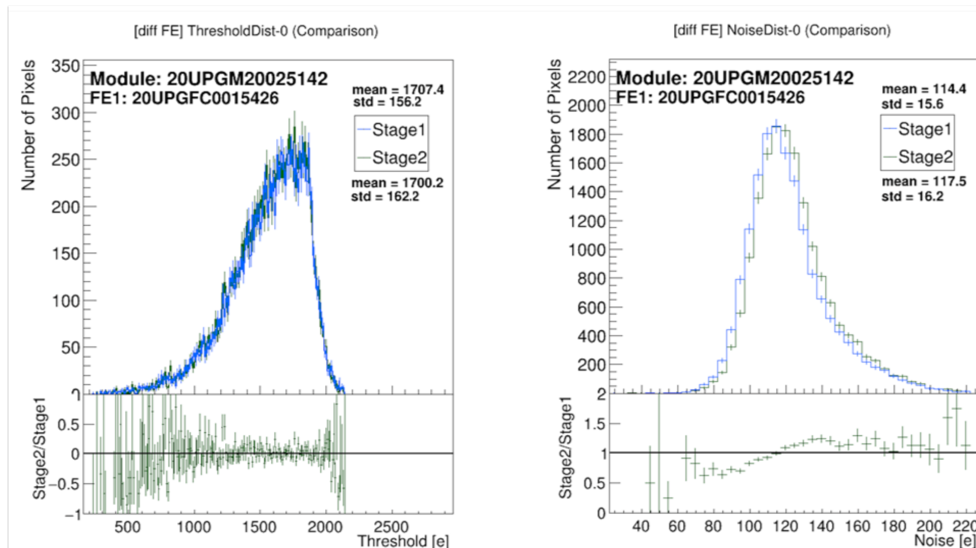

Figure 106: Threshold (left) and noise (right) distributions of differential front-end pixels of chip 15426 belonging to module 20UPGM20025142 before (Stage 1) and after loading (Stage 2) with their ratio.

Finally, a temperature map of a loaded module (see Figure 107) was taken by the thermo-camera installed in the 48 cm high upper shell BOX B (see Figure 139B in Section 6.2.2.2). From this it is possible to appreciate the absence of hot spots in any of the four readout chips.

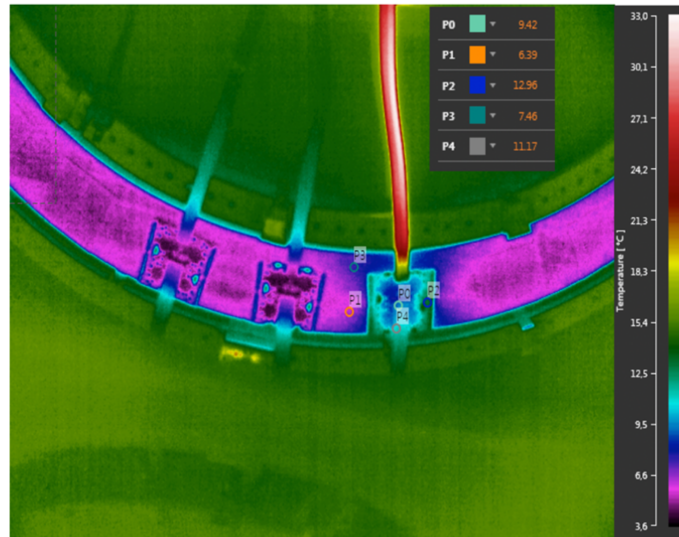

Figure 107: Thermometric map of a loaded module during full bias and testing with CO_2 cooling at 5C circulating in the half-ring titanium cooling pipe.

4.5 Thermal Cycling of a Layer-4 Half-Ring

The module loading test performed in Genova and described in Section 4.4 is actually two-fold. On one hand it is meant to validate the pick-and-place loading techniques and the achievable precisions in terms of X-Y positioning of the module and glue layer thickness. On the other hand, it is intended to validate the robustness of the power pigtail connections to the module and to the power bus tape after thermal cycles. The Ring-1 system test (Section 0) uses version V5 of the bus tape, while the half-ring loaded in Genova is equipped with a V6 bus tape (see Figure 108), which is the version presented at the Services FDR in November 2022. In this sense, thermal cycling the Genova Layer-4 half-ring can provide useful information on the behaviour of a system closer to the final design.

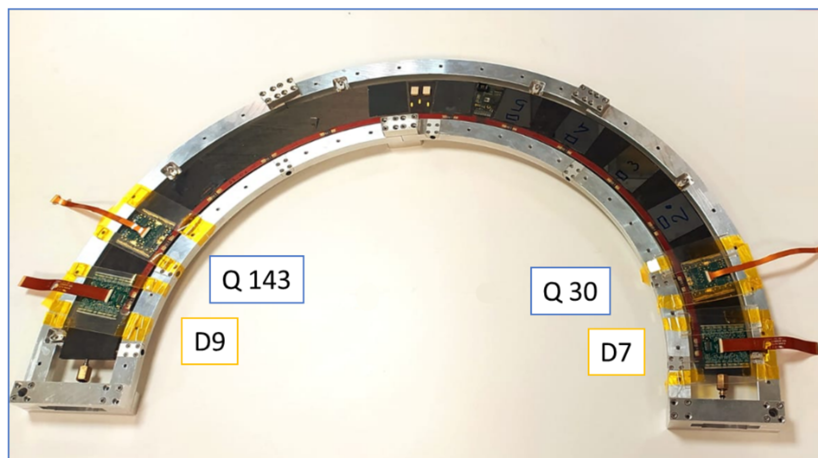

Figure 108: Half-ring after modules and bus tape loading.

In order to maximize the stress induced on the connections by the thermal deformations, a Layer-4 half-ring has been used and two ITkPixV1 modules have been loaded at the two extremes (see Figure 109). Unfortunately, ITkPixV1 full modules were not available in time for this loading exercise, so digital modules (i.e. without sensors) have been used. Two RD53A modules with sensors have been loaded close to the ITkPixV1 digital, in order to have the possibility to verify, at least in part, possible effects of the pigtail soldering procedure on the module bumps. The RD53A modules, however, have not been connected to the bus tape for the initial tests. This decision is motivated by the very limited experience in operating "mixed" ITkPixV1 and RD53A serial power chains. We decided it was safer to start with a pure ITkPix1 serial power chain, postponing the connection of the RD53A modules to the tape to a second stage. RD53A modules can still be operated concurrently with ITkPixV1, but with independent power connections (long pigtails). The connection to the V6 bus tape of a RD53A module requires a non-standard curved pigtail.

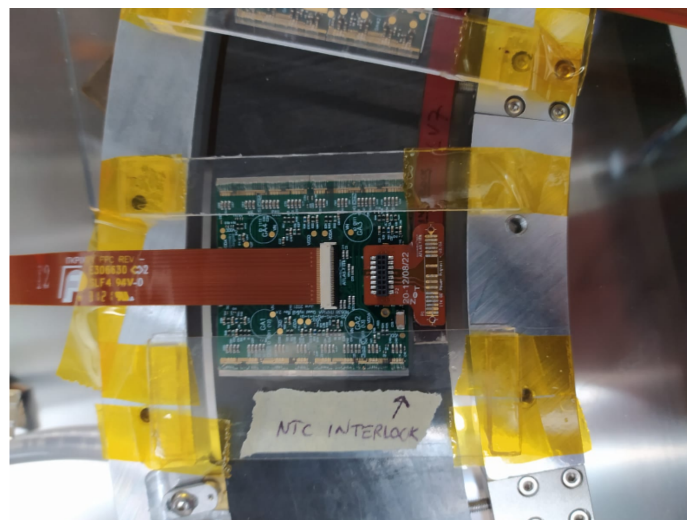

Figure 109: Power pigtail soldered on ItkPixV1 module D9. Long data pigtail used for communication with the readout system (YARR).

After loading of the four modules, the pigtails of the ITkPixV1 modules were soldered (Figure 109) as explained in Section 3.3.4. Short-circuited pigtails were soldered on the other pads to close the serial power chain. The half-ring was then moved in the testing box and connected to the electrical and cooling services. Cooling was provisionally implemented with a chiller circulating plain water[12] at 17°C. The power tape was connected to a LV power supply (Rohde & Schwarz HMP4040) operated in current limitation, to the MOPS chip readout system (ESP32 based) and to a standalone NTC readout for the module designated to be connected to the interlock system (actually one of the two ITkPixV1 loaded). HV connection was not necessary, as the ITkPixV1 modules are purely digital.

The first power-up of the serial power chain at 6.4 A was smooth and the two modules were perfectly functional at the first attempt as well as the MOPS chip. The total voltage drop measured at the power supply was 4.8V (including voltage drop on the cables). The voltage drop measured by the MOPS chip for module D9 (8th element of the serial power chain) and for module D9 (8th element) were compatible with the nominal value of 1.5 V. The temperature

[12] The use of water as a coolant is only allowable because the half-ring is not production grade; a CO_2 cooling system (MARTA) is being commissioned.

measured by the MOPS for module D7 and by the standalone system for module D9 were respectively 27.2 and 27.5 °C, in agreement with the measurement done with the thermal camera (Figure 110, Figure 111).

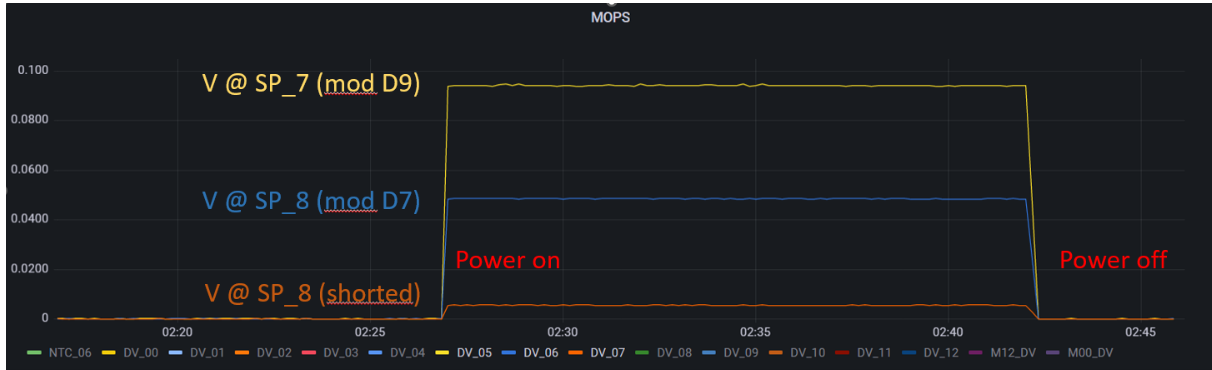

Figure 110: Trace plot showing the raw voltage drop measured by the MOPS ADCs for module D9 and D7.

Figure 111: Thermal image of the Genova half-ring with the two ITkPixV1 modules powered by the V6 bus tape.

The comparison between pre- and post-loading performance is satisfactory. There are not many parameters that can be tested in a digital module, but the stability of threshold and noise using the same configuration is an indication that the behaviour is not affected by the gluing and by the pigtail soldering. Module D9 has a threshold distribution peculiarity (presumably related to a software problem) that is however present in all tests (Figure 112).

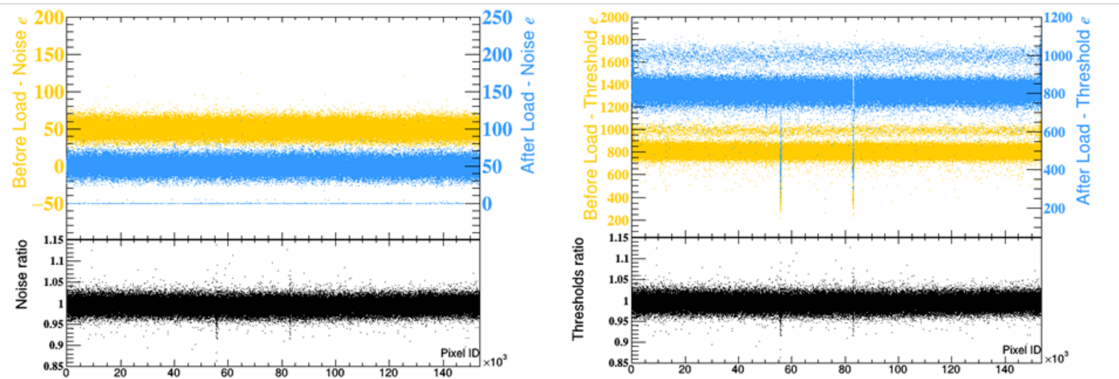

Figure 112: Noise and threshold distributions before and after loading for Module D9. Y scales before and after loading are deliberately shifted to ease the comparison.

The thermal-cycling program foresees a large (100) number of cycles between -55°C and 60°C with a ramp of 5°C/s and a dwell time of 15 minutes. The idea is to proceed in three steps, the first with 10 cycles, the second with 40 cycles and the last one with 50 cycles. After each step the half-ring will be reconnected to the services and the modules will be tested to see if the cycles produced visible effects. The test list includes:

- General functionality tests, integrity of the power chain (D7, D9, Q30, Q143)
- I-V scan (Q30, Q143)
- Analog, digital, threshold scan (D7, D9, Q30, Q143)
- Disconnected bump scan (Q30, Q143)
- X-ray test (Q30, Q143)

Thermal cycles are performed with an environmental chamber (ACS Discovery My DM340CES) flushed with dry air (dew point -70 °C). The handling frame captive screws (holding the inner rim) and the fixation lug clamps are removed during thermal cycles to avoid mechanical stresses induced by the CTE mismatch between the aluminium and the carbon fibre.

During thermal cycles, two temperature and humidity sensors and two temperature sensors (one being the module D9 NTC) placed around the half-ring are continuously readout and logged InfluxDB (Figure 113). This setup is a rough approximation of the setup that may be used in production for thermal cycling the half-rings. Compared to this QA style test, looking for possible fragility in the design of the services, the test foreseen for QC is only a “light” version (one single cycle from -40 °C and +40 °C) to spot and possibly fix weak interconnections. However, given the aggregate value of the parts under test and the potential risks (mishandling, condensation during cycles), a severe protocol will be required, and a comprehensive interlock system will be installed.

Figure 113: Picture of the half-ring inside the environmental chamber.

Figure 114 shows a trace plot of the temperature sensors and of the measured dew-point during the first cycles of the first step. The measurements indicate that the distance between the half-ring temperature and the dew-point is always at least 10°C, and this has been confirmed by several dry run performed with the same setup where no evidence of condensation was seen. It must be said, however, that maintaining a very dry environment at T < -40°C is challenging and require a deep understanding of the behaviour of the climatic chamber, which can adsorb or release humidity during the cycle, and the adoption of special humidity sensors performing well even below -40°C.

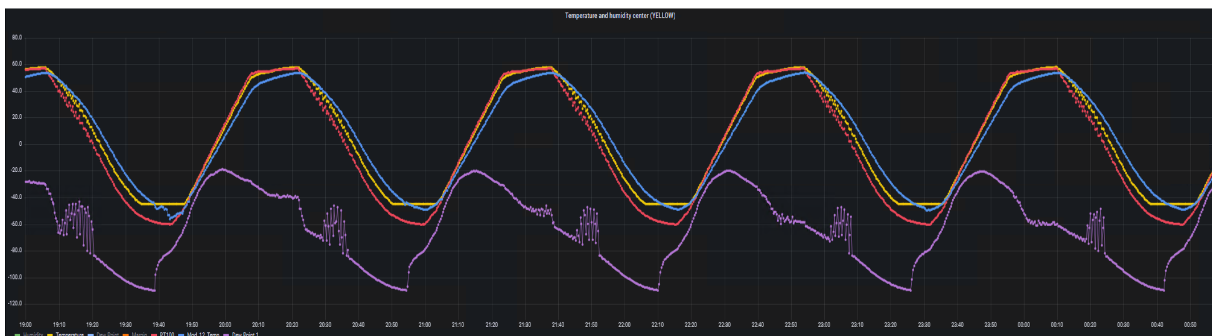

Figure 114: Trace plot of T and Dew Point during the first 5 -55 – 60 °C cycles of the Genova half-ring.

A first quick test of the two ITkPixV1 digital modules gave good results, threshold and noise are identical to the previous test before thermal cycles. Also the serial power chain works as expected, total voltage drop and voltage drops across the two modules measured by the MOPS chip did not change.

5 Electrical Evaluation and design validation of LLS

5.1 Concept of Electrical Validation

To validate the Outer Endcaps loading process and the overall loaded local support system design, a Layer-3 half-ring has been fully loaded with RD53A modules and prototype version-5 bus tape / EoS card combinations with MOPS chips. This demonstrator has the potential to bring together all concepts (serial powering, interlock, multi-module readout) which are relevant for a loaded local support and offers the first opportunity to test a complete detector system.

It must be noted that the RD53A readout chip is not the final readout chip of the ITk Pixel detector, but the first prototype chip that comes with a few features and shortcomings which have direct impact on the evaluation of the demonstrator results:

- **Three different types of analogue front-end**
  The pixel matrix of the RD53A front-end chip is subdivided into sections using a "linear", "differential" and "synchronous" analogue front-end circuitry, which all require different tunings, different configuration parameters, and are differently sensitive to the particular timing of the readout. Since ATLAS and CMS selected the differential and linear FE for the final chip, the support for the synchronous FE in a multi-module readout infrastructure is quite limited and, therefore, the systematic analysis and comparison of the data of the synchronous analogue front-end is dropped under a few circumstances.
- **Different chip geometry**
  The dimensions of the RD53A chip is half the size of the final ITk pixel readout chip, which impacts the power consumption and restricts the sensor coverage of the active pixel matrix.
- **Shunt-LDO start-up problems**
  RD53A has known problems in the shunt-LDO design, which have been fixed in later chip versions, which were not available at the time of the building of the demonstrator modules. Consequently, individual front-end chips can have problems starting up correctly in the serial powering chain of the demonstrator. The problem is especially pronounced at cold temperatures. Separate system tests with very early modules made of ITkPixV1.1 front-end chips have been carried out to validate serial powering. This aspect is not part of this review.

In addition to the shortcomings of the RD53A readout chip, the scarcity of RD53A modules made it necessary to drop some quality requirements for the selection of demonstrator modules. This leads to additional complications in the operation of the demonstrators, which are unrelated to the loaded local support design.

5.1.1 Testing Stages and Test Setups

The electrical performance of the modules on Ring-1 was assessed during different stages and compared to evaluate any changes in performance that could be due to loading techniques or effects from the local support. The testing stages considered are as follows:

- Stage 1 = Module production
- Stage 2 = Reception testing at RAL
- Stage 3 = post loading measurement at RAL
- Stage 4 = single module testing on ring at Liverpool
- Stage 5 = module tested on Serial Power chain
- Stage 6 = multi-module readout test with 4 modules

5.1.2 Pre-/Post-Loading

Twenty-two RD53a quad modules were loaded onto Ring-1 at RAL as shown in Figure 115 and Figure 116 for sides A and B respectively. Before loading, each module was tested to evaluate its performance. After loading each module was tested individually, with the same tests as before loading, to determine if any changes due to loading were seen.

Module performance was evaluated using YARR. Sensor IV scans were also performed. See Section 5.2.2 for details and results.

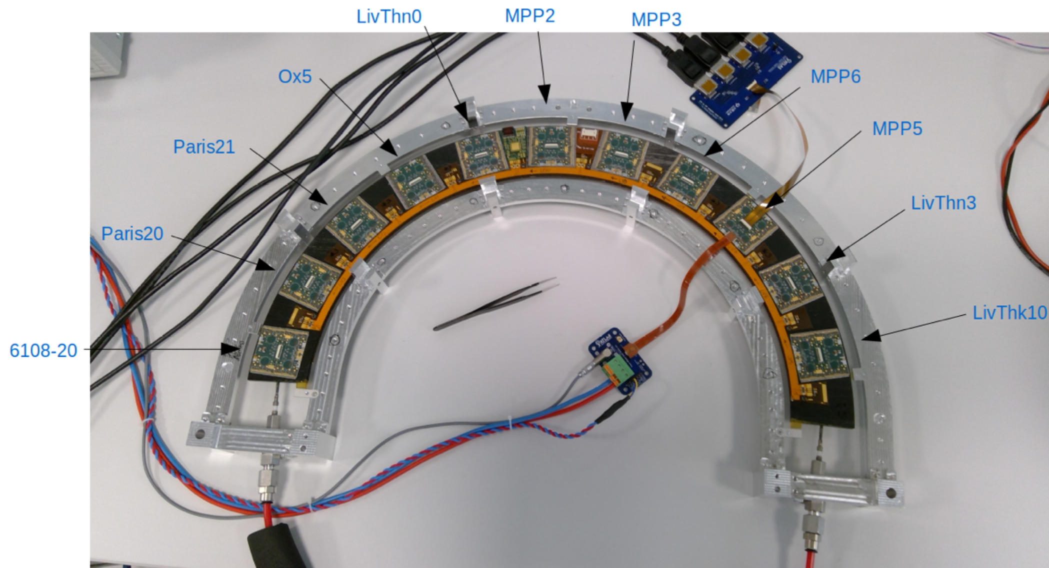

Figure 115: Side A of Ring 1 showing the module placement of the 11 modules and their names.

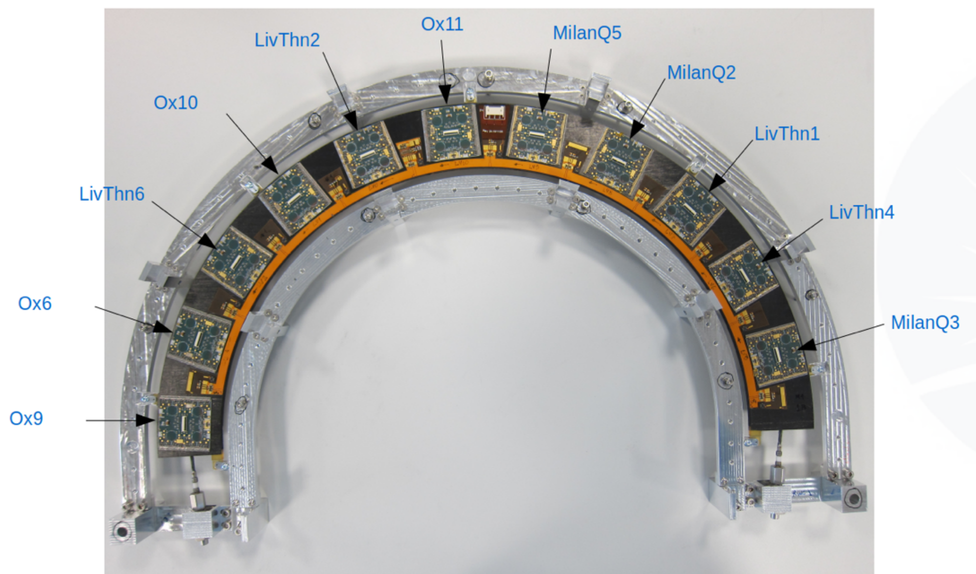

Figure 116: Side B of Ring 1 showing the module placement of the 11 modules and their names.

5.1.3 System Test

5.1.3.1 Cooling systems

Liverpool developed a test box (Figure 117) that can hold half-rings of any size. The box also acts as a thermal and eventually a radiation shielded box. A copy of the box was made for RAL. The half-ring is held in the middle of the box by the top and the bottom of the half-ring's handling frame.

Figure 117: Ring 1 located in its test position inside the test box (left). The Liverpool test box, in its open position, with the lid open, allowing access (right).

The equipment instrumented to control the environment inside the box includes:

- A Keysight 34972A (to monitor module NTCs and Type J thermocouples for the environment).
- BME280 sensors to monitor the humidity, temperature and pressure inside the box (readout with an Arduino).
- Fans to circulate the air inside the box.
- Holes where cables and cooling pipes can enter.
- A motorised rotating arm that can hold a radioactive source in front of each of the modules.

Two cooling systems have been used to cool the modules on the half-ring: a liquid-nitrogen evaporative cooling system and a "Lukasz" evaporative CO_2 plant.

The evaporative liquid-nitrogen system was developed using a NORHOF [24] liquid nitrogen dosing system, see Figure 118. The dosing "pump" is inserted and delivers drops of liquid nitrogen into the box, from the top. The rate of flow is controlled to match the required temperature of the system, via a sensor. Figure 118 also shows the measurements made inside the box when the system was set to –10°C.

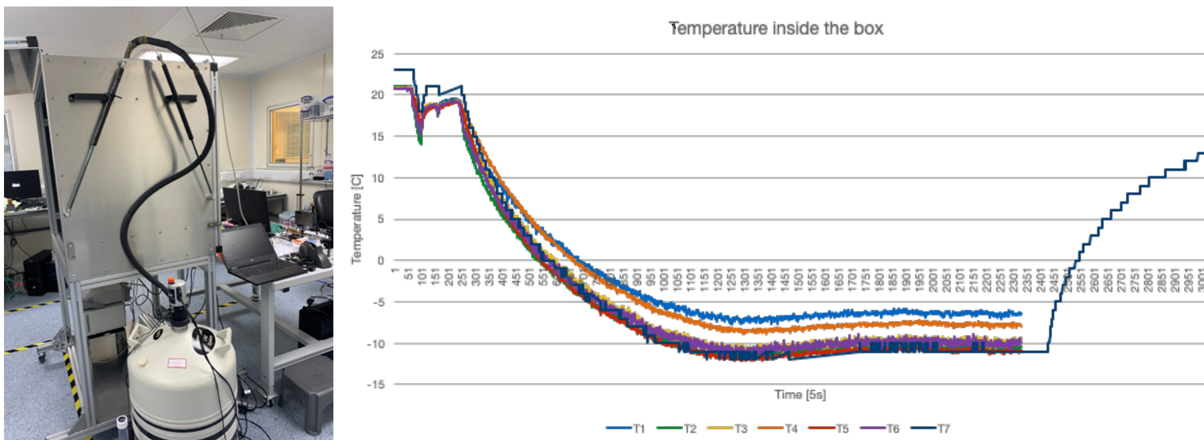

Figure 118: Left: the NORHOF liquid-nitrogen dosing system used to cool the Liverpool test box. Right: measurement made inside the box when the system was set to -10℃.

Lucasz is a circulating CO_2 system designed by the CERN cooling group. The plant comes in two parts (see Figure 119); the first is outside of the clean room and is known as "the plant"; the second part is inside the clean room and is called "the local box".

Figure 119: The Lucasz "plant" (left) and "local box" (right).

The coldest temperature that the Lucasz system can reach is –30°C at the plant. Ring-1 has been successfully connected to the local box. A simple test is shown in Figure 120. Modules were tested at different plant temperature and the modules NTC were read out. – see Table 11. Unfortunately, due to WINCC licensing issues plus software incompatibilities, this system is not currently operational and is awaiting intervention from the CERN cooling group.

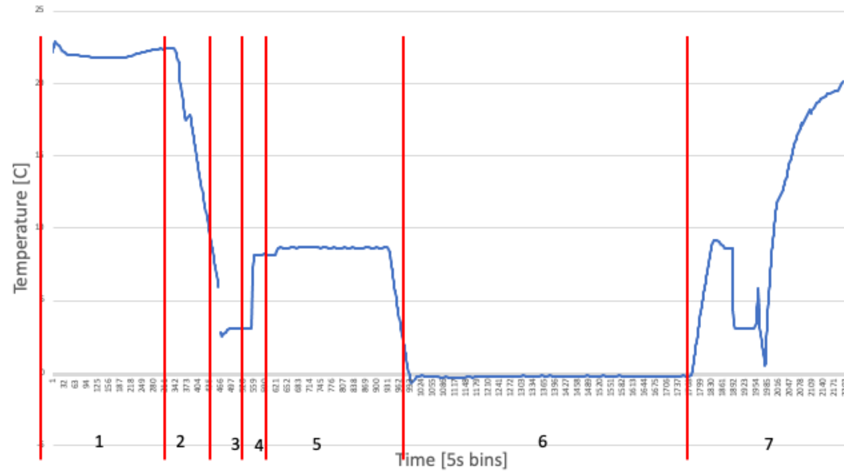

Figure 120: The measured temperature of a RD53A module with the Lucasz system running. Period: 1) Plant preparing to cool, 2) Plant cooled to 0ºC, 3) Left to stabilize, 4) 3 modules powered, 5) All 11 modules powered, 6) Plant cooled to -10ºC, 7) Modules turned off and plant turned off.

Plant Temperature [°C]	*Module Temperature [°C]*
10	*+8*
0	*+3*
-10	*-5*
-20	*-13.9*
-30	*-22.2*

Table 11: Temperature map for a test of cooling with the Lucasz system.

5.1.3.2 DAQ and powering

The DAQ system used was based on YARR. This consists of a Trenz version 2 PCIe card with an Ohio interface card attached. The YARR was run at full speed, 640Mbps, and in two configurations. The first was in the 4x4 mode where one YARR system could read out 1 quad module. This required a 4-display port adaptor card, as shown in Figure 121. And the second was in 16x1 mode where the one YARR system could readout 4 full quad modules (16 chips). This required the 1DP adaptor card. The module on the ring was attached to the adaptor cards using the data flex, again shown in Figure 121.

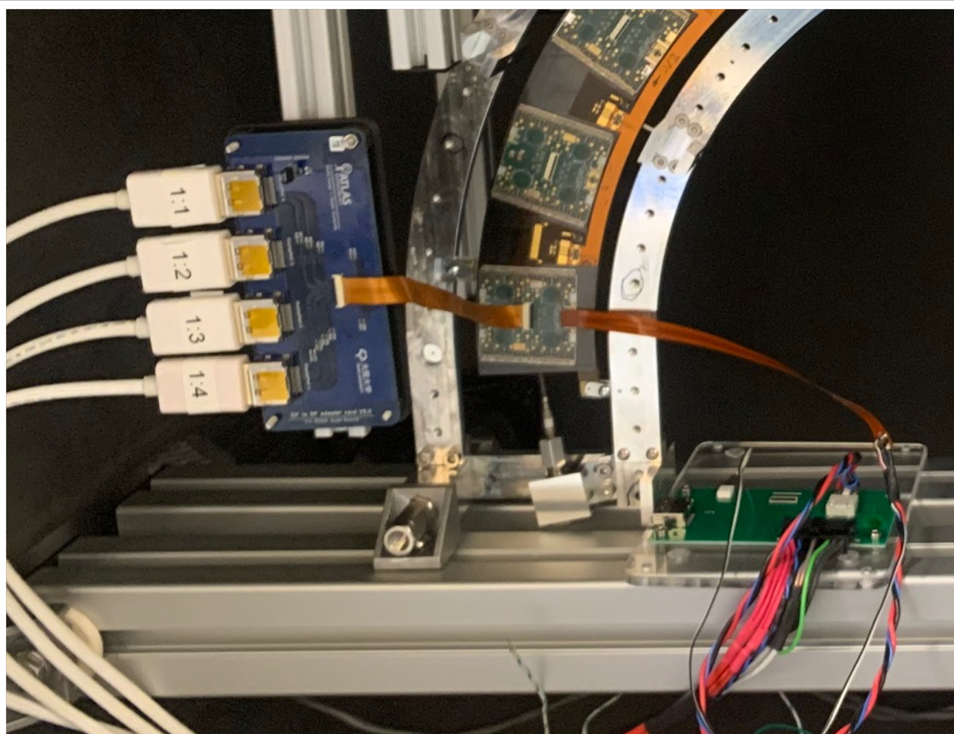

Figure 121: The 4-display port adaptor card (blue) with the display port cables going to the YARR PC and the data flex connecting the card to the module. The power board for single module tests is shown in green.

The modules were powered by two different power supplies depending on what configuration they were in. For the single module tests the power was supplied by a HMP4040 via a single module power board (shown in Figure 121). This power board could also provide high voltage to the module with the use of a Keithley 2410. The module NTC could also be monitored via this board using a Keysight 34972A DAQ. After single-module testing was complete, the modules were connected to the serial power bus tape using the power pigtail, see Figure 122. Once the modules were in the serial power chain, they were powered with a Keysight E3634A. The module temperatures and voltages could now be monitored by the MOPS chip.

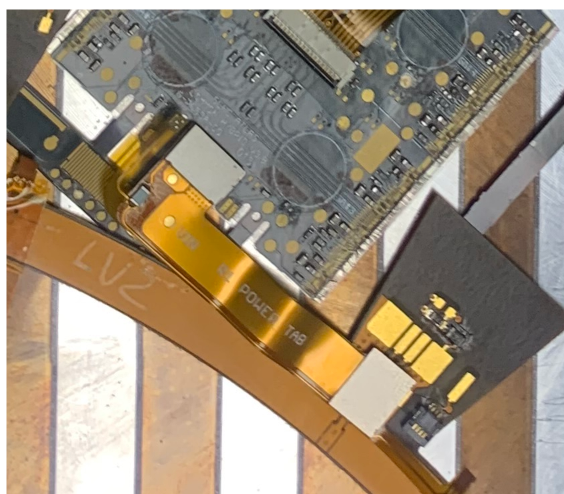

Figure 122:The power pigtail attaching the module to the serial power bus tape.

5.2 Results

The following sections contain the results of the electrical tests of the modules and completed half-ring:

- The performance of the MOPS chip is presented in Section 5.2.1.
- A description of the serial powering chain is presented in Section 5.2.1.2.
- A subset of the comparison plots to compare the data between the difference stages is presented in Section 5.2.2.

5.2.1 MOPS Readout

The modules are listed 1-11 starting with the bottom left module and ending in the bottom right. The modules in the serial power chain are listed differently. See Figure 123 to see the full mapping. The MOPS chip is designed to monitor the module NTCs and input voltages and is integrated into the EoS card on Ring-1, see Figure 115.

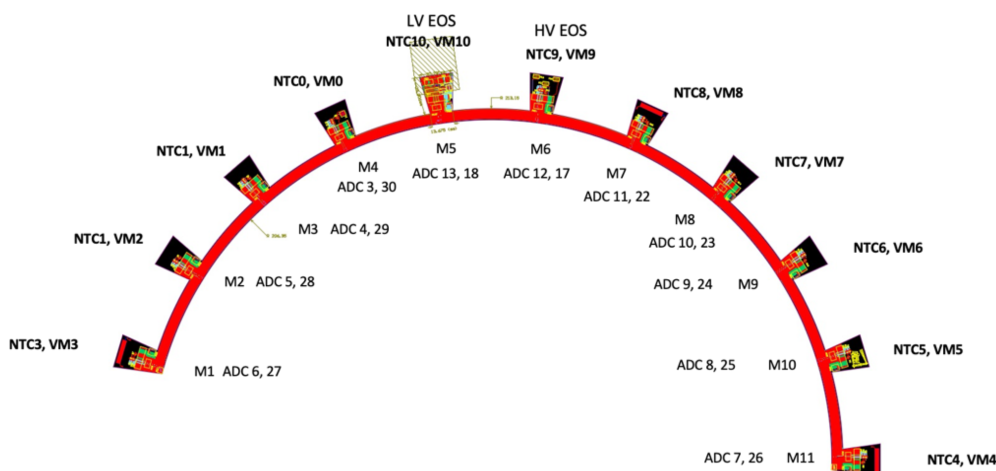

Figure 123: M1 is the module number, NTC/VM number is the number in the serial power chain and the ADC number is the number in the CANMOPS software.

The MOPS chip is read out with a CANbus using the CANMOPS software [25] developed in Göttingen. The CANbus interface is a Kvaser Leaf Lite v2 [26]. This reads out the 64-bit ADCs which are in turn connected to the module NTC's and voltage measurement circuitry. These ADC values can be converted into the module temperatures and voltages.

5.2.1.1 Module Temperature

On the EoS card, each NTC is pulled up to 1.2V through a 100k resistor where the central divider connects directly to the ADC. The supply voltage on the serial power chain is gradually increased until the voltage across each module is approximately 1.6V @ 4.6A, at which point it is then decreased until the supply voltage back to zero. The resistance of each NTC will then decrease and then increase as the power supply voltage is cycled in the way previously described. As a result, the ADC voltage and hence count values will also decrease and then increase as indicated in Figure 124. The Steinhart-Hart Coefficient values from the NTC data sheet can then be used to convert the ADC counts to temperature values as can be seen in Figure 125.

First, a quick test was performed without cooling. The serial power chain was turned on and the ADC values were recorded (see Figure 124). From the single module tests, it is known that the modules would reach about 48°C without cooling; this is confirmed in Figure 125.

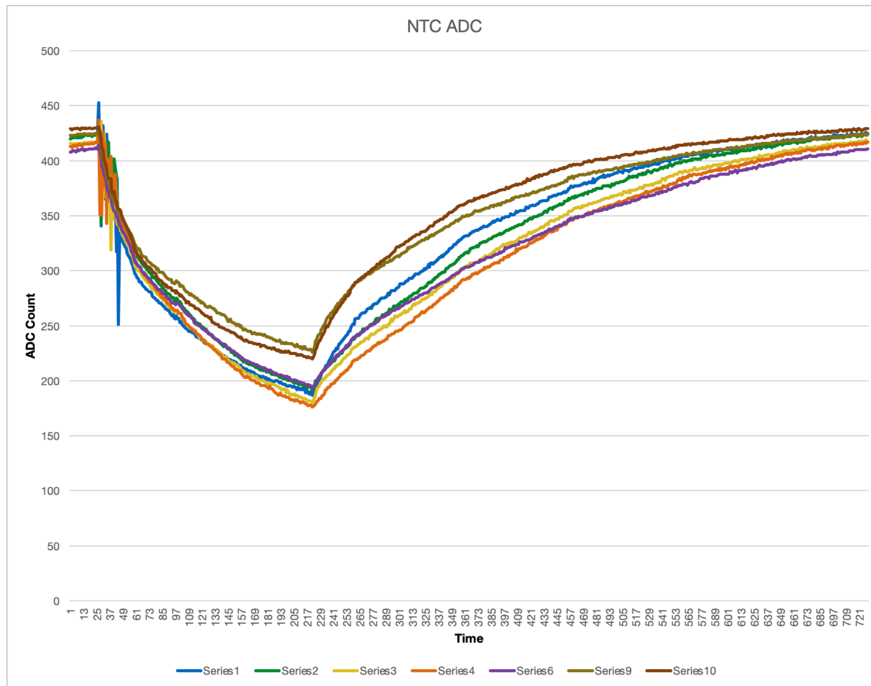

Figure 124: ADC counts from the MOPS chip on Ring-1 (Ring-1 not cooled).

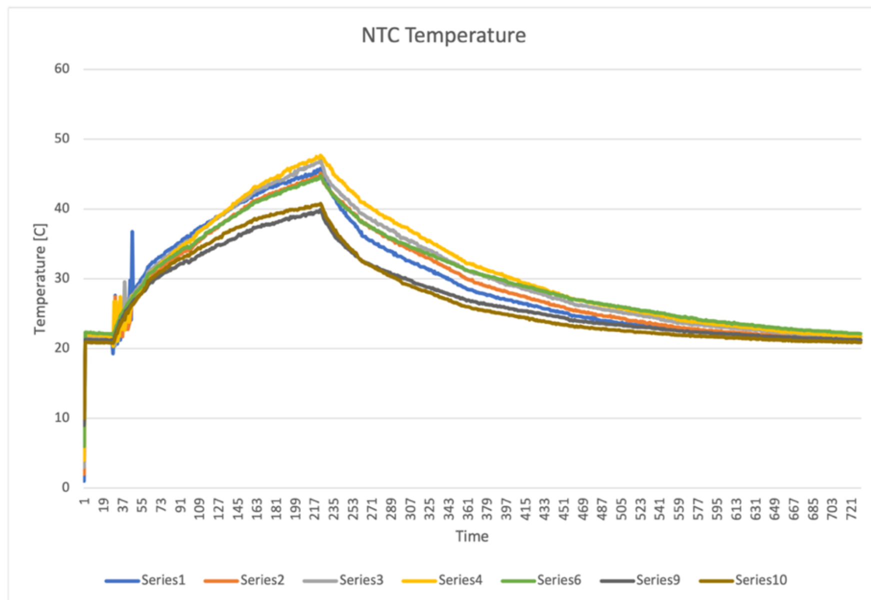

Figure 125: The MOPS chip measurements of the module NTC temperatures (Ring-1 not cooled). These plots start with the serial power chain off and show how the NTC temperature increases after powering the chain on. The peak corresponds to the chain being switched off again and shows the modules cooling to their previous state.

5.2.1.2 Powering in SP chain – without cooling

The serial power chain of 11 RD53A modules on side B of Ring 1 has been powered through the Version 5 bus tape and attached End of Stave (EoS) cards, see Figure 126.

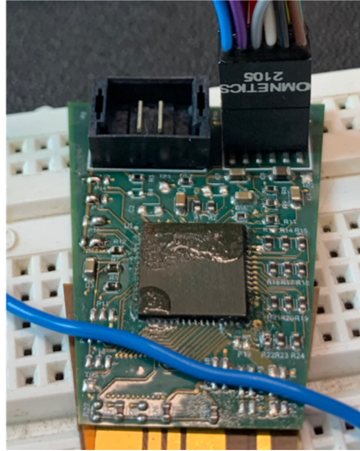

Figure 126: The LV/DCS EoS card on Ring-1.

The power supply was set in constant-current mode with the following values: V_{in} = 18.4V and A_{in} = 4.6A. The V_{in} on each of the modules was measured to ensure that all modules received 1.6V. The results are shown in Table 12. Note that the configuration files for modules 7, 8 and 11 were not available at the time the measurements were made, so these modules were bypassed by soldering wires onto the serial power chain. Module 5, which was connected into the same tab as the EoS card, didn't give any readings; this is being investigated. Apart from these four modules we can see the expected voltage drop along the serial power chain. After these tests and a few more temperature tests the MOPS chip connector on the bus tape came off. This had also happened on earlier tests with a serial power tape (not glued to a CF half-ring). This is not a concern as in future tapes the EoS will be integrated into the bus tape (i.e. not connector).

Chain	Module	MOPS calculated voltage (V)	Measured voltage (V)
VM0	4	0.34	0.328
VM1	3	0.30	0.286
VM2	2	0.26	0.246
VM3	1	0.22	0.206
VM4	11	Not connected (module position shorted)	
VM5	10	0.17	0.163
VM6	9	0.12	0.124
VM7	8	Not connected (module position shorted)	
VM8	7	Not connected (module position shorted)	
VM9	6	0.09	0.081
VM10	5	Bus tape wing shared with EoS card	

Table 12: V_{in} on the modules in the serial powering chain on side B of Ring-1. The table shows the expected behaviour of the voltage drop as we are moving forward in the serial power chain.

5.2.1.3 *MOPS operation when cooled*

As seen above, the v1 MOPS functions as expected when operated at room temperature. It is known that the v1 MOPS does not function below about 0ºC[13], but in addition, noise has been seen on the ADCs at temperatures between 0ºC and room temperature; see Figure 127 and Figure 128. This has been brought to the attention of the rest of the collaboration and must be understood.

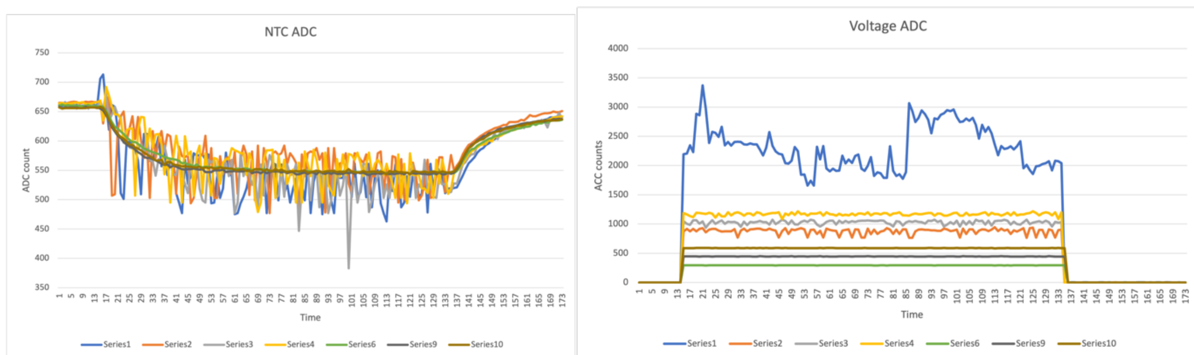

Figure 127: v1 MOPS ADC readouts when Ring-1 is cooled to 10ºC..

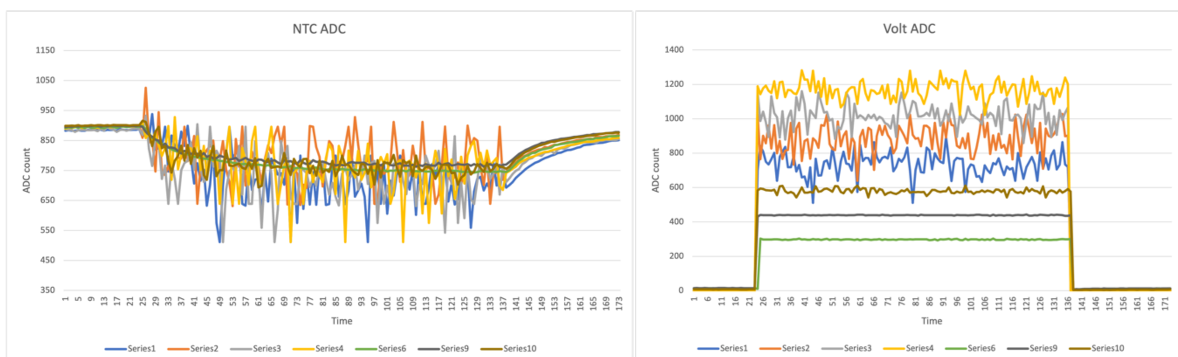

Figure 128: v1 MOPS ADC readouts when Ring-1 is cooled to 0ºC.

5.2.2 *Module Performance Pre-Loading, Post-Loading and System Test*

Twenty-two RD53a quad modules were loaded onto Ring-1 at RAL. Before loading, each module was tested to evaluate its performance. After loading each module was tested individually, with the same tests as before loading, to determine if any changes due to loading were seen. A similar set of tests were carried out in Liverpool on the modules individually after being mounted in the testing box and before the modules were connected together in a serial power chain. Following this more tests were carried out as described in this subsection.

For tests requiring communication with FE chips, YARR was used (as described above). For the duration of Ring-1 work at RAL, the YARR version used there was kept fixed for consistency. This led to a YARR-version mismatch between tests performed at RAL, and subsequent Ring-1 tests at Liverpool.

---

[13] This problem may be solved in v2 MOPS; an EoS card with v2 MOPS is being prepared for use on Ring-1 at the time of writing of this document.

For all YARR tests performed, the FE chip configuration files produced at the respective module-building sites were used, as will be done during ITk production. Due to early differences in module-tuning procedures at different module-building sites, some module-to-module variation in performance results is therefore seen.

As described above, the results have been compared between the various stages of testing. Recall that these stages are defined as:

- Stage 1 = Module production
- Stage 2 = Reception testing at RAL
- Stage 3 = post loading measurement at RAL
- Stage 4 = single module testing on ring at Liverpool
- Stage 5 = module tested on Serial Power chain

All the results were comparable through the different stages of testing, with the exception of the mean Time over Threshold (ToT) which saw a slight shift before and after module loading. A similar effect was observed in the inner and outer barrel system tests. In the sections that follow, plots for a typical-representative module are presented.

5.2.2.1 Digital Scan

Figure 129 shows the digital performance of module 'MilanQ3', for all three front-end architectures, for Module production ('stage 1'), reception testing at RAL ('stage 2'), post-loading at RAL ('stage 3') and module tests on the serial power chain at Liverpool ('stage 5'). No significant change in performance was observed across the stages.

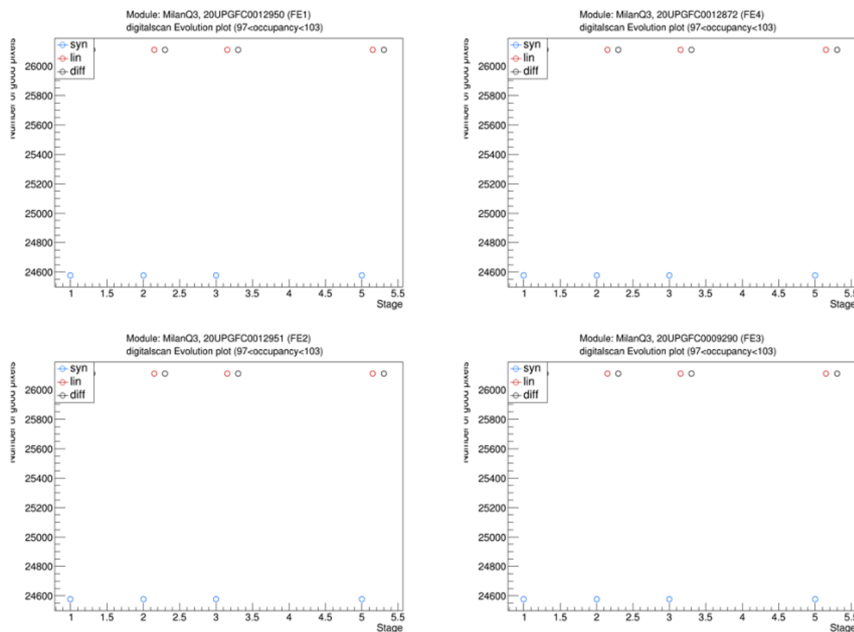

Figure 129: These plots show the evolution of the number of 'good' pixels for the digital scan of each front-end chip on the quad module 'MilanQ2'. A good pixel is defined as a pixel that is not masked at the end of each scan. The vertical scale shows the number good pixels for each front-end (synchronous, linear, and differential), and the horizontal scale shows the testing stage, with the numbers following the convention set in section 1.2.3.

5.2.2.2 Analogue Scan

Figure 130 shows the analogue performance of module 'MilanQ3', for all three front-end architectures, for module production ('stage 1'), reception testing at RAL ('stage 2'), post-loading at RAL ('stage 3') and module tests on the serial power chain at Liverpool ('stage 5'). Again, no significant change was seen across the stages.

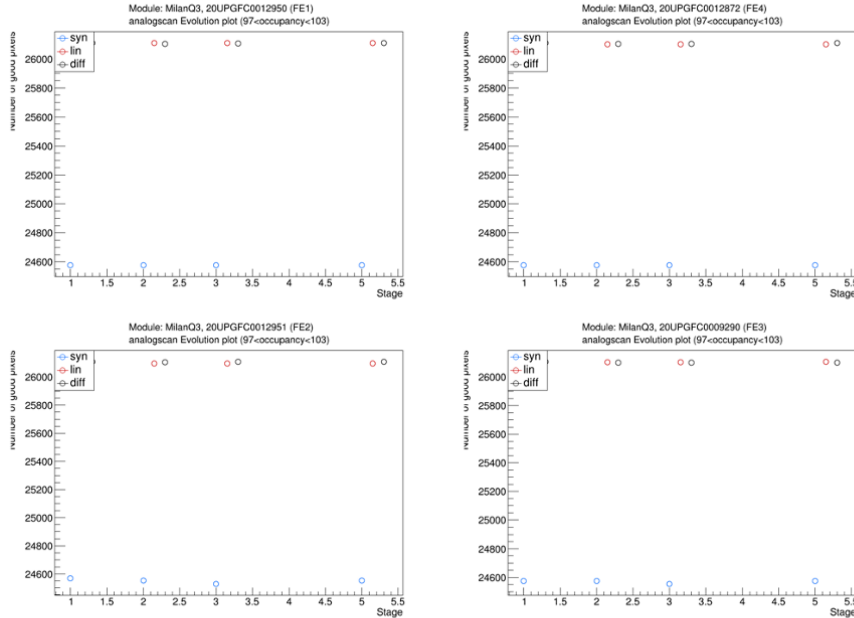

Figure 130: These plots show the evolution of the number of 'good' pixels for the analogue scan of each front-end chip in the quad module 'MilanQ3'. A good pixel is defined as a pixel that is not masked at the end of each scan. The vertical and horizontal scales are defined identically to in Figure 129 above for the digital scan.

5.2.2.3 Threshold/Noise/ToT Measurement

Measurements of the threshold, Noise, and Time over Threshold (ToT) were performed for the sensors for different stages to assess any impact on the loading on the performance or whether there was a difference if the module was tested individually or though the serial power chain. No effect on the threshold or noise was apparent but a slight shift in the mean ToT was observed. The following plots are example plots from some representative modules. Figure 131 and Figure 132 show the evolution of the threshold of each front-end chip in the quad module 'MilanQ2' and LivThn6 respectively. No significant change in performance was observed across the stages.

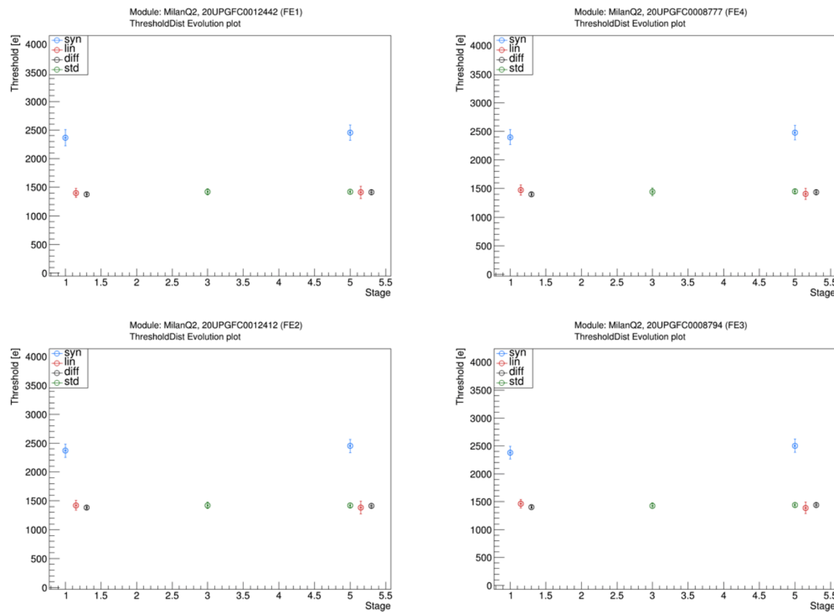

Figure 131: These plots show the evolution of the threshold of each front-end chip in the quad module 'MilanQ2'. The horizontal scale shows the testing stage, with the numbers following the convention set in section 1.2.3.

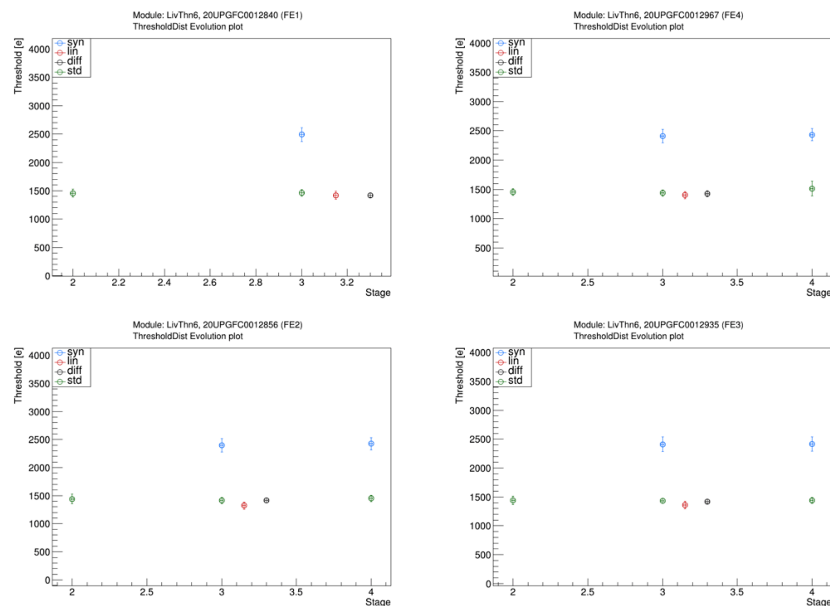

Figure 132: These plots show the evolution of the threshold of each front-end chip in the quad module 'LivThn6'. The horizontal scale shows the testing stage, with the numbers following the convention set in section 1.2.3.

Figure 133 shows the noise of module 'MilanQ3', for all three front-end architectures, for Module production ('stage 1'), reception testing at RAL ('stage 2'), post-loading at RAL ('stage 3') and module tests on the serial power chain at Liverpool ('stage 5').

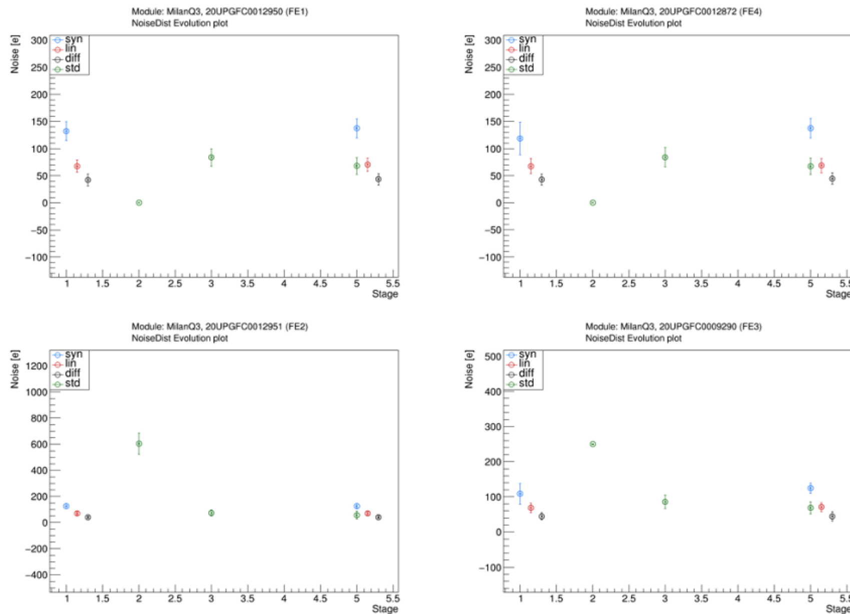

Figure 133: These plots show the evolution of the noise of each front-end chip in the quad module 'MilanQ3'. The horizontal scale shows the testing stage, with the numbers following the convention set in section 1.2.3. No significant change in performance was observed across the stages. Note that RAL (stages 2 and 3) ran 'standard' combined scans only, rather than the series of separate scans (linear, synchronous, differential) as was done at Liverpool (at stages 1 and 5).

Figure 134 shows the time over threshold performance of module 'Liverpool Thin 0', before ('stage 2') and after ('stage 3') loading. A slight shift in mean ToT is observed before and after module loading. It is noted that a similar effect was observed for the inner and outer barrel system tests.

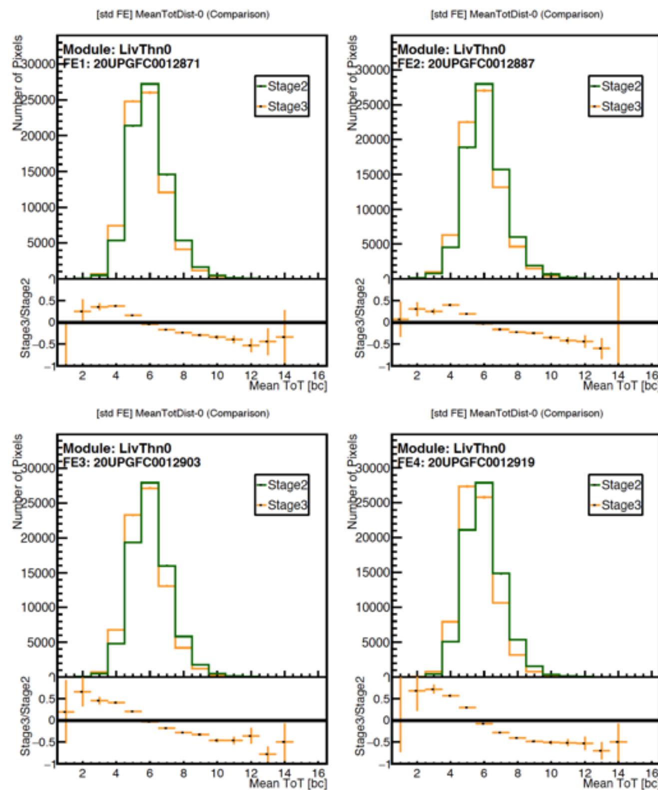

Figure 134: Plots showing mean ToT distribution for each front-end chip on quad module LivThn0 following reception testing at RAL ('Stage2') and following loading onto Ring 1 at RAL ('Stage3'). A shift in the mean ToT can be observed following loading.

Figure 135 shows the time over threshold performance of module 'Liverpool Thin 1', at module production ('stage 1') and after testing on the ring at Liverpool ('stage 4').

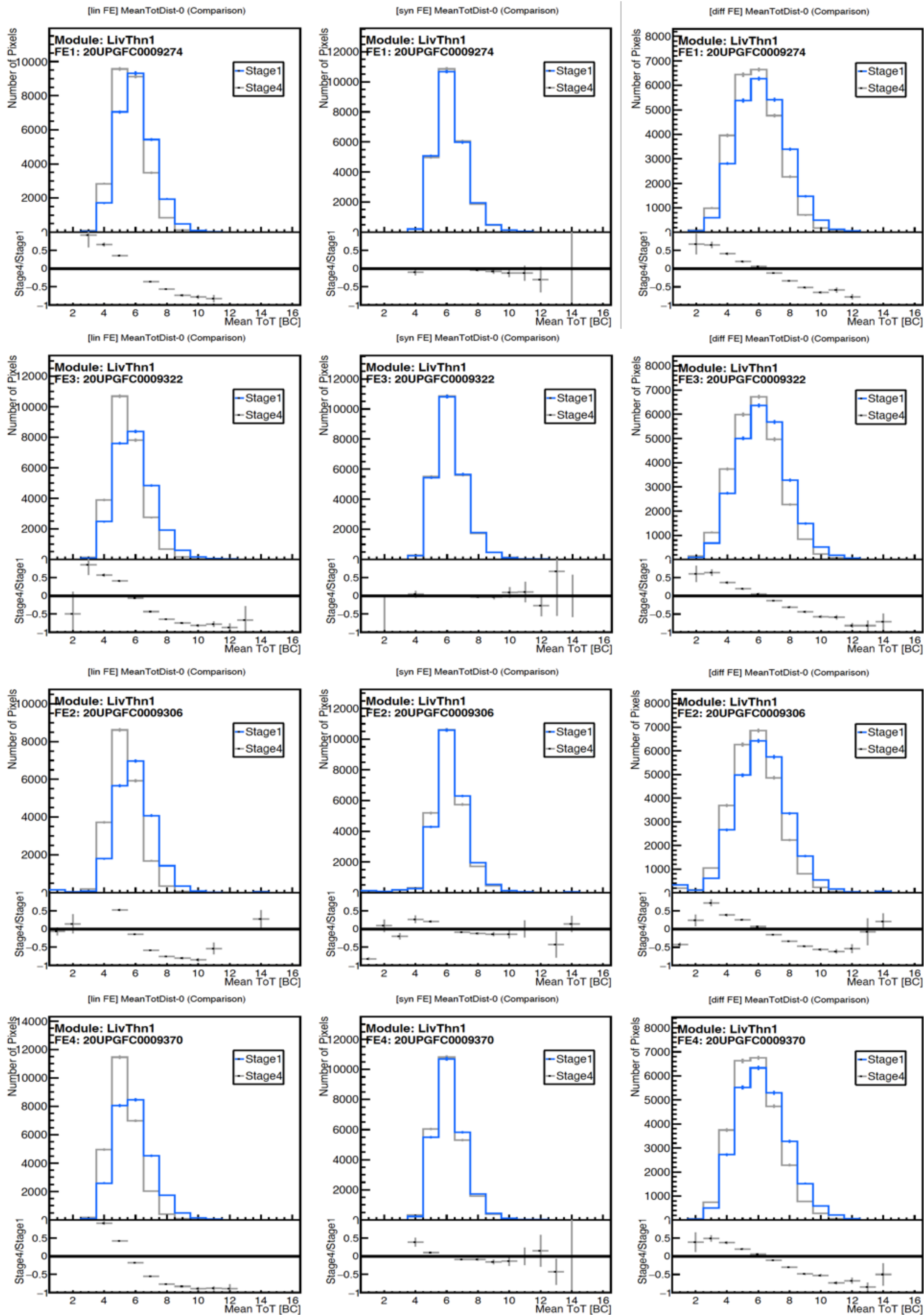

Figure 135: Plots showing mean ToT distribution for each front-end chip on quad module LivThn1 following reception testing at module production ('Stage1') and testing at Liverpool ('Stage4') for the "linear" (left), "synchronous" (middle) and "differential" (right) analogue front-end circuitry. A shift in the mean ToT can be observed, corroborating the RAL observation from Figure 134.

5.2.2.4 Disconnected Bump Bond Evaluation

Figure 136 shows the number of disconnected bump bonds of module ‘Liverpool Thin 1’, at production at Liverpool (‘stage 1’), after reception test at RAL (‘stage 2’), following loading at RAL (‘stage 3’), and following single module testing on the ring at Liverpool (‘stage 4’). There is a slight difference observed between the results at RAL (stages 2 and 3) and at Liverpool (1 and 4). This is believed to be due to the different YARR versions used.

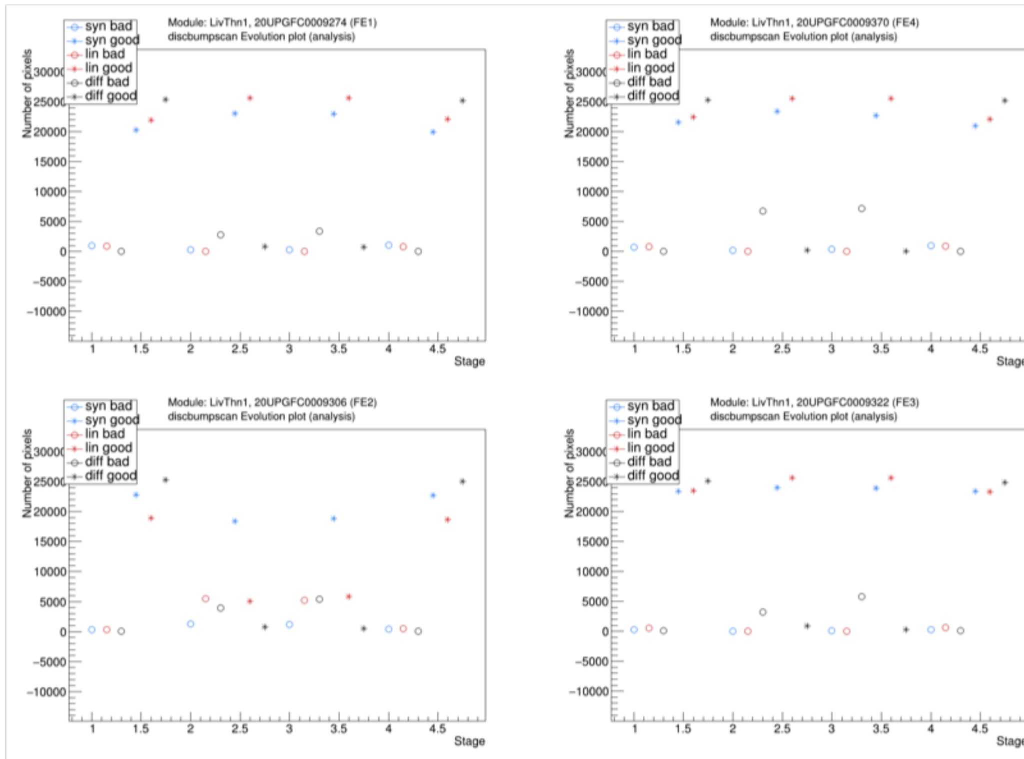

Figure 136: These plots show the evolution of the number of ‘good’ and ‘bad’ pixels for each front-end chip on the LivThn1 quad module during disconnected bump scans at each stage. The vertical scale shows the number good (or bad) pixels for each front-end (synchronous, linear, and differential), and the horizontal scale indicates the testing stage as defined in section 1.2.3. Given that stages 1 and 4 took place at Liverpool, and 2 and 3 took place at RAL, different YARR versions used led to a discrepancy in results between testing sites. However, no significant change in performance is observed between stages measured at Liverpool, or stages measured at RAL.

5.2.2.5 Sensor I(V)

Sensor IV curves were produced for all sensors on the ring before and after loading at RAL, and again at Liverpool. Good agreement was observed for all sensors demonstrating that the behaviour of the sensor was unaffected by loading the module onto the half-ring, and shipping to Liverpool.

Figure 137 and Figure 138 show the sensor IV curves of a few representative modules (LivThn1, MilanoQ3, MPP5 and Ox10).

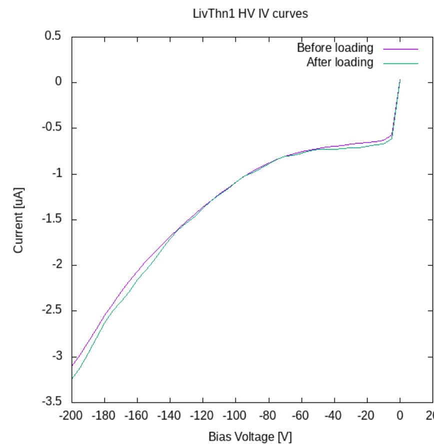

Figure 137: The HV IV curves measured for the LivThn1 sensor before and after the module was loaded onto Ring 1 at RAL. No significant change in behaviour was observed.

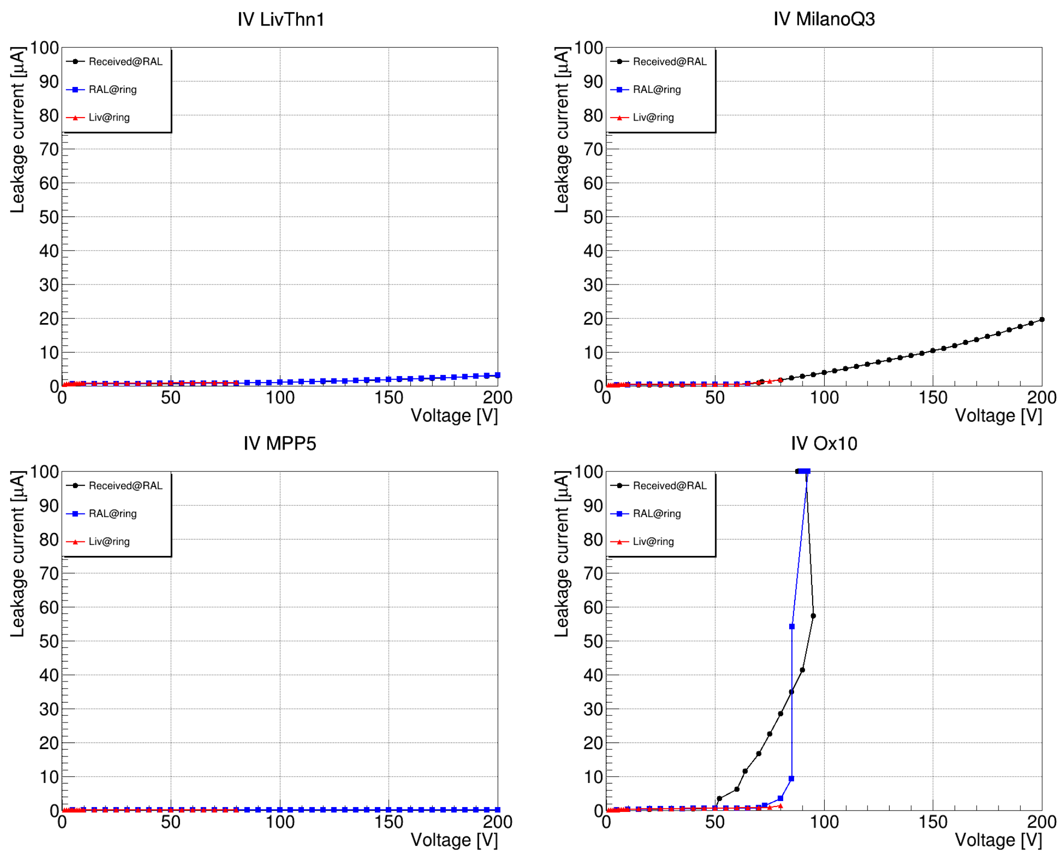

Figure 138: Representative I-V distributions for 4 modules on Ring, clockwise from top left: LivThn1, MilanQ3, MPP5 and Ox10. No significant difference was observed in the curves measured before and after loading at RAL and again at Liverpool.

5.3 Summary

Due to problems with the Lukasz cooling system described in section XX, the full testing program of Ring 1 is yet to be completed. The electrical tests taken so far, of which a representative sample is presented here, show consistent performance and behaviour of the modules loaded onto Ring-1 from module production, through loading to operation by the serial power chain. The only exception is an observation of a slight shift in the mean of the ToT distribution which occurs after loading of the modules onto Ring-1.

The testing program to follow includes:

1. Testing of all eleven modules in a serial power chain together.
2. Adding the other side of Ring-1 → front/back measurements.
3. Upgrading the MOPS from v1 to v2.
4. Noise injection studies.
5. Source and X-ray scans.
6. Thermal camera measurements.
7. Addition of more realistic cables (e.g. full-length).

6 Quality Control

6.1 Philosophy of QC Procedures

The electrical test procedures for the testing of the loaded local supports are detailed in [27]; here only a conceptual summary is given.

The goal of the electrical QC testing is to

1. identify any problem related to the connections made on the loaded local supports during the loading process,
2. identify any degradation of the module performance after the mechanical loading process,
3. test aspects of the loaded local support as a system that could not be tested at earlier integration levels (i.e. MOPS system, serial powering in a large chain, problems with cooling interface).

The electrical test sequence has been grouped in three logical units:

- Checkout
    - 1 – Module temperature interlock (“Tilock”) and MOPS check
    - 2 – Bit Error Rate Test
    - 3 - front end temperature readback
    - 4 - Tilock and MOPS readback
- Performance QC
    - 5 - I-V scan
    - 6 - digital scan
    - 7 - analogue scan
    - 8 - threshold/noise measurement
    - 9 - disconnected bump bond scan
    - 10 - front end temperature readback
    - 11 - Tilock and MOPS readback
- Low power tests
    - 12 - Tilock and MOPS readback
    - 13 - front end temperature readback

The purpose of the checkout is to validate very quickly the basic functionality of the different systems allowing a save and successful operation of the loaded local support. In the performance QC, frontend and sensor performance figures will be measured in order to be able to compare the results with earlier QC stages. The low power mode tests check the basic functionality of the system while powered in the low-power mode, which is very relevant for later integration stages.

6.2 Outline of electrical QC setups

Electrical QC of the loaded half-rings will be performed at the module loading sites immediately after module loading. In this section the setups that will be used in the three QC sites will be described. The intention is to use as much as possible identical components, but for a number of reasons, this will not always be possible. Differences will be described and motivated in the various sections below and the equivalence between adopted solution will be demonstrated with specific tests or repeated measurements on the same part.

Part of the equipment is already installed in the four labs and was used during the preparation of the FDR. However, electrical test setups are not yet at the production level. During pre-production all the elements will be commissioned, and a formal qualification procedure of the

four loading will be performed before the PRR to ensure that all specifications are met. The qualification procedure is described in Section 5.3.

6.2.1 UK test box and environmental control

The test box and environmental control at the UK loading sites will be similar to what has been used for the Ring-1 demonstrator testing; see Section 5.1.3.

6.2.2 Italy test box and environmental control

During electrical tests in the Italian sites the half-ring is placed in a modified version of the storage and transport, specialised with appropriate feed-throughs for electrical services and cooling pipes. This box defines the main humidity-controlled environment around the half-ring during cold operations. The box is then inserted in a larger shielded container equipped with a movable X-ray gun. The second box provides an extra thermal isolation and humidity control. It is equipped with door, light, temperature and humidity interlocks to prevent operations in improper conditions.

In general, especially if cold operation with CO_2 at –30°C is considered sufficient to demonstrate the stability of the half-ring connections during thermal cycles, the ideas would be to keep the half-ring inside the two boxes for the entire duration of the QC program. However, if thermal cycles at –40°C are required as a part of the QC program, it will be necessary, after a first set of electrical tests, to disconnect the half-ring from the services, extract it from the two boxes, place it in the climatic chamber and repeat the connections for the final round of tests.

6.2.2.1 Preparation of the half-ring

After module loading and power pigtails connection, data PP0 flex circuits are connected to the modules and attached to support structures fixed to the handling frame. The data PP0 are the final ones and will not be disconnected during the integration step.

6.2.2.2 Transport box adaptation

As for the normal transport box, the test inner box is made of two plastic shells. The half-ring is placed in the lower shell with its handling frame secured to an aluminium frame and the data PP0 connectors pointing up. Power and data cables enter in the box via gas tight feed-through and are connected to the half-ring power and data tapes. The upper shell is placed above and seal off the internal environment with rims gasket. See Figure 139.

The CO2 cooling is delivered by two Swagelok feed-through and stainless-steel inner pipes placed on the lower box front face. The dry air is flushed by push-pull feed-through fitting and plastic pipes placed on the lower box side wall. The dew point is measured by a Vaisala sensor readout by a USB connector placed on the upper box side wall. The environmental parameters (Temperature, Humidity and Light) are measured by sensors placed on a PCB board powered and readout by a feed-throw connector placed on the lower box side wall.

The thermal and moisture isolation is strongly increased, with respect to the storage/transport box set up, by an internal layer of 3 mm thick ARMAFLEX on the lower and upper shells.

The QC is done keeping the half-ring in horizontal position, which makes it easier to install pipes and cables. The internal structure is however reversible, so that the lower half-ring face can be exposed in case of need, after disconnection of the cooling pipes.

The inner box is transparent to X-ray, so a test of the module bumps integrity can be performed without opening the box. In addition, a thermo-camera could be placed inside the upper box of 48cm height to take a temperature map of the half-ring during operation. It must be noted that X-ray test and temperature maps are not mandatory parts of the loaded half-ring QC procedure.

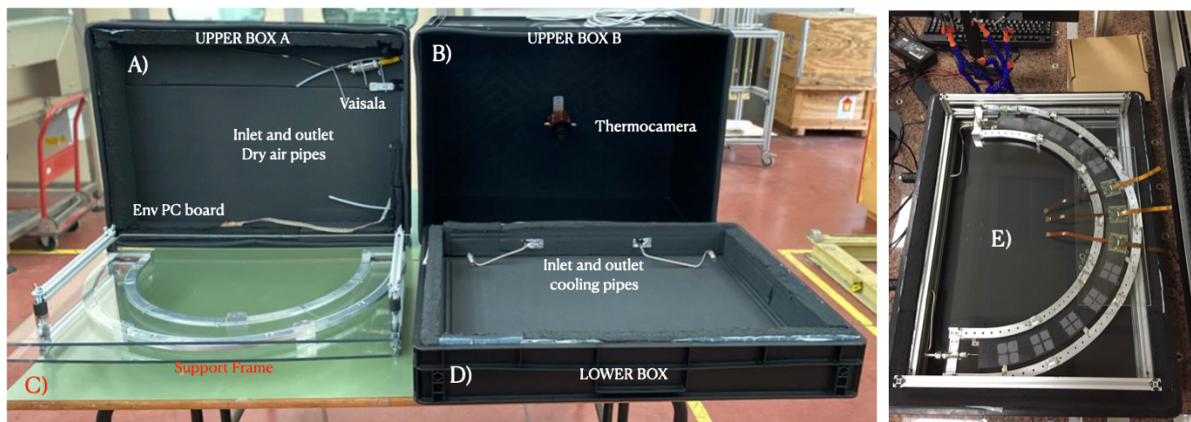

Figure 139: Test box for half-ring QC during production for the Italian sites. A) Upper Box for production QC tests B) Upper Box for cross-check with thermal camera C) Support frame and Layer-4 handling frame with a Layer-4 plexiglass half-ring D) Lower box for QC tests and E) Old style lower box with old style support frame.

6.2.2.3 Insertion in the outer box

Once all the connections to the half-ring are completed, the inner box is closed and inserted in the outer box. Power services from the inner box are connected to the external power supplies. Twinax data cables are connected to an opto-box located inside the other box and connected to the readout system with optical links.

The outer box is closed, flushed with dry air with dew point of –60°C (as well as the inner box) and conditioned to a temperature around 5°C. When the humidity inside the two boxes is sufficiently low, the half-ring can be powered.

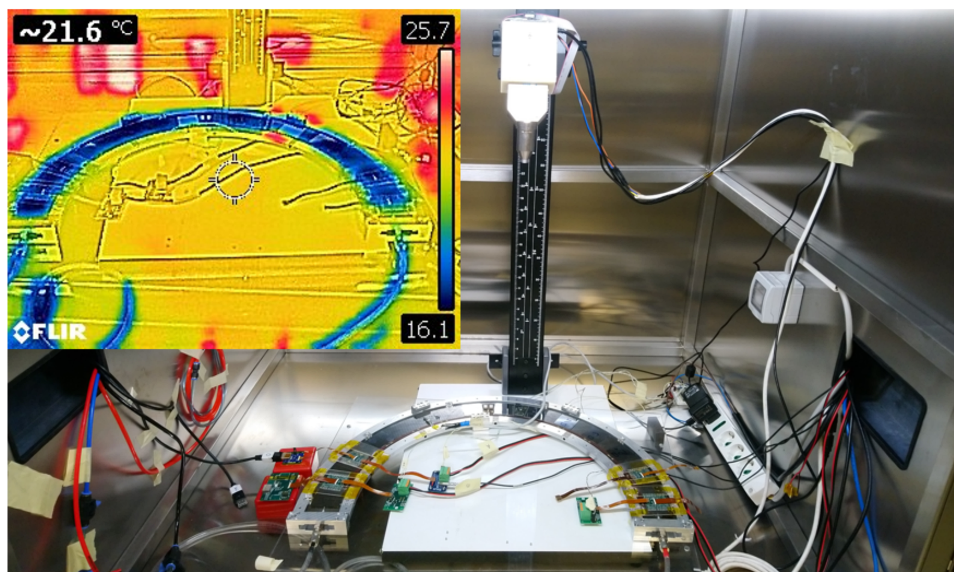

Figure 140: Picture of the outer box (in a very preliminary stage and with a non-motorized support of the x-ray tube) with a half-ring under test. In the upper left corner is a thermal picture of the half-ring during operation.

6.2.3 Power supplies

The initial idea was to use pre-production power supplies in the loading sites. The market survey for the power supplies has been delayed several times, and it is now foreseen in 2023, which means that pre-production units will not be available before 2024.

For the EC loading sites, a natural alternative is to look at power supplies already qualified in the context of the Module QA/QC program. This is a viable solution, considering the fact that each half-ring consists of two serial power lines, hence only two HV and LV channels are needed to power it up. Power supplies for the MOPS chip and for the optobox/optoboards are needed as well, but the total number of channels remains sufficiently small and does not require a highly integrated solution.

Rohde & Schwarz HMP4040 units provide 4 LV channels (max 10 A / 160 W per channel) and are already qualified for use with ITkPixV1.1 modules in serial power mode. Two units should be sufficient to power a half-ring, including ancillary supplies (DCS, MOPS chips, optoboards). This is the solution adopted for Ring 1 tests and it and should be adequate for the loaded local support pre-production phase. We expect to be able to switch to pre-production units as soon as they become available.

For the HV, we can consider using a pair of Keithley Instruments 2410 or similar source meters already largely used in ITk labs to bias sensors and qualified for module QA/QC for the two serial power lines. An alternative, being considered for QA/QC, would be CAEN DT8032, an 8-channels HV (500V, 10 mA) power supplies or old ISEG power supply units currently available as spares for the legacy ATLAS Pixel Detector. Again, migration to pre-production units will be considered when possible.

In order to facilitate the migration from QA/QC units to pre-production multi-channels power supplies we would like to simplify as much a possible the impact on the DCS software side. A good way to achieve this result would be to base the DCS software on OPC servers for low level communication with the hardware and WinCC OA for user interface and automated controls. In this way, and as long as an appropriate OPC server is available, any unit can be used with limited modification on the WinCC OA side. Pre-production units will be delivered with an embedded OPC server. For the R&S and Keithley units a custom OPC server has been developed and can be used in the early stages of the loaded local supports QC. This custom OPC server can be adapted to more power supplies if needed.

6.2.4 Cables

Connections of the half-rings with the power supplies will be organized as in the real detector, trying to mimic as closely as possible the same connection and grounding schema. However, given the fact that we will not use production grade power supplies at least at the beginning, we may be forced to use custom cables to connect to HV and LV power supplies.

6.2.5 Detector Safety and Interlock concept

The conceptual design of the interlock system will follow that of the full detector. In particular the temperature sensors of the modules located at the inlet of the cooling fluid will be used to assess the proper functionality of cooling system and humidity sensors located close to the half-ring will be used to monitor environmental conditions and prevent condensation. The remaining temperature sensors will be readout via the MOPS chips on the bus tapes and routed to the DCS system. As already prescribed for individual module QC, temperature measured on the module NTC will not be allowed to exceed 40 C. In case of improper operating conditions, the HV and LV power supplies will be interlocked by and hardware signal and the cooling system will be stopped in case the humidity gets too high.

The implementation of the interlock, considering the limited number of channels (just two serial power lines), will be based on custom micro-controllers or PLCs.

A complete DCS system, based on WinCC OA, is being prepared for loading sites and intermediate size system tests. This system will provide an extra level of detector protection based on software, as well as a complete logging of the operating conditions on a database (InfluxDB).

6.2.6 Readout System

A FELIX based readout system is the baseline for QC tests during production, even if a transition phase from the existing single module readout system to a complete multi-module readout is foreseen during pre-production.

Each loaded half-ring QC site is equipped with a phase I FELIX server and is about to receive a pre-production optobox with four optoboards. This setup is sufficient to read fully populated Layer-2, Layer-3 and Layer-4 half-rings at the same speed as in the final detector setup. Presently, the only missing component are the twinax cables to connect data PP0 with the optoboards. The availability of twinax bundles is very limited and the pre-production seems not imminent. Moreover, depending on the half-ring type, different types of twinax bundles will be required as the channel mapping between the data PP0 and the optoboard depends on the layer. The hope is that the four bundles per site needed to start the Layer-2 production will be available at the end of 2023, in time for the site qualification and the loaded local supports PRR in August 2024.

The readout software is expected to evolve in the next two years. A minimal version with basic functionality already exists, but the discussion on the software readout architecture for large systems is still in progress. We are confident that a first mature release of a FELIX based multi-module readout will be available at the beginning of 2024 to support loaded half-ring QC.

6.3 Site Qualification Plan

To prepare this FDR we focused on the qualification of the loading procedures. Before the PRR, scheduled for August 2024, a formal qualification of the four loading sites (Genova and Lecce for the Italian end-cap, Oxford and RAL for the UK end-cap) will follow a formal qualification procedure to assess readiness for production.

The key element of the qualification procedure will be the loading of a full (two-sided) half-ring with pre-production services and ITkPixV1 pre-production modules and the corresponding QC. These are the key points that each site will have to demonstrate:

- Appropriate working environment (clean room cleanness, temperature and humidity control, anti-static measures).
- Availability and functionality of all the elements of the loading setup (depending on the loading technique used), including ancillary tools and jigs to perform preparation and post-loading steps assigned to the site.
- Module handling, starting with the mandatory reception test, must follow the recommendations from the module working group and the corresponding qualification procedure applies to the loading sites as well.
- For sites in charge of gluing bus tape on the half-ring: availability of the gluing tool, capability to perform metrology in order to verify the correct placement of the tape in the half-ring reference system.
- Capability to glue modules on a local support respecting the specifications in terms of glue layer (thickness between 50 and 200μm, coverage > 80%) and position (150μm with respect to the nominal position) demonstrated producing a fully populated half-ring and performing the necessary metrology.

- Tools to connect the modules to the service distribution tapes (power and data).
- Availability of a full setup to cool down and operate a complete half-ring, equipped with an interlock system functionally equivalent to the one foreseen for the full detector. Complete comparison of module performance pre- and post- loading, demonstrating no degradation on the complete pre-production loaded half-ring.
- Packaging and shipping procedures to move the loaded half-rings to the integration sites.
- Capability to log operating conditions during the loading process on a condition DB. Appropriate long term archival of all the measurements and testes performed during the loading procedure and the corresponding preparation and QC. Availability of tools to load summary results of the loading process and of the corresponding QC to the ITk Production DB.

The exact details of the requirements for the qualification of each loading sites will be defined during pre-production and published on EDMS.

7 Production Plan

7.1 Number of Parts

As can be understood from Table 1 in Section 2.2.1 of this document, each endcap requires 56 loaded half-rings. Table 13 is adapted from the Basis of Estimate (BoE), which includes agreements about how many parts are required for production and pre-production. The actual number of loaded half-rings made during pre-production will of course depend upon the number of modules available, which is expected to be fewer than the number needed to produce four loaded half-rings per endcap; it is however vital that each loading site fully load at least one half-ring in pre-production.

Sub-system	Needed for detector	Production (includes yield)	Pre-production	Total to produce
Endcap A	56	58	4	62
Endcap C	56	58	4	62

Table 13: Number of loaded local supports required for the Outer Endcaps

7.2 Production Flow and Involved Institutes

7.2.1 Production Flow Diagram

Figure 141 shows the Production Flow Diagram for the ITk-Pixel Outer Endcaps Loaded Local Supports. As has already been mentioned in this document, and as if reflected in the diagram, Endcap-A will be delivered by Italy and Endcap-C will be delivered by the UK.

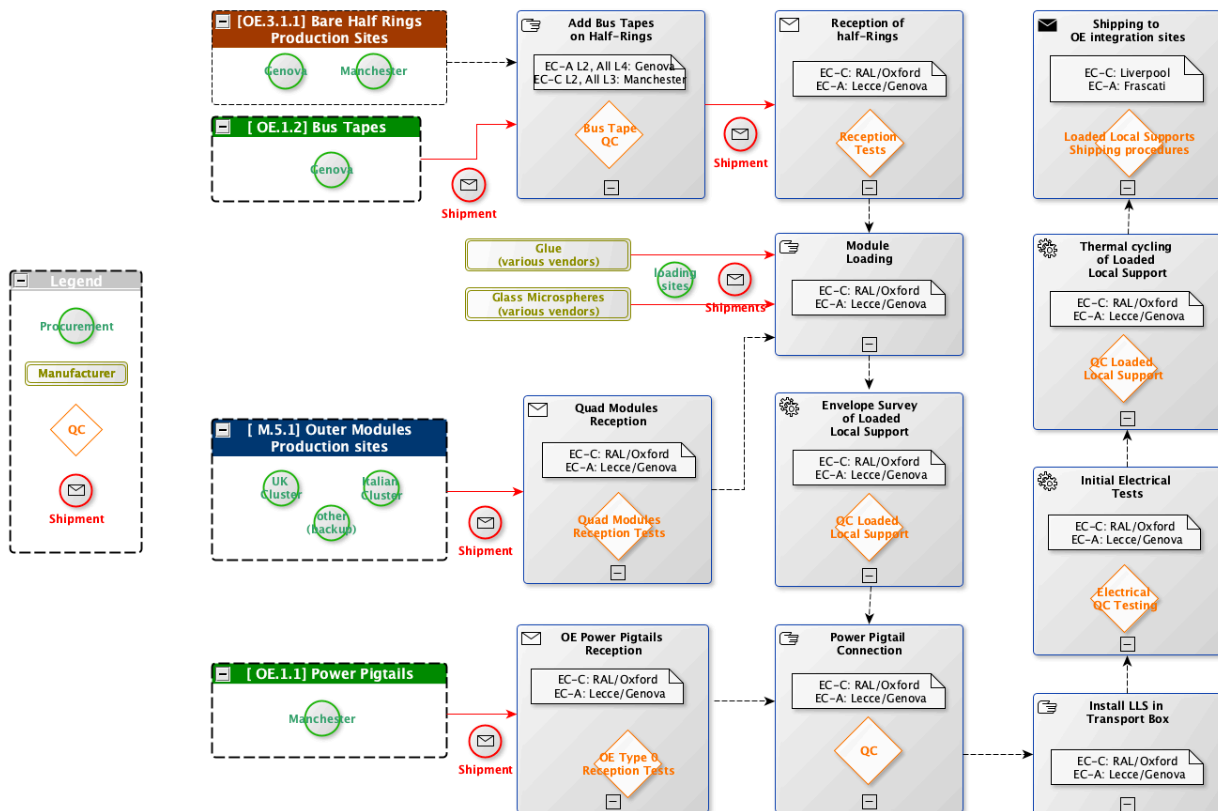

Figure 141: Production Flow Diagram for the Outer Endcaps Local Support Loading.

7.2.2 Description of Production QC

This topic is covered in AT2-IP-QA-0051 [27], which also covers the production database implementation.

7.3 Transport of loaded supports to Integration Sites

A half-ring is ready for testing only after being loaded with modules on both faces and the power pigtails of each module are soldered on the bus tape and plugged into the modules. A complete half-ring is then sandwiched between two anti-static Perspex plates, enclosed in a vacuum bag with desiccant salts and placed inside a storage and transport box surrounded by thick foam to protect the half-ring from shocks. The half-ring is removed only for thermal cycling and qualification tests, and finally for integration into an endcap.

Two potential solutions exist for the transport and storage box.

In the first solution, pictured in Figure 142a, the Perspex plates that sandwich the loaded half-ring have dimensions of 700 mm x 500 mm x 6 mm anti-static perplex plates, with two handles on both plates, using vertical bars crossing the not-threaded lateral holes of the handling frame end pieces. The transport box is made from two inexpensive commercial coverless ESD black boxes (ESDEG86/12HG, 800mm x 600mm x 120m) one on top of the other. An adhesive gasket (12mm x 14mm D-shaped rubber) is placed on the rim of the bottom ESD black box to improve the light and gas tightness. The two boxes are held together by clamping the two rims of the boxes, separated by the gasket, with 6 custom made plastic H-shapes (2 H-shapes on the long sides 33 cm long and 1 H-shape on the short sides 48 cm long). The H-shapes are placed by hand pushing them horizontally while pushing the upper box down. During transportation between sites the two boxes are safely keep together by strapping. The transport box with loaded half-ring could travel between loading and integration sites in a commercial large hermetic box full of foam, see Figure 142b. Two or more support frames could be piled-up inside a storage/transport box and/or two storage/transport boxes could be piled-up inside a bigger hermetic box.

Figure 142: a) stacked commercial storage boxes for containing a half-ring in its protective Perspex plates. b) commercial hermetic box to contain one or two storage boxes for transport.

The second solution (see Figure 143) is a similar concept but uses different commercial items and was employed to transport the loaded Ring-1 from RAL to Liverpool. The Perspex plates

enclosing the loaded half-ring in this solution are arcs and the outer box is a “PeliCase” fitted with pre-cubed foam which can be easily shaped to cushion one or more half-rings for transport.

No matter which solution is used, a USB temperature, humidity, and shock data logger will be placed on the base plate of the support frame to monitor the transport conditions.

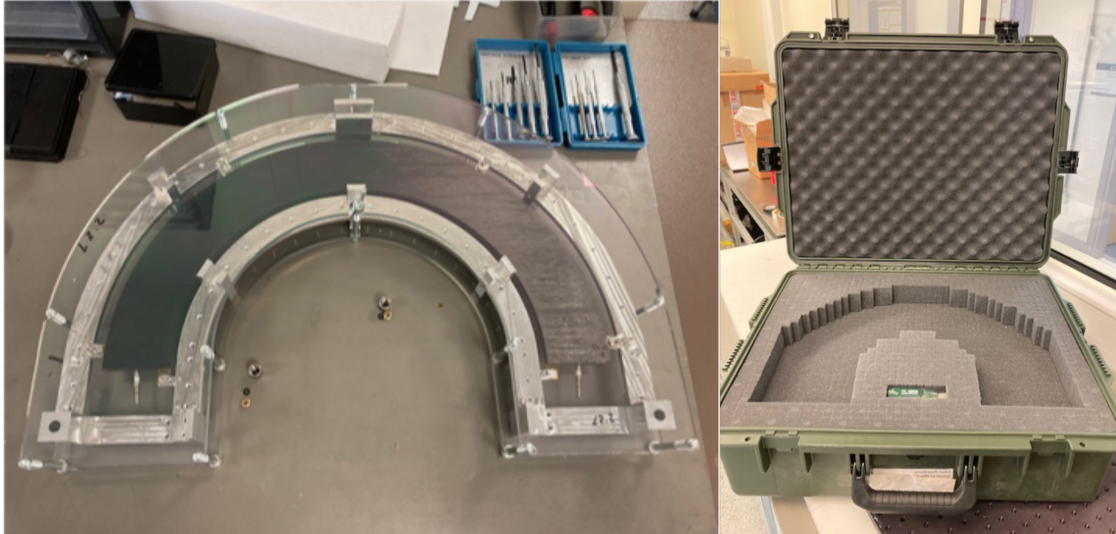

Figure 143: Left: A bare half-ring in its handling frame with Perspex covers; when loaded this will be enclosed in a vacuum bag with desiccant. Right: a commercial parts suitcase fitted with pre-cubed foam that has been shaped to cradle the half-ring in its frame.

7.4 Schedule

Figure 144 shows the current Outer Endcaps pre-production schedule leading up to the Outer System Production Readiness Review, currently foreseen for June 2024. The timeline also shows the availability of the modules and services needed for loading.

Figure 145 shows the pre-production and production schedules together on the same timeline.

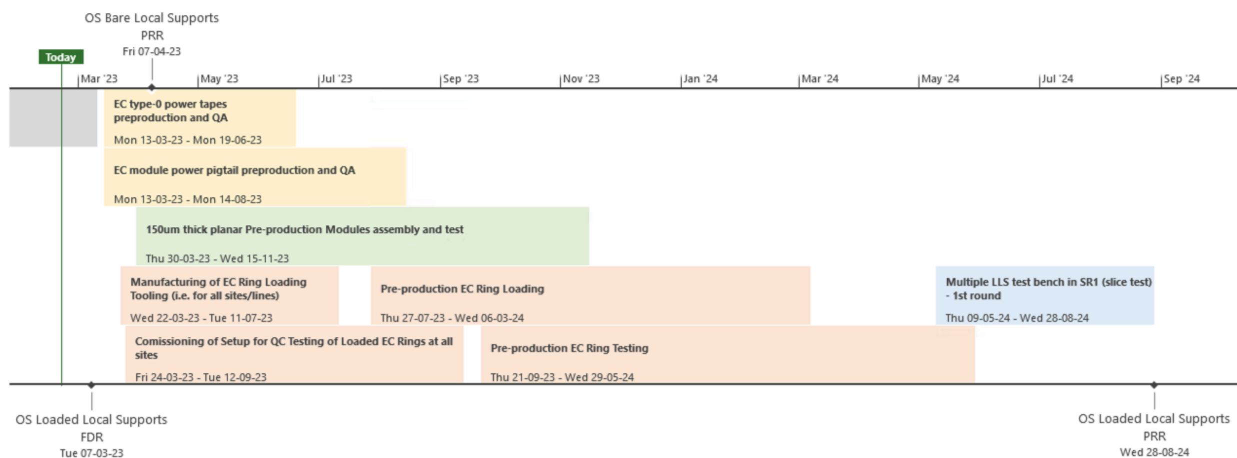

Figure 144: Outer Endcaps Pre-production Schedule (1-January-2023 version). The grey bar is the bare local supports pre-production. Services pre-productions are shown in yellow, modules pre-production in green, and system tests in blue.

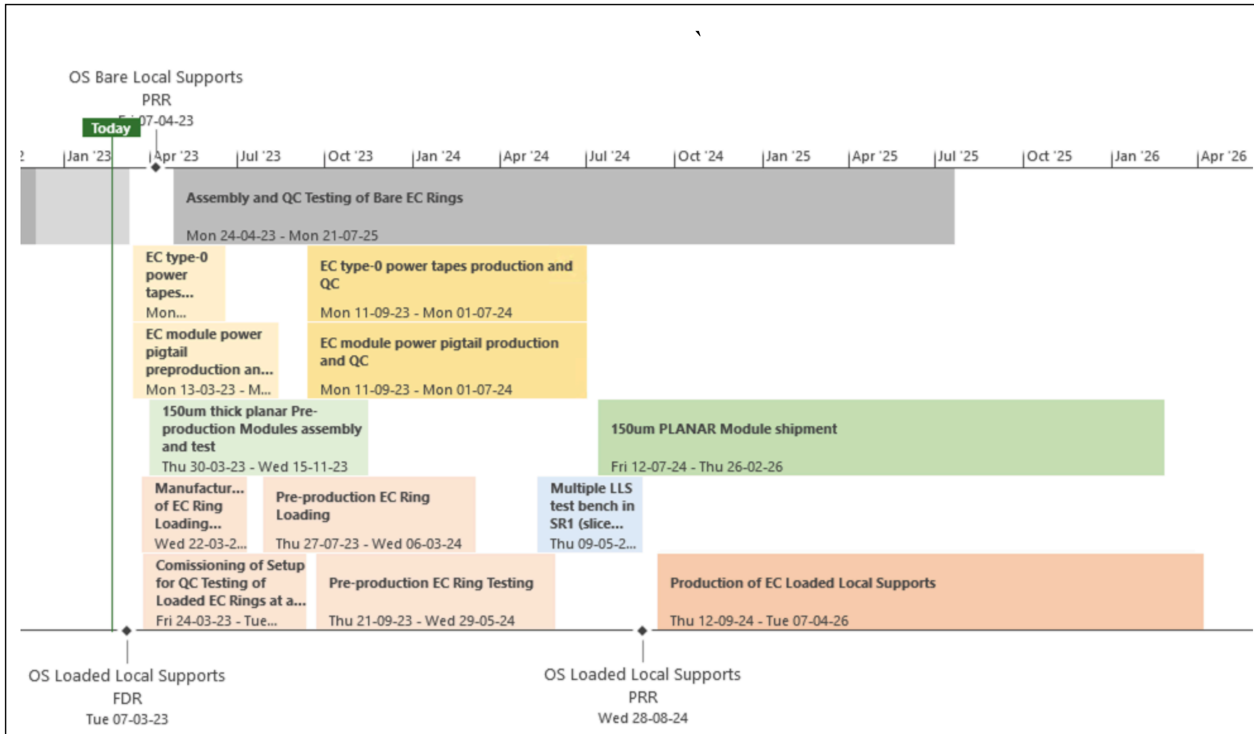

Figure 145: Outer Endcaps Schedule (1-January-2023 version) from now through production.

8 References

[1] J. Pater et al., “AT2-IP-ER-0012 ITk Pixel Outer endcaps Bare Local Supports - for FDR,” 30 September 2021. [Online]. Available: https://edms.cern.ch/document/2632350.

[2] Dow, “DOWSIL™ SE 4445 CV Gel Technical Data Sheet,” 2020. [Online]. Available: https://www.dow.com/documents/en-us/productdatasheet/11/11-18/11-1823-01-dowsil-se-4445-cv-gel.pdf.

[3] STFC Composites & Material Testing Group, “SE4445 CV Thermal Analysis Report - Rheometer,” UK Science & Technology Facilities Council, 23 May 2019.

[4] Henkel, “LOCTITE STYCAST 2850FT,” 2021. [Online]. Available: https://www.henkel-adhesives.com/uk/en/product/potting-compounds/loctite_stycast_2850ft.html.

[5] T. Jones, “AT2-IP-EN-0024 "Description of the Global Mechanics and Integration Sequence for the Endcaps",” 4 December 2020. [Online]. Available: https://edms.cern.ch/document/2446824.

[6] D. Giugni, “AT2-IP-ES-0005: ITk Pixel Local Support Design Specifications,” September 2018. [Online]. Available: https://edms.cern.ch/document/1534572.

[7] E. Vigeolas-Choury, “ITk-Pixel Specficiations for modules loading,” 3 September 2018. [Online]. Available: https://edms.cern.ch/document/1936936.

[8] C. Gemme, “AT2-IP_ER_0026 "Design Overview of the ITk Pixel EC Tapes, Pigtails and Data PP0,” 30 November 2022. [Online]. Available: https://edms.cern.ch/document/2788370/. [Accessed February 2023].

[9] A. Grillo, E. Spencer and N. Starinski, “AT2-I-EP-0001: ITk Grounding & Shielding Requirements,” 2 July 2019. [Online]. Available: https://edms.cern.ch/document/1841188.

[10] L. Cunningham, “AT2-IP-DF-0002 OEC Half Ring Handling Frames,” 12 October 2021. [Online]. Available: https://edms.cern.ch/document/2632309/1. [Accessed February 2023].

[11] S. Coelli and M. Monti, “AT2-IP-ER-0010 "Thermo-Mechanical Finite Elements Analysis of the Pixel Outer End-Cap Half-Rings",” 23 September 2021. [Online]. Available: https://edms.cern.ch/document/2474998.

[12] CERN, “Lap shear test on EA 9396 AERO to 15 MG,” [Online]. Available: https://cernbox.cern.ch/index.php/s/uV8vEW7KZktcxqg.

[13] WikipediA, “ImageJ,” [Online]. Available: https://en.wikipedia.org/wiki/ImageJ. [Accessed February 2023].

[14] OGP Metrology Systems, “SmartScope,” [Online]. Available: https://www.ogpnet.com/products/metrology-systems/multisensor-metrology-systems/smartscope-video-multisensor-systems/. [Accessed February 2023].

[15] Samtec, “FTM Series 1.0mm Surface Mount Micro Low Profile Terminal Strip,” [Online]. Available: https://www.samtec.com/products/ftm. [Accessed March 2020].

[16] CERN, “PS-IRRAD Proton Facility,” [Online]. Available: https://ps-irrad.web.cern.ch/ps-irrad/. [Accessed February 2023].

[17] S. F. Koch, “ATLAS Qualification Task Report: ITk Pixel Outer Endcap Loaded Local Supports : Pixel Module Transport, Half-ring Loading Adhesive Studies, Half-ring Loading Gantry Operation,” 17 November 2022. [Online]. Available: https://cds.cern.ch/record/2841168 . [Accessed February 2023].

[18] J. Pater et al., “AT2-IP-EN-0017 "Allcomp Foam for the ITk Pixel Local Supports",” 26 October 2020. [Online]. Available: https://edms.cern.ch/document/2390267.

[19] CERN, “YARR: Yet another Rapid Readout,” [Online]. Available: https://yarr.web.cern.ch/yarr/. [Accessed February 2023].

[20] G. Gebbia, “A PCI Express board proposed for the upgrade of the ATLAS TDAQ read-out system,” in *PoS(LHCP2018)076* , Bologna, Italy, 2018.

[21] M. Ressegotti, “ITk Pixel DCS meeting: Qualification task report,” 22 April 2021. [Online]. Available: https://indico.cern.ch/event/1022719/. [Accessed February 2023].

[22] CERN, “OpcUaCanOpenServer,” 13 December 2021. [Online]. Available: https://twiki.cern.ch/twiki/bin/view/AtlasPublic/DcsCanOpenOpcUa. [Accessed February 2023].

[23] Cracow University of Technology, “MARTA (Monoblock Approach for a Refrigeration Technical Application),” 2017-2018. [Online]. Available: http://icp.mech.pk.edu.pl/martaco2/. [Accessed February 2023].

[24] NORHOF, “NORHOF LN2 microdosing systems,” [Online]. Available: https://www.norhof.com/. [Accessed February 2023].

[25] CERN GitLab, “CANMOPS,” March 2022. [Online]. Available: https://gitlab.cern.ch/mops/canmops/-/wikis/home. [Accessed February 2023].

[26] Kvaser, “Kvaser Leaf Light HS v2,” 2023. [Online]. Available: https://www.kvaser.com/product/kvaser-leaf-light-hs-v2/. [Accessed February 2023].

[27] M. Wielers, “AT2-IP-QA-0051 Production Flow and QA.QC of Outer Endcap Loaded Local Supports,” 16 February 2023. [Online]. Available: https://edms.cern.ch/document/2822991.

[28] WikipediA, “Open Platform Communications,” [Online]. Available: https://en.wikipedia.org/wiki/Open_Platform_Communications. [Accessed February 2023].

Appendix A: Responses to Actions and Recommendations from Previous Reviews

To be provided before the Review.